# 國 立 交 通 大 學

## 機 械 工 程 學 系


博士論文

# 複合金屬板件冷輥接合與板液壓製程之分析

# Analysis on cold roll-bonding and sheet hydroforming process of clad metal sheets


研 究 生：曾煌棊

指導教授：洪景華 教授



中 華 民 國 一百 年 一 月

# 複合金屬板件冷輥接合與板液壓製程之分析

# Analysis on cold roll-bonding and sheet hydroforming process of clad metal sheets


研 究 生: 曾煌棊　　Student: Huang-Chi Tseng

指導教授: 洪景華　　Advisor: Chinghua Hung


國 立 交 通 大 學
機械工程學系
博 士 論 文

A Thesis
Submitted to Department of Mechanical Engineering
College of Engineering
National Chiao Tung University
in Partial Fulfillment of the Requirements
for the Degree of
Doctor of Philosophy
in

Mechanical Engineering

January 2011

Hsinchu, Taiwan, Republic of China

中華民國一百年一月

# 複合金屬板件冷輥接合與板液壓製程之分析

學生:曾煌棊　　指導教授:洪景華教授

國立交通大學機械工程學系

## 摘要

本研究針對複合金屬薄板，分為冷輥接合，成型極限及板液壓製程等三部分進行深入探討。研究首先探討複合金屬薄板冷輥軋接合製程，針對不同初始厚度及減縮率之複合金屬薄板，利用剛塑性有限元素法，考慮熱傳導、塑性熱及摩擦等熱力項，計算鋁/銅複合金屬薄板之介面溫度，比較不同參數下之差異。結果指出，高輥速、高減縮率及非對稱輥速等，將可提高介面溫度，有助於複合金屬薄板之接合。

其次，應用實驗成型極限圖預測複合金屬薄板之破裂，由成形極限圖可以比較出，厚度減縮率(初始厚度)將影響鋁/銅複合金屬之成型性，而後搭配深引伸試驗比較模擬結果，由結果指出，實驗成型極限圖確實可作為預測複合金屬薄板之破裂。

針對複合金屬薄板之應用，本研究利用板液壓製程來提高複合金屬薄板之成形性。研究中透過有限元素分析，探討鈦/鋁複合金屬薄板於不同製程參數下之厚度減薄率，在數值分析中，本研究提出一虛擬薄膜之概念來應用於數值分析之模型，能夠真實模擬出液壓作用於試片之變化；並提出預鼓脹製程及模具修整的方式，藉此降低鈦/鋁複合金屬薄板之厚度減薄情況，並有效降低加工道次與模具成本。

關鍵字:複合金屬薄板，冷輥接合，成型極限圖，板液壓製程，有限元素分析

# ABSTRACT

This study comprises three sections that include cold roll-bonding, forming limit diagrams (FLDs), and sheet hydroforming (SHF). First, the bonding performance of Al/Cu clad metal sheet with different initial thickness and reduction rate were discussed. The heat flux calculation with thermal conduction, plastic heat and friction consideration were adopted in finite element analysis (FEA). The temperatures of clad metal sheet at maximum reduction region were obtained by rigid-plastic FE code (DEFORM-2D), and then the temperature distribution of Al/Cu clad metal sheets with different combinations of process parameter were determined. The simulation results pointed out that higher rotation speed, higher reduction rate, and asymmetrical rotation are positive to improve the bonding performance for clad metal sheets.

The possibility of applying FLDs to fracture prediction of clad metal sheets is examined. The forming limits of Al/Cu clad metal sheets with different thickness reduction are investigated via FLD test. Moreover, deep drawing tests are carried out to compare the numerical results. The results pointed out that the fractures of clad metal sheets are predicated by experimental FLDs.

For clad metal sheet application, the SHF was adopted to improve the formability of Ti/Al clad metal sheet used in 3C product housings. Some significant process parameters were analyzed for improving formability of clad metal sheet by FEA. In numerical simulation, a virtual film technique was proposed to realistically approach the hydraulic loading for SHF. And pre-bulging and tool modification are proposed to reduce thinning ratio of Ti/Al clad metal sheet, operation stage, and tooling cost.



Keywords: Clad metal sheet, cold roll-bonding, FLD, SHF, FEA

# 致　謝

在完成博士論文之後，慢慢回想起當初與指導教授 洪景華老師，首次面談時的情境，時間匆匆一轉眼就過了五年半，從過往求學歷程來看，本人在大學時期，並未投入足夠的時間在學業上，唯有在研究所期間，才稍微有較為積極正面的投入，個人資質方面，更是很難與正面名詞有所關聯，不過這樣的我，在工作一年後，仍然期望能夠有再回到學校進修的機會，首次與老師面談時，深怕過去所累積的知識基礎不夠充足，無法把握再次回到學校的機會，面談後，老師給了我這個機會讓我能夠再度進入學術領域中學習進修，在五年半的研究過程中，老師除了不厭其煩在學術方面給予指導及方向指引，對於面對研究議題時，秉持精益求精，絕不輕易妥協的原則，這些都對將要取得博士學位離開校園的我，最為寶貴的物品，感謝老師這段時間的指導與教誨。

再者，必須感謝口試委員 賀陳弘，陳復國，陳申岳，向四海，徐瑞坤教授等人，撥空擔任本人的口試委員，並在口試過程中，針對論文提出相當多寶貴的建議與問題指正，讓本人的論文能夠更趨向完整正確。

其次感謝，高雄金屬研究發展中心 產品設計組 黃金川組長，江俊憲博士，金屬成型組 鄭炳國組長，李明富先生，還有板液壓機台操作師傅，同時感謝在計畫執行期間，曾經協助材料實驗及有限元素建模的學弟 忠諭及宗錞，感謝高雄金屬研究發展中心的計畫支助，由於你們的協助，本人才能順利完成論文著作，並讓此論文更為豐富。

感謝，精密工程與模擬實驗室的學長，榮崇學長，深厚的實驗設計與經驗，足以作為我未來實驗規畫的表率；宇中學長，擔任大學長最長的一段時間，在這段時間的相處下，讓我見識到研究與生活，原來是能夠也必須要有所彈性取捨，兩者兼備才是王道；政成學長，圓融的個性以及專業的生物力學研究態度，同樣令我佩服，以及齒輪實驗室冠宇學長，工研院能環所岳儒學長，同學 陽光，立碁，

正展等人，平時對本人研究的關心。

在博士班期間，歷經了數任碩博班學弟，感謝 麒禎，嘉偉，銘傑，彥彬，宗駿，理強，黃詠，志嘉，俊羿，運賢，世璿，建榮，時恆，麒翔，聖平，立釗，維堂，筱偉，正一，馨勻，書麟，雅喬，彥佑，品帆，志豪，怡君，呂翔等，大家各有特色，無法一一說明，但陪伴我渡過五年多的實驗室研究生活的回憶，都將會永遠存在於我腦海中。

再來感謝養育我長大的爸媽，雖然從小到大，兩人忙碌於公司事務，但是平時仍舊對我相當關心與期待，求學過程提供無間斷的經濟支援，讓我能夠無後顧之憂完成學業，對於某些事情，無法盡如兩老之意，本人深感愧歉。

我的女兒 旖婕，感謝妳在兩年前來到這個世界，融入我與媽咪的生活之間，帶給我們世上最甜蜜的幸福，在撰寫論文時，一想到你的笑容就是給我最好的動力，妳永遠都是我最大的驕傲。

最後，最感謝的人當然是我的太太 瑞芬，謝謝你，在我博士班期間及完全沒有事業基礎時，就選擇嫁給我，又替我生了一個可愛女娃，十幾年來的相處過程中，容忍我相當多的缺點，體諒我長時間不在你們身邊，獨自一人照顧旖婕，雖然妳不懂我的研究，但妳卻是這份論文得以完成的最大功臣，在此將要本論文獻給妳。

曾煌棊 謹誌於

國立交通大學機械工程學系

中華民國 100 年 1 月 4 日

# TABLE OF CONTENTS

## LIST OF TABLE

## LIST OF FIGURE

# CHAPTER 1 INTRODUCTION

## 1.1 Clad metal

The clad metals considered in this study are multilayer sheets that possess various properties that surpass single material sheets. Generally, clad metals has advantageous properties such as good thermal conductivity, anti-corrosiveness, wear-resistance, high strength, etc.. Therefore, it can be used in many fields, for example, the electronics, the maritime industry, and the automobile industry. Clad metals not only preserve the original characteristics of the layer metals but also create additional functional properties. The use of clad metals to reduce product weight is also garnering a lot of attention from the viewpoint of environmental preservation. Altogether, the applications of clad metal will bring great improvement in terms of functionality. Table 1.1 shows some applications of composites produced by cold roll-bonding. By using clad metals, such as an Al/Cu sheet with 80% Al, the weight of building sheets is reduced by half compared with those of conventional Cu sheets [1].

Table 1.1 Some applications of different metal produced by cold roll-bonding [2]

| Metals | Applications |
|---|---|
| Al/Cu | Cooking utensils; roof and wall plate; heat exchangers; special engraving plates; electrical components |
| Al/Cu/Steel | Cookware; roast and bowl for induction heater |
| Al/Fe | Reflectors in electric heaters; automobile silencers |
| Al/SUS | Automobile trims |
| Al/Steel/Al | In automotive exhaust systems |
| Ti/SUS/Ni | Bipolar electrode in fuel cell |
| Al/Zn | Printing plate for high-speed wrap-around press |

## 1.2 Cold roll-bonding

Clad metals can generally be made by several processes, for example, explosive

bonding, adhesive bonding, and hot/cold roll-bonding. In this research, all clad metals were made by cold roll-bonding from MIRDC (Metal Industries Research & Development Centre). Cold roll-bonding process has many advantages over hot roll-bonding, it is carried out at low temperatures, and thus, undesirable phase transformations and microstructures can be avoided [2]. Moreover, it yields good surface quality and is low cost. The two-ply clad metal sheets were arranged as illustrated in Figure 1.1.

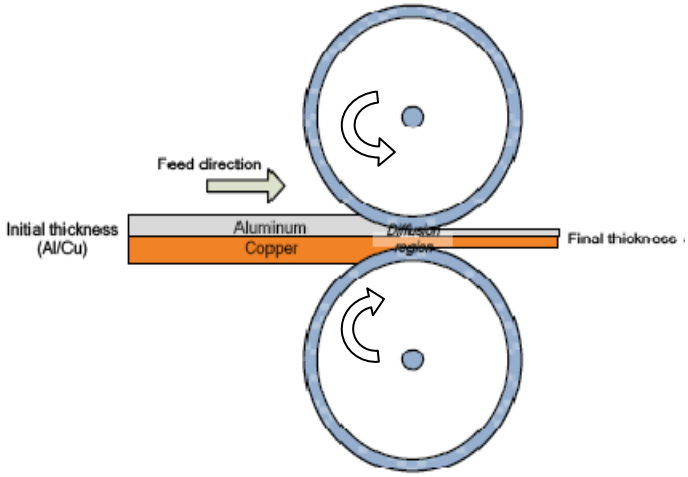


Figure 1.1 Schematic illustration showing principle of cold roll-bonding

### 1.3 Sheet hydroforming

SHF, Figure 1.2 (a), is the process that metal sheets were formed by deep drawing punch with a hydraulic counter pressure. The counter pressure was controlled by a relief valve and an additional safety relief valve avoids bursting of the counter pressure. Nowadays, SHF have been widely accepted by industries for the production of components characterized by fine surface quality, higher dimension accuracy, better formability, lower tooling cost, fewer forming operations, and economical for small lot production. The application of SHF on clad metal can combine the advantages of both process and material, and thus become promising in producing

outward products. Figure 1.2 (b) is sample by SHF.

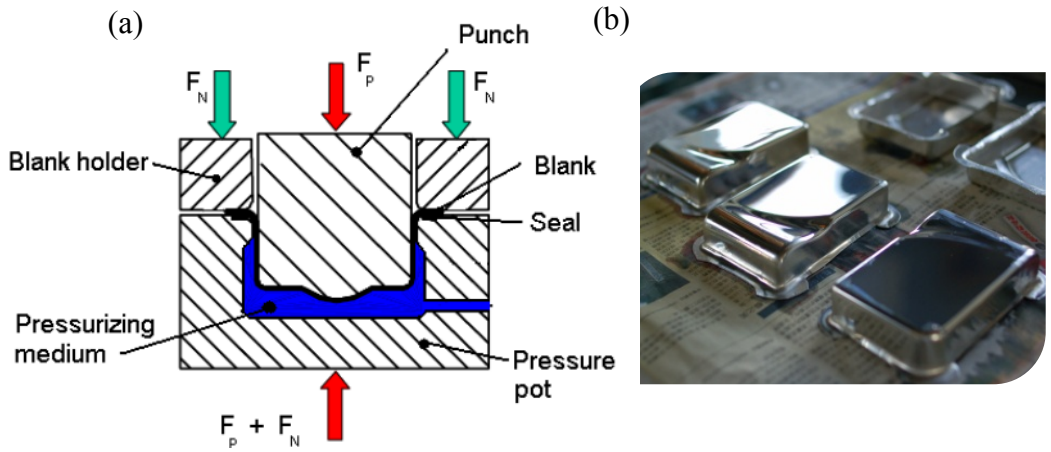


Figure 1.2 (a) Schematic of SHF, (b) Formed sample

## 1.4 Literatures reviews

***Clad metal and rolling process***

Some researchers have presented studies on estimating the bonding performance of clad metal in terms of long holding time, and high diffusing temperature [3,4]. Dyja et al. investigated the deformation zone of a bimetallic cylinder (Cu/Steel、Cu/Al) by a three-dimensional rigid plastic finite element method [5,6]. Mahendran developed diffusion bonding windows for the effective joining of AZ318B magnesium and commercial grade copper alloys [7]. Nowicke considered that the unwanted strain localization of clad metal sheets can be delayed significantly with the use of a small roll radius [8]. There have been some studies on the performance of diffusion bonding, the evolution of textures and the effect of rolling process parameters concerning the production of clad metal sheets at high temperature [9~12].

Over the past decades, many researches have been presented to explain the mechanism of cold roll-bonding [13~15]. Vaidyanath et al. [16] have expressed that the film theory is the major mechanism of cold roll-boning because of the low rolling temperature. It has been found that bonding can be obtained when deformation causes

fresh metal surfaces to be exposed and that the deformation reaches a value sufficiently large to establish contact bonding between two sheets. The fracture of the work-hardened surface (the cleaned surface) and the extrusion of fresh metals through the cracks played very important roles in the real contact between metals. Bay [14] suggested two mechanisms, namely, the fracture of the work-hardened surface and that of the contaminant film of oxides and water. Figure 1.3 [13] shows the simplified illustration of the film theory mechanisms suggested by researcher, namely, the fracture and extrusion of the work-hardened surface.

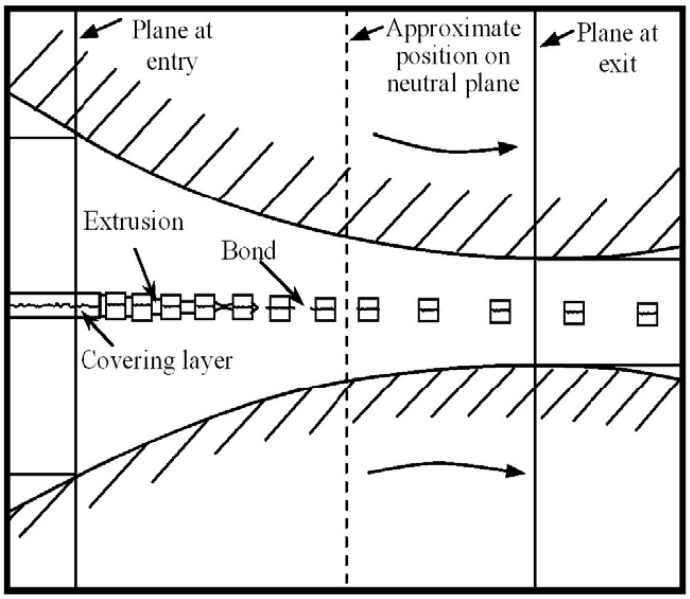


Figure 1.3 Schematic illustration of fracture and extrusion of surface during cold roll-bonding [13]

For rolling parameters, some studies on the parameters controlling bonding have been carried out to understand the complex condition of the bonding mechanisms of clad metals. It has been reported that the roll-bonding of clad metal sheets is affected by various factors, such as material reduction, the temperature of bonding, the amount of pressure, the bonding time, the surface preparation conditions, and the type of post-heat treatment etc.. Generally, the bond performance and mechanical properties of the clad metal sheets are controlled by both the rolling conditions (such as interface

temperature, relative interface displacement, and normal pressure) and materials, but the parameters combinations of cold roll-bonding have been solely analyzed empirically.

***Forming limit diagram***

In general, most of the research on deep drawing tests has analyzed the formability of a single material during the forming process [17], but there have been few studies done on the formability of clad metal sheets made by cold roll-bonding process.

During the forming process, sheet metals can deform only to a certain level, which is dependent mainly on the combination of the ratio of the major and minor strains before necking occurs. Keeler first introduced the forming limit diagram (FLD) [18]. The FLD is widely applied for predicting the fracture of sheet metals during the deformation process [19,20]. In this research, in order to understand the formability of clad metals with different thickness combinations, the punch-stretching test (forming limit test), the deep drawing test, and associated FEA were carried out.

***FE simulation***

FE simulation has become an established tool for predicting the formability of sheet metals. It has enabled significant reduction in the cost and time for design, and facilitation in improving the quality of products. FE simulation has also been integrated with optimization procedure to efficiently obtain the most suitable process parameters for many forming process including SHF and cold rolling.

Kim et al. compared an implicit and an explicit FE method for the hydroforming simulation of an automobile lower arm. The influences of time scaling and mass scaling were investigated [21]. Shim et al. and Pegeda et al. introduced optimization

based method to estimate the initial blank shape through FE simulations [22,23]. Lang et al. presented an optimization of the blank shape and studied the effect of the pressure in the die cavity on the formed parts by using a typical aluminum alloy for aircraft manufacturing [24]. Several researchers have attempted to design the blank geometry using the FE analysis of the forming process.

***SHF process***

Kim et al. and Chen et al. proposed a multi-stage SHF, which have increased the formability of structural parts with complex shape [25,26]. Palumbo et al. and Zhang et al. adopted a moveable inferior plate to enhance the SHF [27,28]. Thiruvarudchelvan et al. provides a technique that uses a hydraulic pressure to apply peripheral push on the flange, which apply counter pressure in the die cavity to provide excellent lubrication at the die radius [29]. Kleiner et al. provides an investigation on the residual stresses induced in HBU-formed workpieces by numerical and experimental. The results show that a higher fluid pressure leads to significantly lower residual stresses in addition to an improved accuracy of form and dimensions [30]. Dankert et al. provides the modified hydromechanical deep drawing process and experimental results obtained are compared to results obtained using FEM. The modified hydromechnical deep drawing process has been investigated experimentally and the experiments show that the concept works in practice; cylindrical cups made from aluminium have been draw successfully with a drawing ratio as high as 3.0 [31].

## 1.5 Motivation

From literature review, deformation (normal pressure) and temperature of clad metal sheets are two significant factors for bonding. However, short bonding time,

thin specimen, and experimental error make it difficult to measure real interface temperature and pressure distributions of the clad metal sheets in the bonding process. Therefore, this research will focus on analyzing the numerically effects of pressure and temperature of the clad metal sheets during bonding processing. In the finite element simulation, the heat generated by friction, material plastic deformation, different roller speed/gap, and material reductions were all considered.

In this research, the clad metals were made through cold roll-bonding process. Because the clad metals are produced at low temperature, the residual stresses generated in the rolling process cannot be released by the conventional annealing process. Therefore, the effect of secondary formability on the application of the clad metal sheet is significant.

Conventionally, in product design, the process parameters often depend on engineer's experience; it is difficult to estimating using trial and error, especially for complex part. However, increase in the complexity of the parts and emphasis to use clad metals with low formability requires the use of FEA to better control material flow.

Due to limited application of SHF, it is still a relatively new forming process. There is limited experience-based knowledge of process parameters for SHF. For wide application of SHF, a design methodology to provide robust process needs to be developed. Thus, there is a need for a fundamental understanding of the influence of process and tool design variables on part quality in the SHF.

### 1.6 Organization of dissertation

To achieve the research objectives, the research approach was divided into four major tasks as follows:

Task 1 : Development of a methodology to estimate the heat flux vector with plastic

work and friction of clad metal during rolling process using DEFORM.

Task 2 : Estimate the flow stress and anisotropy of the clad metal sheets. (Al/Cu, and Ti/Al)

Task 3 : The possibility of applying forming limit diagrams to the formability and fracture prediction of clad metal sheets is examined. The forming limits of clad metal sheets with different thickness combinations are investigated via forming limits test.

Task 4 : Development of a methodology to analyze the suitable process parameters that will result in a rectangular pan formed and complex parts using ABAQUS.

This research has 6 chapters. The contents of each chapter are as follows:

Chapter 1 Brief introduction to clad metal, cold roll-bonding, SHF, and use of FE simulation in sheet metal forming is discussed. The motivation behind the research is explained.

Chapter 2 Chapter 2 is devoted to task 1 of this study, estimate the heat flux vector with plastic work and friction was applied to estimate the temperature and pressure distribution of clad metal bonded by cold rolling process.

Chapter 3 In chapter 3, the true stress-strain curves of Al/Cu clad metal sheets (the thicknesses are 1.2 mm and 1.5 mm) are obtained through tensile tests. Using the experimental forming limit diagrams and the stress-strain curves, the fracture prediction of clad metal sheets are simulated by FEA. Moreover, deep drawing tests are carried out to compare the experimental with the numerical results. Finally, significant differences in formability are found, and comparisons of the fracture prediction of clad metals with

different initial thickness ratios are analyzed both numerically and experimentally.

Chapter 4 In chapter 4, the material property of Ti/Al clad metal (the thickness is 0.45 mm) were tested. The flow stress and anisotropy of clad metal were used in SHF simulation. And development of a virtual film was applied to estimate effect of process parameters for rectangular pan formed by SHF. The results from simulation and experimental validation are presented in this chapter.

Chapter 5 In chapter 5, the Ti/Al clad metal (the thickness is 0.9 mm) with complex shape were formed by SHF. Through finite element simulations, several significant process parameters such as tooling geometry, single-stage (with pre-bulging effect) and multi-stages SHF were analyzed for improving formability of the Ti / Al clad metal housing during SHF.

Chapter 6 Final chapter provides the summary and conclusion of the findings and future works for this study.

# CHAPTER 2 COLD ROLL-BONDING

In this chapter, the progress of deformations in various layers of the clad metal was simulated with commercial FEM package DEFORM-2D. In addition, the temperature distribution and heat flux vector with plastic work and friction were also determined. In DEFORM-2D, the metal sheets were assumed to be rigid-plastic during forming, which will reduce computation time.

The simulation results of temperature of the clad metal sheets in the various layers were applied to estimate the effect of parameter for improving bonding performance of clad metal sheets.

## 2.1 Material diffusion mechanisms

Many reactions and processes that are important in the treatment of materials rely on the transfer of mass either within a specific solid or from a liquid, a gas, or another solid phase. This is necessarily accomplished by diffusion, the phenomenon of material transport by atomic motion. The phenomenon of diffusion may be demonstrated with the use of a diffusion couple, which is formed by joining bars of two faces; this is illustrated for copper and aluminum in Figure 2.1, which includes schematic representations of atom positions and composition across the interface. [32]

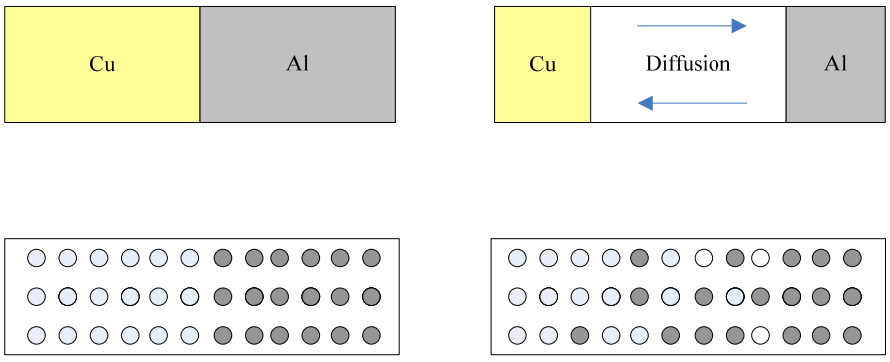


Figure 2.1 Material diffusion mechanisms

From an atomic perspective, diffusion is just the stepwise migration of atom from lattice site to lattice site. In fact, the atom to make such a move, two conditions must be met: (1) there must be an empty adjacent site, and (2) the atom must have sufficient energy to break bonds with its neighbor atoms and then cause some lattice distortion during the displacement. At a specific temperature some small fraction of the total number of atoms is capable of diffusion motion, by virtue of the magnitudes of their vibration energies. This fraction increases with rising temperature.

For rolling process of clad metal, the atoms of material must have sufficient energies that are temperature and pressure. Heat is generated during a metal forming process (friction and plastic heat), and if dies are at a considerably lower temperature than the workpiece, the heat loss by conduction to the dies and by radiation and convection to the environment can result in severe temperature gradients within the workpiece. Thus, the consideration of temperature effects in the analysis of metal forming problems is very important. The temperature distribution and the heat transfer equations were proposed for a coupled thermo-viscoplasitc deformation problem by Kobayashi et al. [33]. The heat flux vector Q has several components and is expressed with the interpolation function N by

$$\mathbf{Q} = \underbrace{\int_V \kappa(\bar{\sigma}\dot{\bar{\varepsilon}})\mathbf{N}dV}_{1} + \underbrace{\int_{S_r} \sigma\varepsilon(T_e^4 - T_s^4)\mathbf{N}dS}_{2} + \underbrace{\int_{S_t} h(T_e - T_s)\mathbf{N}dS}_{3} + \underbrace{\int_{S_c} h_{\text{lub}}(T_d - T_w)\mathbf{N}dS}_{4} + \underbrace{\int_{S_c} q_f \mathbf{N}dS}_{5} \tag{1}$$

1. First term on the right is the heat, generated by plastic deformation inside the deforming body.

   $\bar{\sigma}\dot{\bar{\varepsilon}}$ plastic work, $\kappa$ heat generation efficiency (0.9)

2. Second term defines the contribution of the heat radiated from the environment to the element.

$\sigma$ is the Stefan-boltzman constant, $\varepsilon$ is the emissivity

3. Third term describes the heat convected from the body surface to the environment with heat convection coefficient $h$.
4. Fourth term represents the contribution of the heat transferred from the workpiece the die through their interface.
5. Last term is the contribution of the heat generated by friction along the die-workpiece interface, $q_f$ being the surface heat generation rate due to friction. $q_f = f_s|u_s|$ $f_s$ is the friction stress, and $|u_s|$ the relative velocity between die and workpiece.

During rolling process, the temperature of material will directly influence the bonding performance of clad metal. Therefore, in simulation, if the terms of plastic and friction heat were applied in FE model, the temperature distributions can be used to realistically analyze the effect of rolling parameter for bonding performance of clad metal.

Most practical diffusion situations are nonsteady-state ones. That is, the diffusion flux and the concentration gradient at some particular point in a solid vary with time, with a net accumulation or depletion of the diffusing species resulting.

The magnitude of the diffusion coefficient $D$ is indicative of the rate at which atoms diffuse. Temperature has a most profound influence on the coefficients and diffusion rates. The temperature dependence of diffusion coefficients is related to temperature according to

$$D = D_0 \exp(-\frac{Q_d}{RT}) \tag{2}$$

$D_0$ =a temperature-independent preexponential ( $m^2/s$ )

$Q_d$ =activation energy ($J/mol$)

$R$ =the gas constant

$T$ =absolute temperature (K)

The activation energy may be thought of as that energy required producing the diffusive motion of one mole of atoms. Large activation energy results in a relatively small diffusion coefficient.

Table 2.1 Diffusion coefficient of the material [32]

| **Diffusing species** | **Host metal** | $D_0$ ($m^2/s$) | $Q_d$ | $D$ |
|---|---|---|---|---|
| Cu | Al | $6.5\times10^{-5}$ | 136 $kJ/mol$ 1.41$eV/atom$ | $4.1\times10^{-14}$ |

$R=8.31J/mol-K$, $1.987cal/mol-K$ $or 8.62\times10^{-5}eV/atom-K$

When diffusion condition at same depth x and material composition, the two different diffusion coefficients with corresponding temperatures were be obtained.

$D\cdot t=$ constant

$$D_{T_1}t_{T_1}=D_{T2}t_{T2} \tag{3}$$

According to above equation, the magnitudes of the diffusion coefficient with corresponding times $D\cdot t$ were be obtained, then, the total magnitude of the diffusion coefficient $D_{tol}$ during specific time history were be determined by integral.

$$D_{tol}=\int D_1\cdot t_1 dt=\int D_2\cdot t_2 dt \tag{4}$$

**2.2 FE simulation**

The real rolling process has many extrinsic variations that will affect the results of forming. In simulation case, some assumptions and effects were applied for simplification. The workpiece was assumed to be isotropic, and homogenous.

- The mass effect of roller was neglected.
- The deformation of roller was neglected.
- The bonding condition was neglected. (focus on temperature distribution of workpiece)
- The interface friction coefficient was assumed to be constant. Friction at all contact surfaces were treated with constant shear friction law.

**FE model**

The rolling process of Al and Cu metal sheets was first modeled and rigid-plastic code was selected. The workpieces and rollers were meshed with quadrilateral plane strain elements while the pusher plate was considered to be rigid bodies. The heat transferred was estimated between workpiece and die. A finite element model was constructed as shown in Figure 2.2.

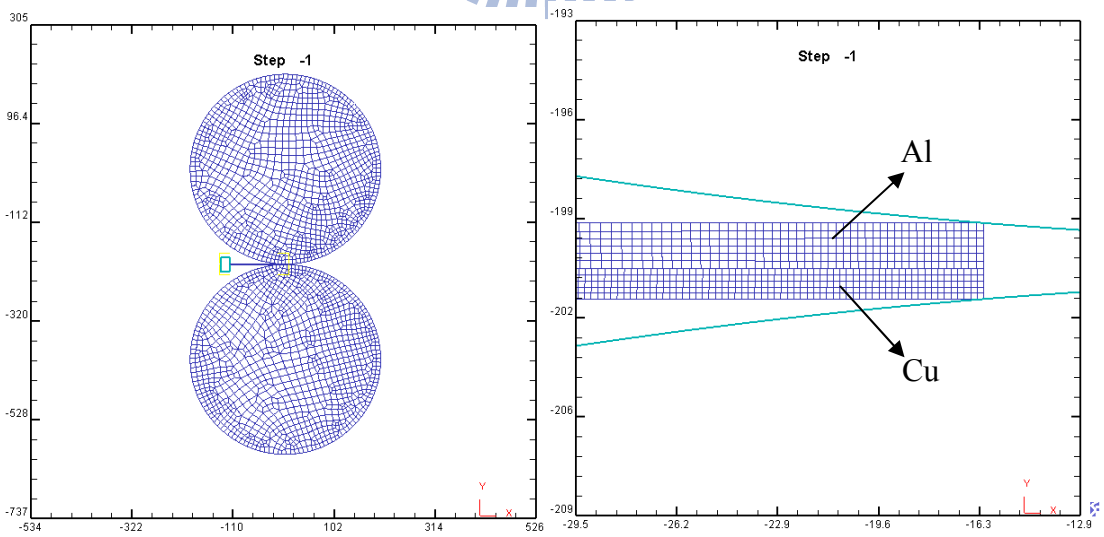


Figure 2.2 FE model of rolling

**Material properties**

Table 2.2 shows the material properties of A1050 and C1100 used in this

research.

Table 2.2 Material properties of A1050 and C1100

| Material | c | n | y (yield stress) MPa |
|---|---|---|---|
| A1050 | 30.38 | 0.36 | 103.1 |
| C1100 | 296.72 | 0.78 | 261.5 |

$$\overline{\sigma} = c\varepsilon^{n}\dot{\varepsilon}^{m} + y$$

**Boundary conditions**

The rotational speed and roller gap have significant influences on bonding performance of clad metal. Table 2.3 shows the list of parameter combinations, with which simulation results were be compared.

The pusher plate was specified to push workpieces into the gap. Figure 2.3 (a) illustrated the relationship of each parts. Figure 2.3 (b) is the movement control curve for pusher plate.

Table 2.3 Parameter combinations for rolling process

| No. | Al<br>Initial thickness | Cu<br>Initial thickness | Roller speed<br>Top/Lower(rpm) | Gap<br>(mm) |
|---|---|---|---|---|
| **1** | | | 0.8/0.8 | |
| **2** | | | 0.5/0.5 | |
| **3** | 1.5mm | 1.0mm | 1/1 | 1.2 mm |
| **4** | | | 2/2 | |
| **5** | | | 1.0/0.5 | |
| **6** | | | 1.5/1 | |
| **7** | | | 0.8/0.8 | |
| **8** | | | 0.5/0.5 | |
| **9** | 1.5mm | 1.0mm | 1/1 | 1.5 mm |
| **10** | | | 2/2 | |
| **11** | | | 1.0/0.5 | |
| **12** | | | 1.5/1 | |

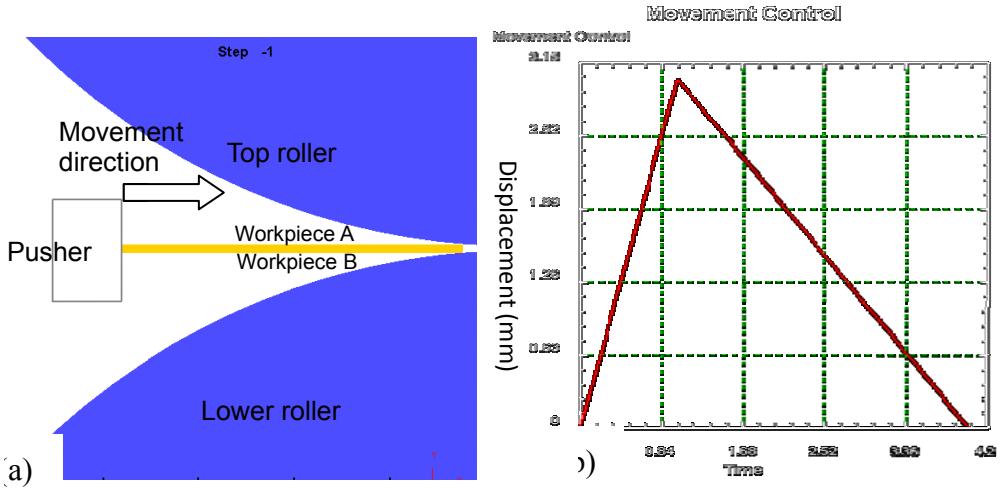


Figure 2.3 (a) The schematic of relationship of each parts, (b) Movement control curve of pusher

**Contact and friction model**

In this research, three contact pairs (top roller-Al, Al-Cu, and Cu-lower roller) were defined in this study. The constant shear friction factor was treated for all of contact surfaces. Recently, many friction tests were presented, which were discuss the friction effect with different lubricant conditions between die and workpiece.

Chang compared the extension rates of different region of clad metal sheet during roll bonding process by experiment and FE simulation. The Coulomb friction coefficients 0.2 and 0.25 were determined between roller-workpiece, and Al-Cu materials respectively [34]. Because, the friction model was shear friction factor law in DEFORM, in this research, the relationships of Coulomb friction coefficient and shear friction factor were compared by ABAQUS. Therefore, the test of ring compression was simulated; the internal diameter changing and load-displacement with different friction condition were observed.

Figure 2.4 shows the FE model of ring compression for ring geometry 6: 3: 2 (external diameter: internal diameter: height). The workpiece was meshed with

axisymmetric element. The top and lower dies were assumed to rigid body.

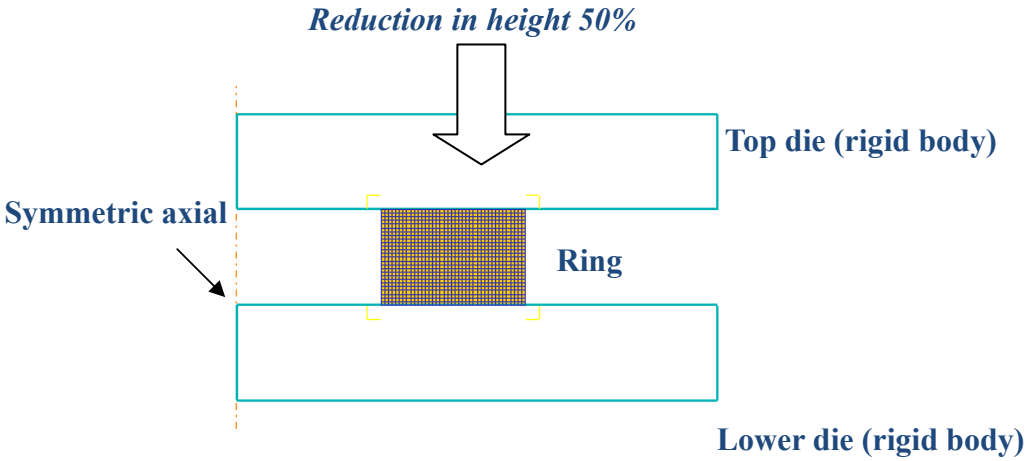


Figure 2.4 The FE model of ring compression

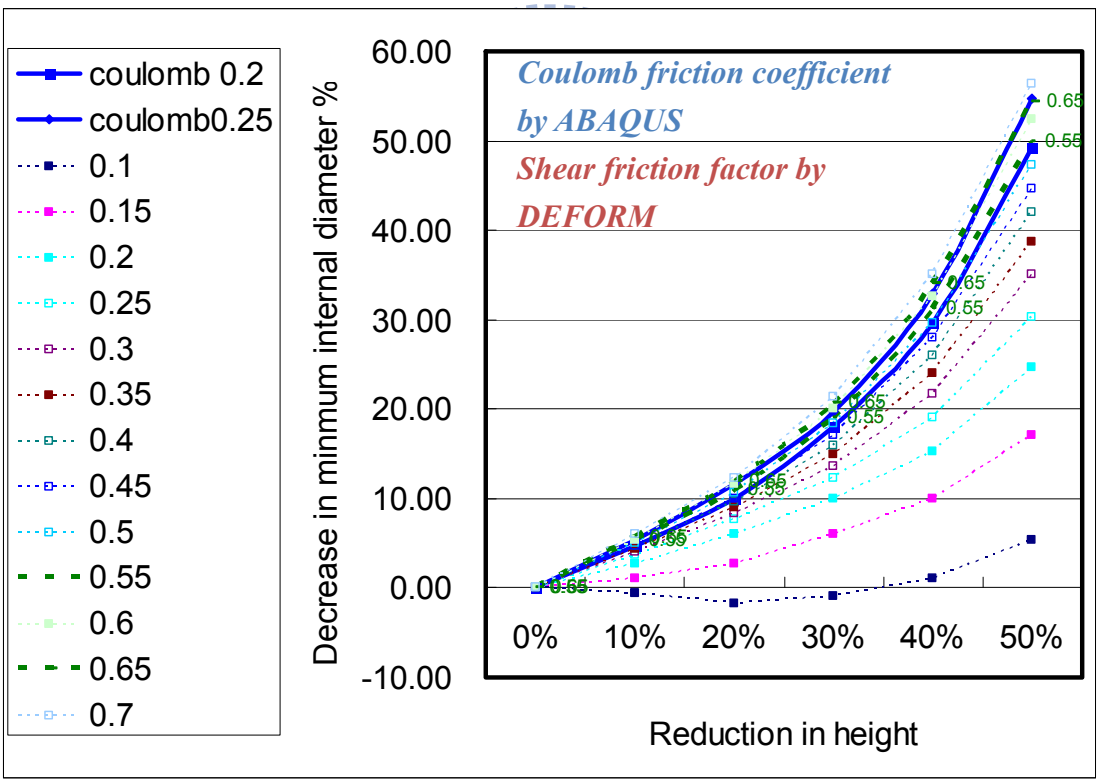


Figure 2.5 The comparisons of decrease in minimum internal diameter with different friction conditions（Material : A1050）


Figure 2.6 The comparisons of decrease in minimum internal diameter with different friction conditions（Material：C1100）

From the comparisons of Figure 2.5~6, the friction factor 0.55, and 0.65 with corresponding friction coefficient 0.2, 0.25 between roller-workpiece and Al-Cu were obtained.

## 2.3 Simulation results with different parameter combinations

### Maximum temperature

Figure 2.7 shows the simulation results of temperature distribution with case No. 1~6 of Table 2.3. Figure 2.8 shows the simulation results of temperature distribution with case No. 7~12 of Table 2.3.

Case 1. rpm=0.8/0.8, Bonding history=1.3 sec, Max. temperature=60.6°C at Cu

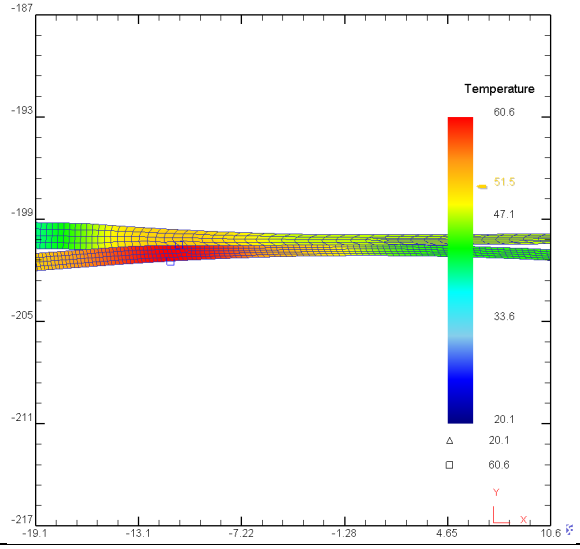


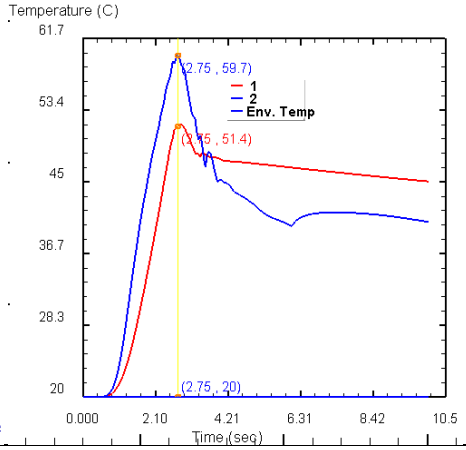


Case 2. rpm=0.5/0.5, Bonding history =2 sec, Max. temperature=49.2°C at Cu

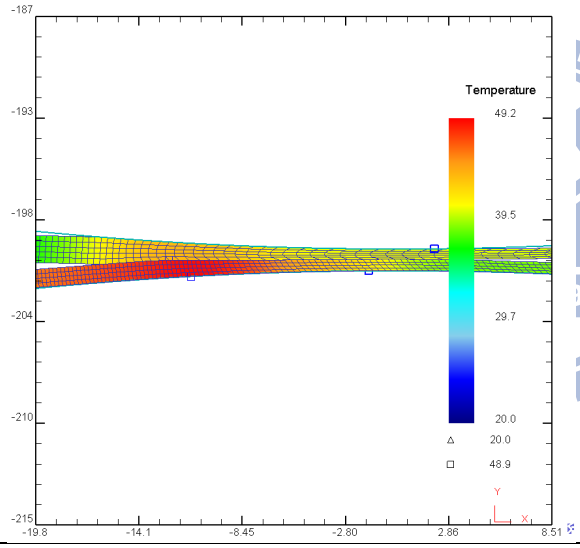


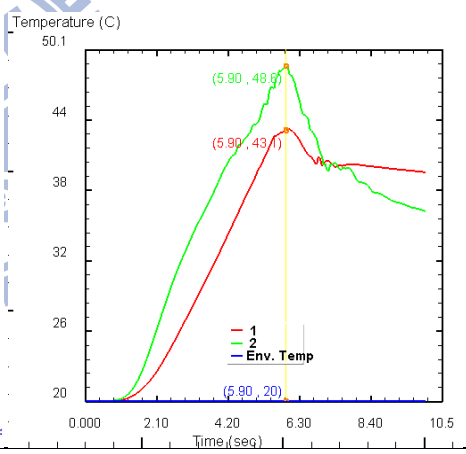


Case 3. rpm=1.0/1.0, Bonding history =1 sec, Max. temperature=73.6°C at Cu

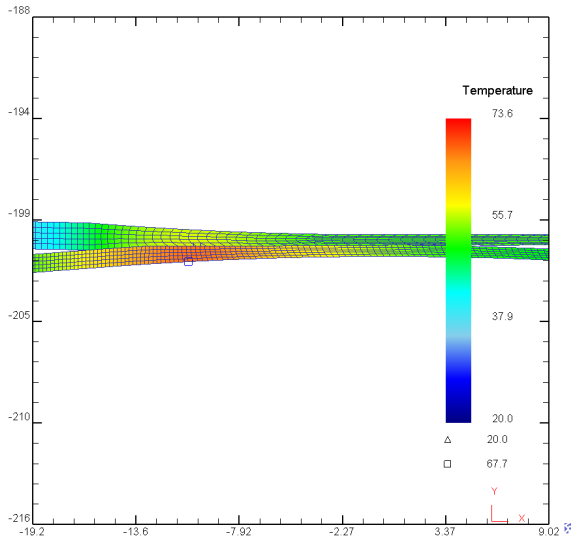


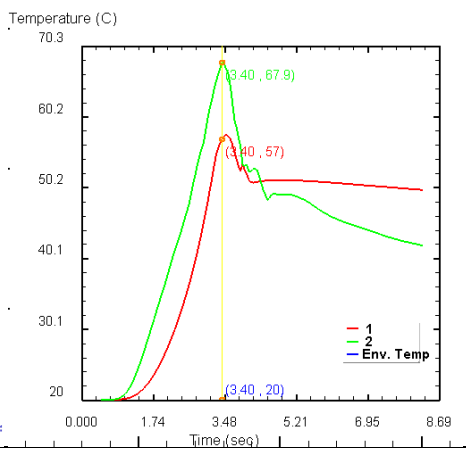

Case 4. rpm=2.0/2.0, Bonding history =0.5 sec, Max. temperature=117°C at Cu

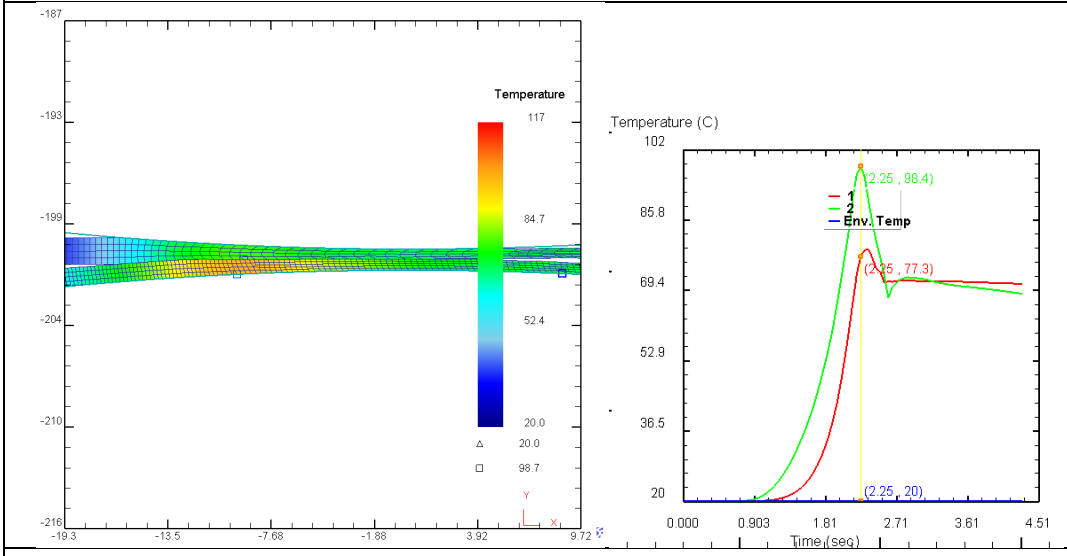


Case 5. rpm=1.0/0.5, Bonding history =1.8 sec, Max. temperature=68.8°C at Al

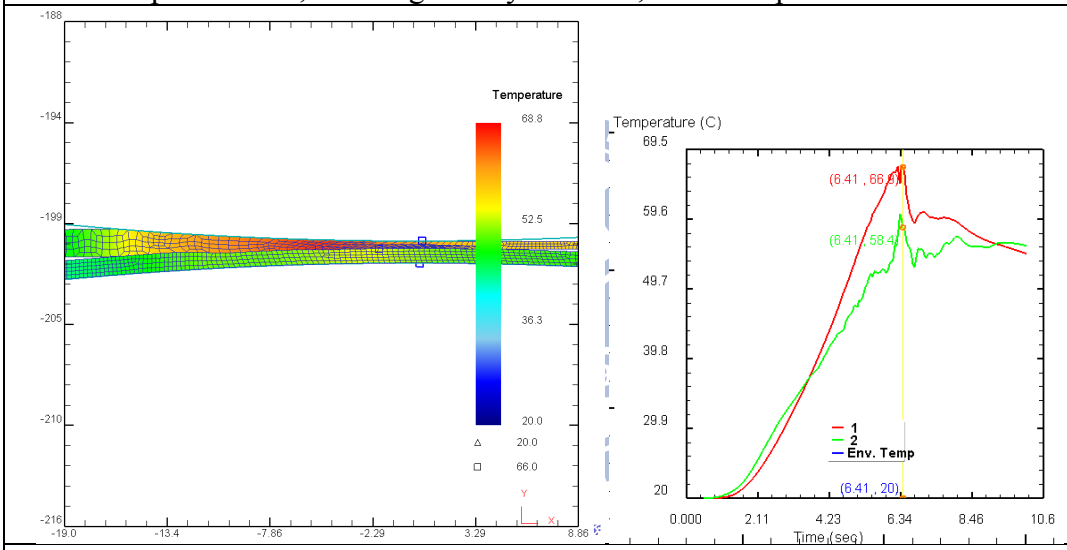


Case 6. rpm=1.5/1.0, Bonding history =1 sec, Max. temperature=77.1°C at Al

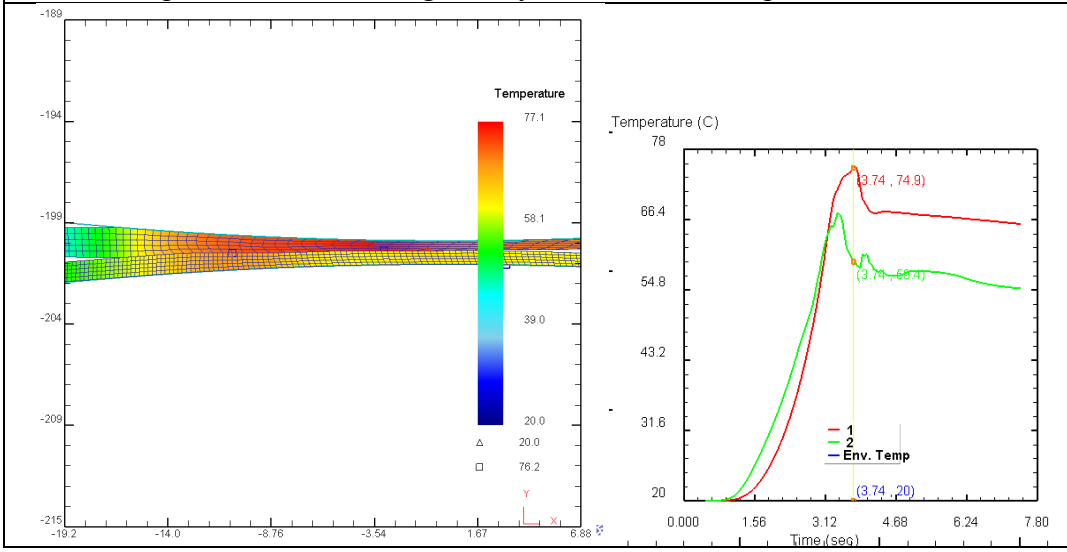


Figure 2.7 Simulation results with different rotational speeds（case 1~6, gap=1.2mm）

Case 7. rpm=0.8/0.8, Bonding history =1.3 sec, Max. temperature=49.6°C at Cu

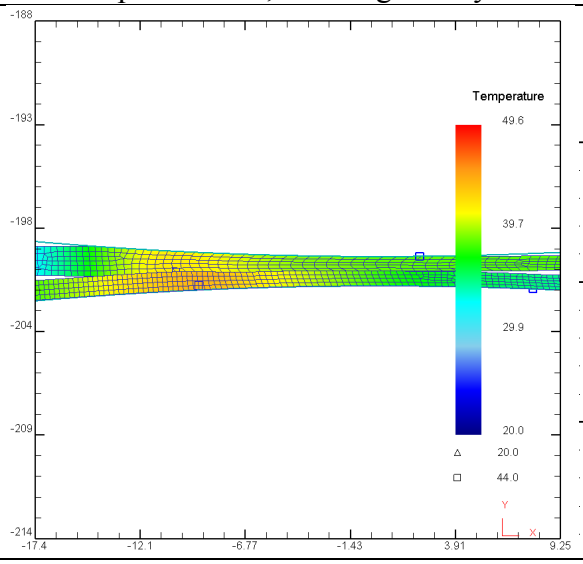


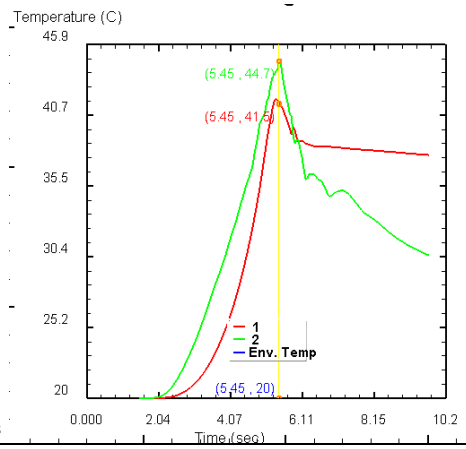


Case 8. rpm=0.5/0.5, Bonding history =1.8 sec, Max. temperature=39.1°C at Cu

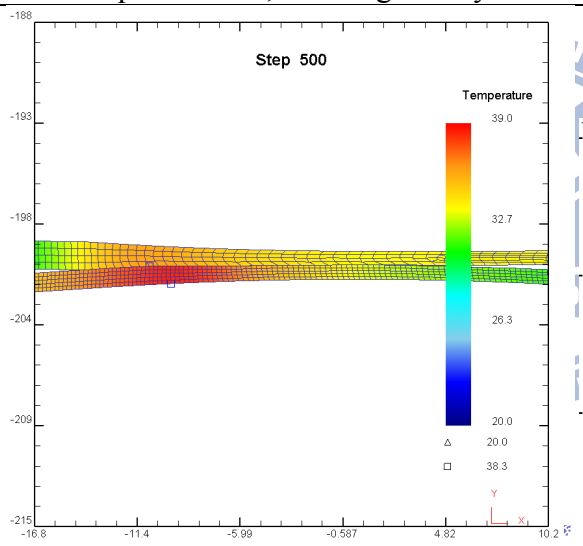


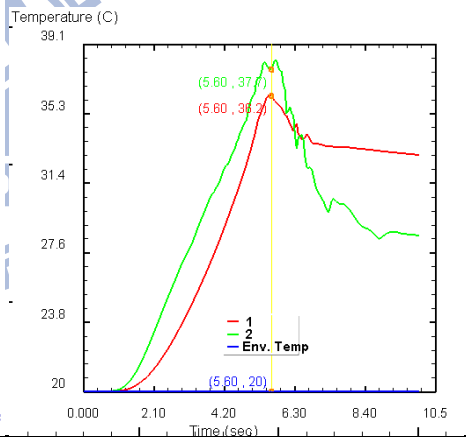


Case 9. rpm=1.0/1.0, Bonding history =0.8 sec, Max. temperature=51.6°C at Cu

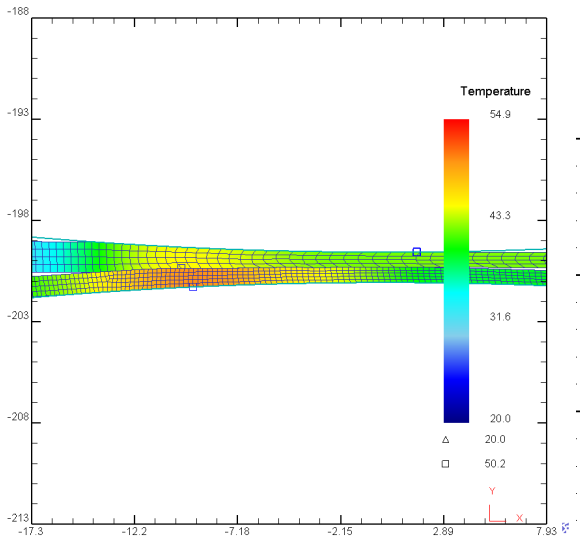


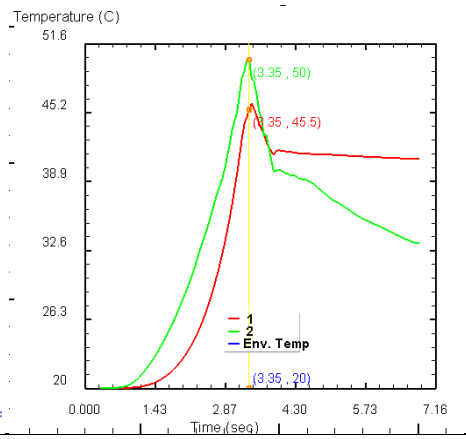

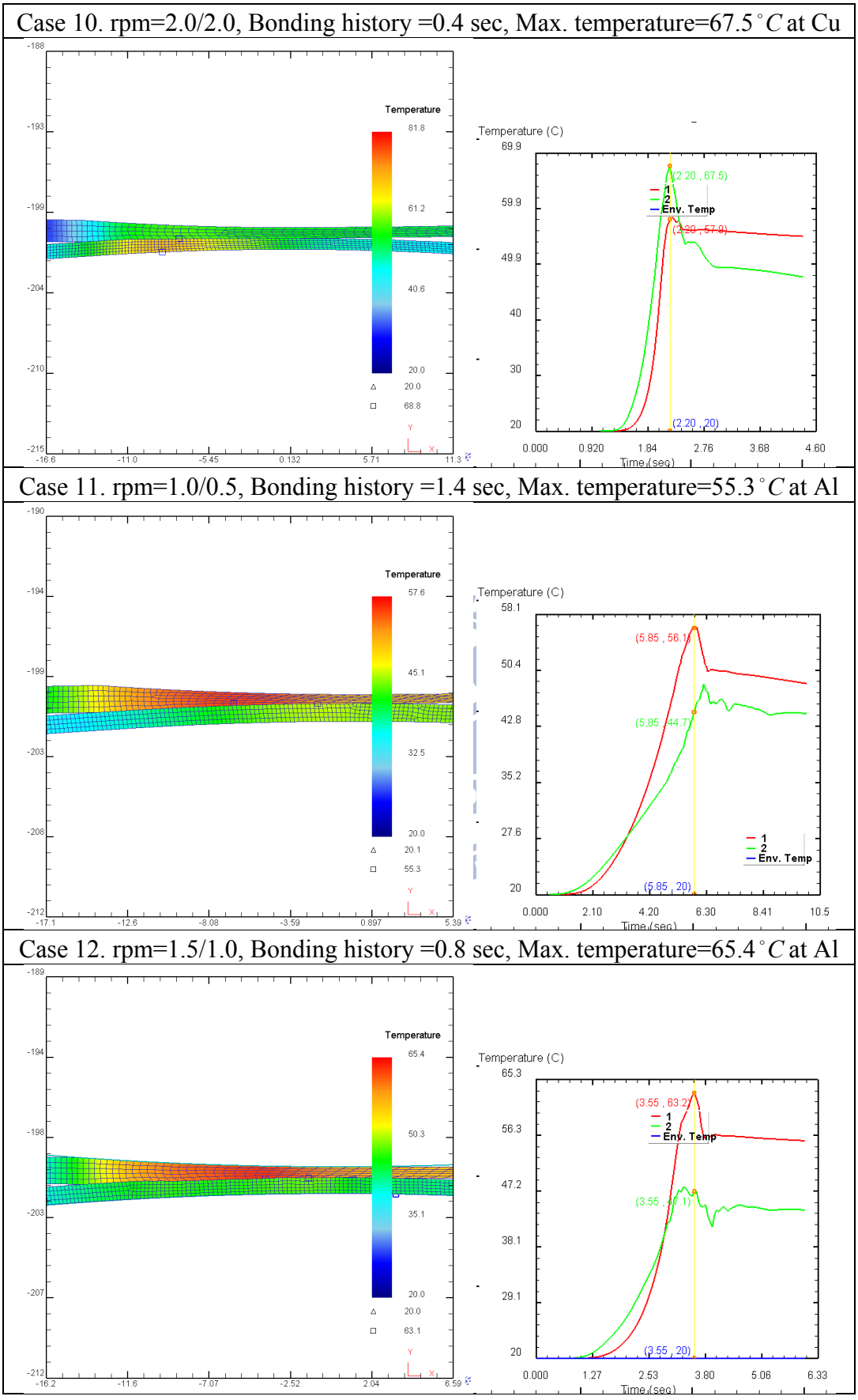


Figure 2.8 Simulation results with different rotational speeds（case 7~12, gap=1.5mm）

In cases of symmetric rotational speed (case No. 1~4, and 7~10), temperatures of lower material (Cu) were high than upper material (Al). When rotational speed increasing, the temperatures of material were increased. From simulation results, increasing rotational speed during rolling process can increase frictional heat that was effective for bonding performance.

In cases of asymmetric rotation speed (case No.5~6, and 11~12), the temperatures of material are higher than those of symmetric cases (case 3, and 9). It might result from the relative displacement which causes more friction heat between layers of material. The compared cases of roller gap 1.2mm and 1.5mm show that larger rolling gap resulted in smaller plastic deformation and thus lower temperature (10~20$^{\circ}C$ lower).

From the comparisons of case No.4 with 10, the difference of temperature was found to be about 50$^{\circ}C$ (maximum temperature was 117$^{\circ}C$, 67.5$^{\circ}C$, respectively).

**Pressure distribution**

In this research, before roll bonding process, the surfaces of material have been cleaned to remove oxides and to improve bonding performance. For same gap setting (1.2 mm or 1.5 mm), the maximum pressure are similar to press materials together for bonding. Figure 2.9 and 2.10 show the pressure distribution of materials at maximum reducing region with different parameter combinations.

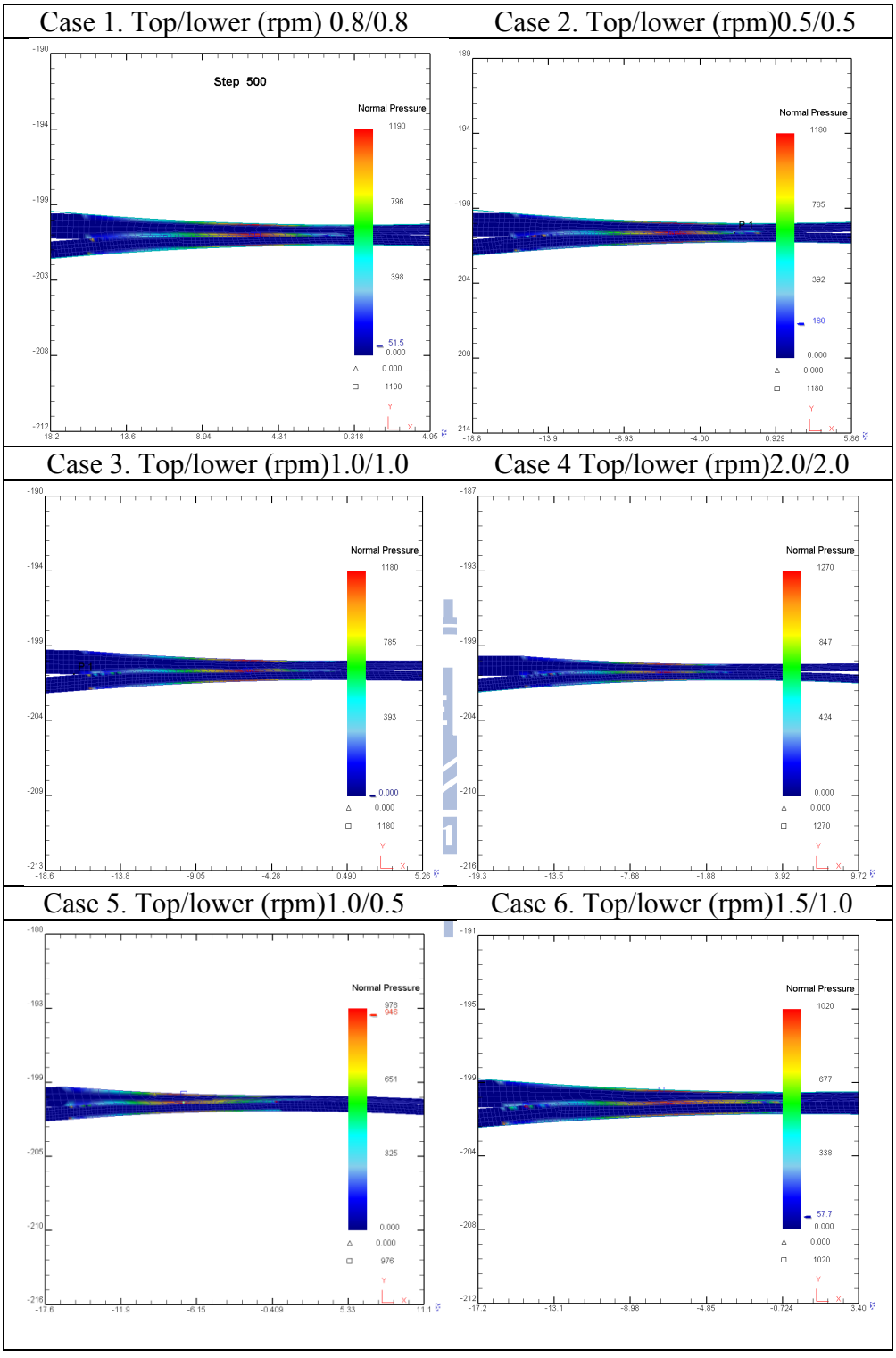


Figure 2.9 Pressure distribution with different rotational speeds（gap=1.2mm）

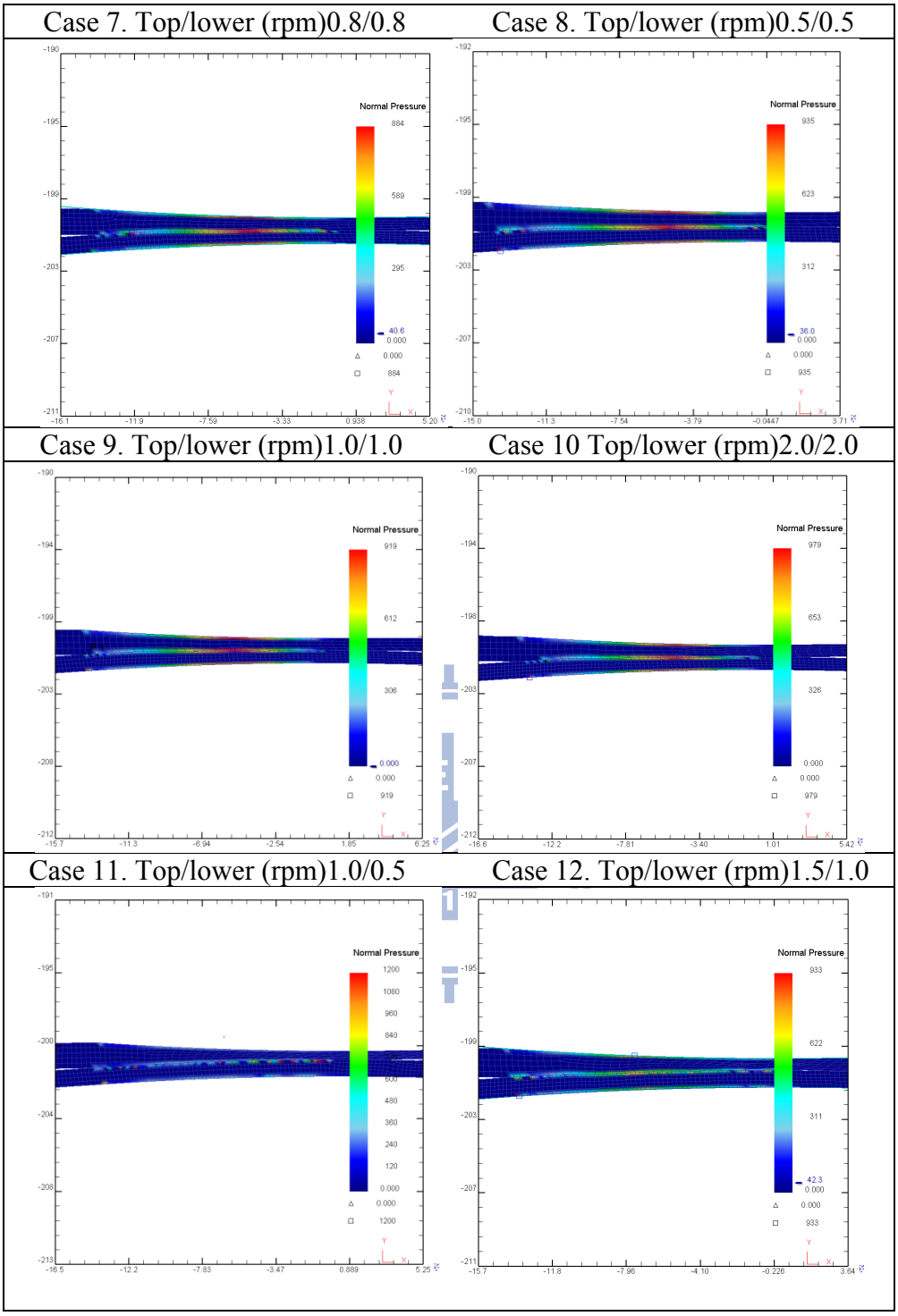


Figure 2.10 Pressure distribution with different rotational speeds（gap=1.5mm）

From above simulation results, the magnitudes of pressure were mostly between 900 to 1200 MPa. From the comparisons of case No.1 with 7, the difference of pressure was found to be about 300MPa (maximum pressures were 1190, and 880 MPa respectively).

According to diffusion equations, the temperature was the most important factor for diffusion process. In DEFORM-2D, large pressure caused higher friction stress along the interface of roller-material and Al-Cu, and therefore influenced the temperature distribution of materials. Therefore higher pressure distribution was positive for raising the bonding energy during cold roll-bonding.

### 2.4 Diffusion coefficient with different combinations

In this section, the magnitudes of diffusion coefficient $D_{tol}$ were estimated according to the diffusion equation in section 2.1 and the results of temperature distribution of materials in section 2.3. Figure 2.11~12 show the comparisons of the magnitude of diffusion coefficient $D_{tol}$ with different parameter combinations.

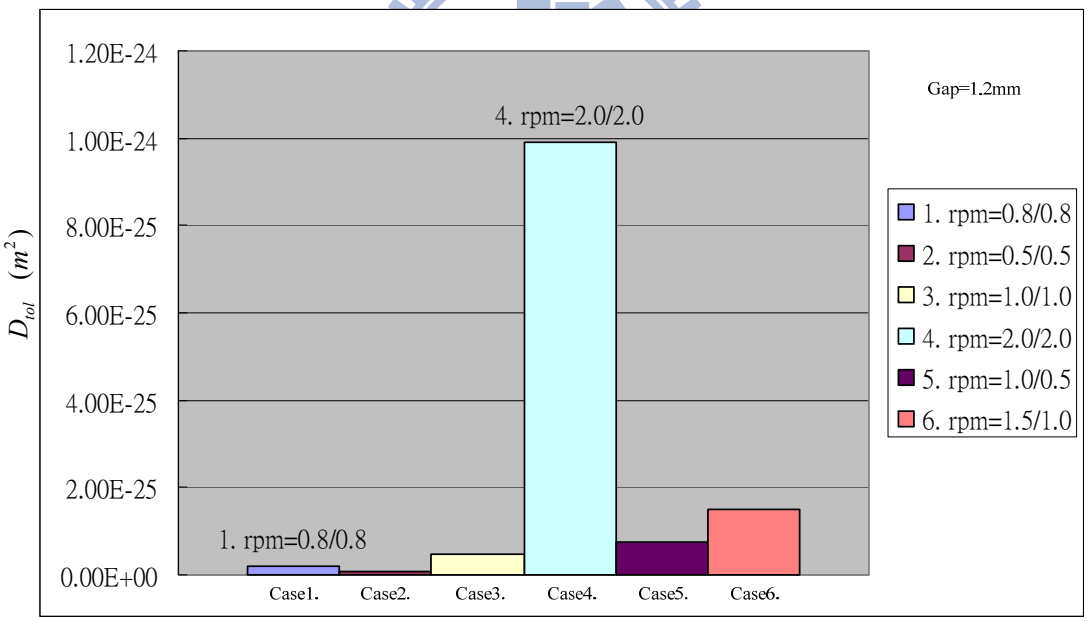


Figure 2.11 The comparison of the magnitude of diffusion coefficient $D_{tol}$ with different rotational speed (gap=1.2mm)

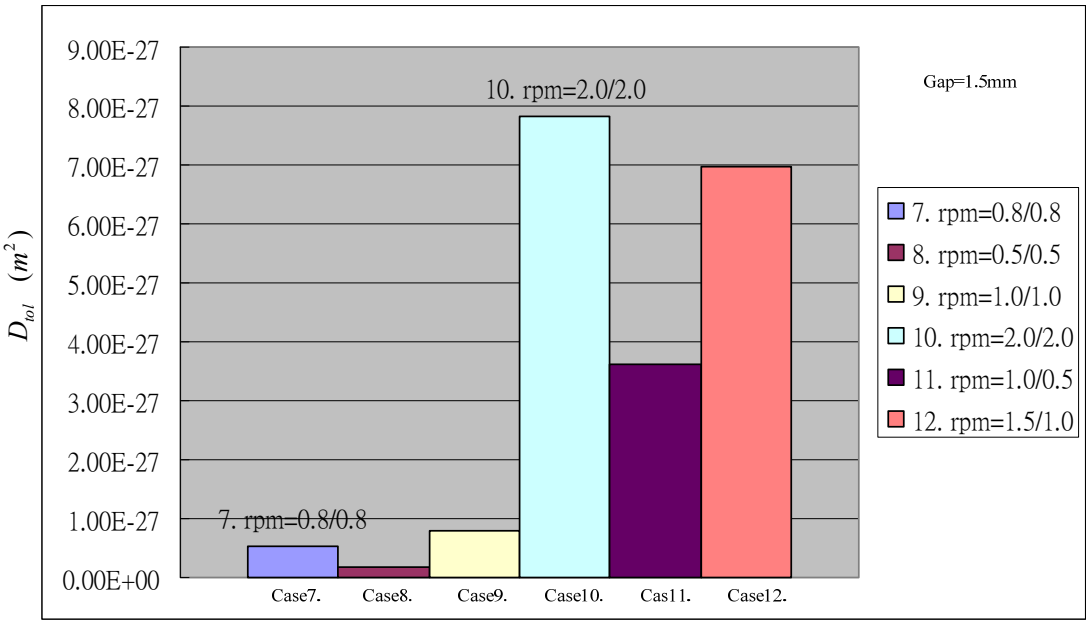


Figure 2.12 The comparison of the magnitude of diffusion coefficient $D_{tol}$ with different rotational speed (gap=1.5mm)

From Figure 2.11, the magnitude of diffusion coefficient $D_{tol}$ of case No. 4 was the highest （4.57e-24 $m^2$ ）according to relative high temperature compared to other cases. Same trend of diffusion coefficient were observed for another roller gap (i.e. 1.5mm).

From preliminary experimental validation, the Al/Cu clad metal sheet was bonded successfully with case No. 1 (Max. temperature=60.6 ° , Max. pressure=1190MPa, $D_{tol}$ = 2.81e-26 $m^2$ ) combination, unsuccessfully with case No. 7 (Max. temperature=49.6 ° , Max. pressure=884MPa, $D_{tol}$ = 5.3e-28 $m^2$ ) combination. Comparisons of the magnitude of diffusion coefficient, maximum temperature, and maximum pressure with other cases indicate that the parameter combinations of case 3~6 (case No. 3 = 49.2° , 1180MPa, 7.7e-26 $m^2$ , case No. 4 =117° , 1270MPa, 4.57e-24 $m^2$ , case No. 5 =68.8° , 976MPa, 2.44e-25 $m^2$ , case No.

6 = 77.1° , 1020MPa, 8.21e-26 $m^2$ ) are possible for good bonding with increasing rotational speed. For case No.10, and 12 (case No. 10 =67.5° , 979MPa, 7.83e-27 $m^2$ , case No. 12 = 65.4° , 933MPa, 6.96e-27 $m^2$ ), the results were closed to case No. 1, which proves that those parameter combinations are also possible for good bonding.

**2.5 Remarks**

In this research, the plastic heat of material and frictional heat were considered during rolling simulation. The temperature and pressure distribution were obtained to realistically analyze the bonding performance for clad metal.

The results show that high reducing rate (gap=1.2mm) were effective for increasing material temperature (caused by plastic heat), which in turns increase the bonding performance of clad metal sheets. In cases of symmetric rotational speed (case No. 1~4, 7~10), the magnitudes of temperature and diffusion coefficient were increased by rising rotational speed. Since case 1 was successfully bonded from experiment. The magnitudes of temperature and diffusion coefficient of case No. 3, 4, and 10, indicated that they were be successfully bonded. In cases of asymmetric rotation speed (case No. 5, 6, and 11, 12), the magnitudes of temperature, pressure distribution, and diffusion coefficient are higher than those of symmetric cases (case No. 3, and 9). It might result from the relative velocity between roller-material and Al-Cu which cause more fresh materials and friction heat to influence the bonding performance.

Although the most significant index to estimate whether the metals can bonded together was not clearly indicated in this analysis, the analysis process and results in this section still provide positive parameter combination for improving bonding performance of clad metal. In future, more experiments (roll-bonding and microscopy) will be carried out to validate numerical result.

# CHAPTER 3 FORMING LIMIT OF THE CLAD METAL

In general, the cold roll-bonding process made clad metal that has many advantages, especially accurate dimension control and straight bonding layers. However, because the clad metals in this research are produced at room temperature, the residual stresses generated in the rolling process cannot be released by the conventional annealing process because the melting temperatures of the individual layer sheets are often different from each other. Therefore, the effect of residual stresses on the secondary formability of the clad metal sheet is significant.

In this section, the specimens of Al/Cu clad metal sheets were obtained through a cold roll-bonding process. Second, the mechanical properties of clad metal sheets with different initial thicknesses were measured by tensile tests. Then, the punch stretching test was carried out to determine the forming limit data of Al/Cu clad metal sheets with different initial thickness ratios. After that, deep drawing tests of clad metal sheets using a square punch were carried out. The deep drawing tests were also simulated with ABAQUS to validate the possibility and accuracy of using FE models. During this verification process, fracture initiations during the deep drawing of the clad metal sheets were carefully inspected.

## 3. 1 Cold rolling process and mechanical property test

### 3.1.1 Experimental procedure for roll-bonding

Specimens of Al/Cu clad metal sheets were prepared in the following manner. The base materials were aluminum sheets with thicknesses of 2.0, 1.5, and 1.0 mm and copper sheets 1.0mm thick. The two-ply clad metal sheets were arranged as illustrated in Fig. 3.1. Before the roll-bonding process, all contact surfaces of the base materials were cleaned to remove impurities such as oxides, grease, and vapor in

order to enhance the bonding performance of the Al/Cu clad metal sheets. The rolls were set to a small roll-gap opening, resulting in a nominal deformation. However, the final thickness of the clad metal sheet was always larger than the initial roll-gap opening, which is attributed to elastic recovery of the blank. Table 3.1 shows the list of thickness combinations of the clad metal sheets. All Al/Cu clad metal sheets were made by the cold rolling process, as shown in Figure 1.1.

Table 3.1 Different thickness combinations of clad metal sheets

| Sample | Initial thickness (mm)A1050 | Initial thickness (mm) C1100 | Final bonded thickness (mm) | Stages of Rolling |
|---|---|---|---|---|
| **1** | 2.0 | 1.0 | 1.3 | 1 |
| **2** | 1.5 | 1.0 | 1.3 | 1 |
| **3** | 1.0 | 1.0 | 1.3 | 1 |
| **4** | 2.0 | 1.0 | 0.97 | 2 |
| **5** | 1.5 | 1.0 | 0.97 | 2 |

### 3.1.2 Tensile test of clad metal sheets

In order to measure the mechanical properties of the Al/Cu clad metal sheets, tensile tests were carried out on a MTS-810 tensile machine. In this research, all specimens of Al/Cu clad metal sheets were produced at room temperature, and thus the residual stresses of two base materials cannot be released by conventional annealing process. After the roll-bonding process, the specimens were very thin, and it was difficult to obtain the flow rule of each of the two materials. Based on the iso-strain deformation behaviors of Al/Cu clad metal sheets, these sheets were considered to be equivalent to a single material in the FE simulation. Therefore, the fracture of Al/Cu clad metal sheets was predicted according to the forming limit data of the equivalent

single material.

Figure 3.1 shows the true stress–strain curves obtained for the Al/Cu clad metal sheets with three different initial thickness combinations (Al 2.0 mm/Cu 1.0 mm, Al 1.5 mm/Cu 1.0 mm, and Al 1.0 mm/Cu 1.0 mm) and two different bonded thicknesses (0.97 mm and 1.3mm). These tensile properties were used in the following FE simulations.

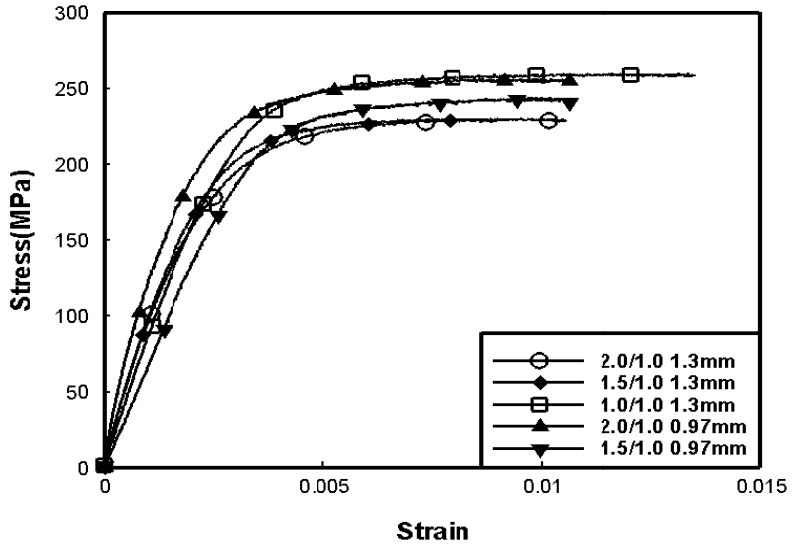


Figure 3.1 True stress–strain curves of the Al/Cu clad metal sheets

### 3.1.3 Punch-stretching test (forming limit test)

The punch-stretching tests were carried out to evaluate the forming limit of the Al/Cu clad metal sheets. In the forming limit diagram, the major and minor strains at a critical site are plotted at the onset of visible, localized necking in a deformed sheet, and the locus of the strain combinations that will produce failures in an actual forming operation can be drawn. The major axes of the ellipses are parallel to the direction of the greater elongation. If the area of the original circle before deformation is less than the area of the ellipse after deformation, the thickness of the sheet has changed at the point because the volume remains constant during deformation. Experimental

methods were used to construct the diagram. First, the clad metal sheets were clamped at their edges and stretched by a 50 mm diameter hemispherical punch, as shown in Figure 3.3. Specimens 100 mm long and of various widths from 10 mm to 100 mm were prepared to cover various stretch modes. Talcum powder was used for lubrication; the blank holding force was set to 160 KN. The aluminum side of the Al/Cu clad metal sheets was in contact with the punch. Before these tests, the surfaces of the copper side of the Al/Cu clad metal sheets were etched with circular meshes so that the major and minor strains could be measured after the stretching test.

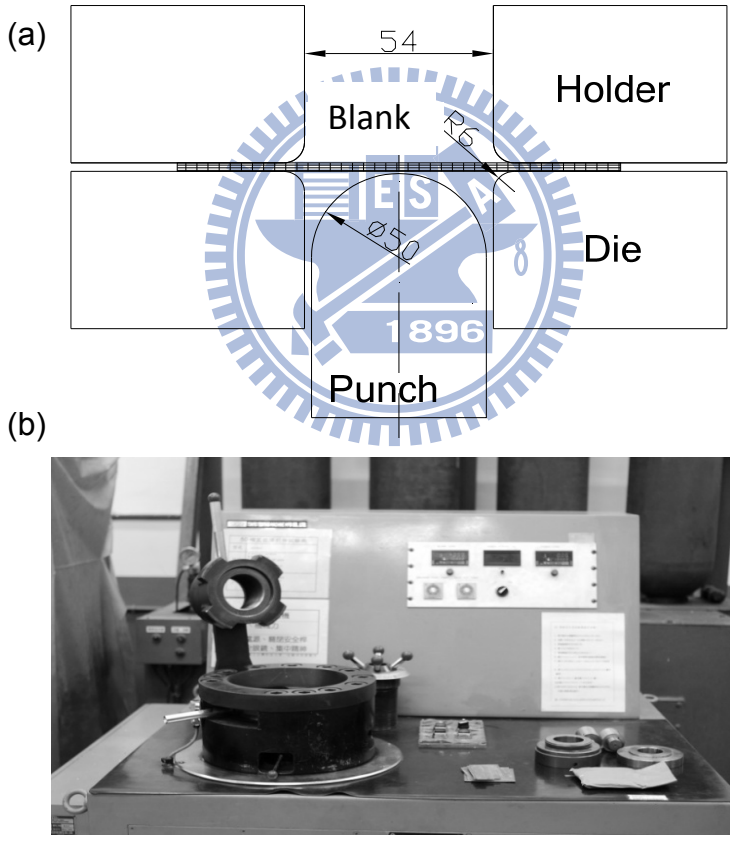


Figure 3.2 (a) Tooling dimension; (b) 50 ton universal material test machine

### 3.1.4 FLD results

*Different initial thickness combinations (Al 2.0 mm, 1.5 mm, and 1.0 mm/ Cu 1.0 mm)*

The fractured conditions of the Al 1.5 mm/Cu 1.0 mm clad metal after the punch stretching test are shown in Figure 3.3(a). The FLDs of different thickness ratios are shown in Figure 3.3(b). The trend of the forming limit curve of Al 2.0 mm/Cu 1.0 mm is obviously higher than those in other cases and thus indicates better formability during the forming test. On the other hand, the clad metal sheet of Al 1.0mm/Cu 1.0 mm has a lower ductility limit. According to this result, the initial thickness ratio (related to the reduction rate because the final thickness is the same) influences the trend of the FLDs of the clad metal sheets; this is due to the work-hardening effects during the roll-bonding process. Therefore, the higher reduction rate of the material is significant factor for raising the forming limit of the clad metal sheets in the secondary forming process.

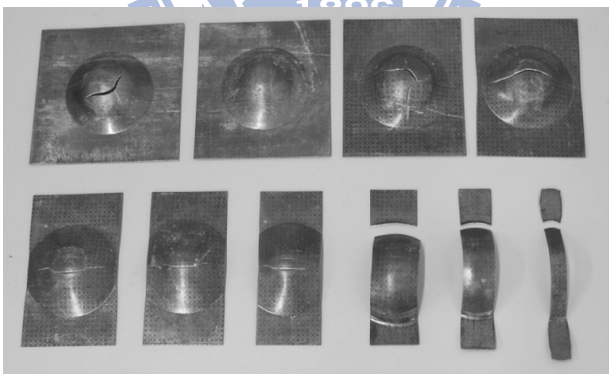

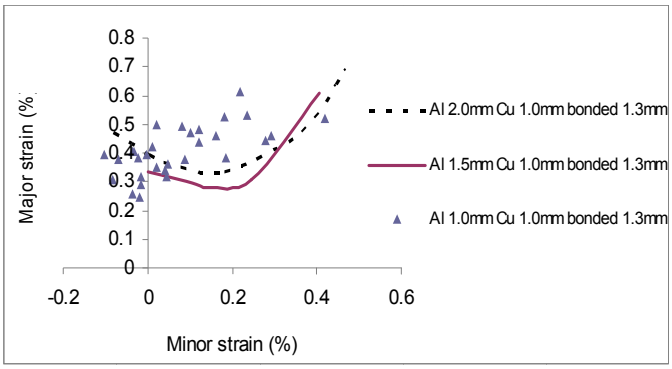


Figure 3.3 FLDs of the Al/Cu clad metal sheets for different initial thickness ratios

*Single metal sheet (Al 1.5 mm and Cu 1.0 mm)*

The comparison of the formability between the clad metal sheets and single metal sheets (Al 1.5 mm and Cu 1.0 mm) is shown in Figure 3.4. The fracture points of the single metal sheets are mostly located above the forming limit curves of the clad metal sheets, revealing the better formability of the single metal sheets than the clad metal sheets.

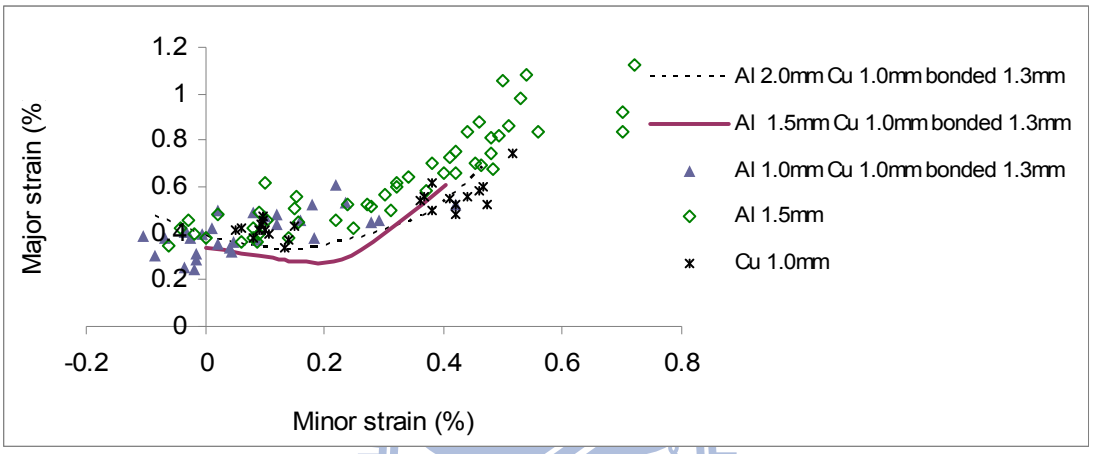


Figure 3.4 FLDs of the clad metal sheet and single metal sheet

## 3.2 Deep drawing tests

Deep drawing tests were carried out on the Al/Cu clad metal sheets with a 50 ton universal material test machine to evaluate the drawing depth and fracture conditions directly. A square punch with an associated die set was used for the deep drawing test, as shown in Figure 3.5. By changing the blank holding force and the blank dimensions, the drawing depth of the blank can be measured. In order to compare the forming variation for different bonded thicknesses, the clad metal sheets were rolled to 0.97 mm and 1.3 mm in thickness. Circular specimens with various diameters (70, 80, and 90 mm) were used. To reduce the effect of friction of the punch, talcum powder was also used between the punch and the blank. The blank holding force was set to 5, 10, 15, 20, and 50 kN, respectively. The same as above punch-stretching tests,

the aluminum side of clad metal was considered to be the contact surface. Table 3.2 lists the fracture conditions for the different combinations. Compared the experimental results of 80mm specimen with those of the 90mm specimen, the fracture mostly occurs near the punch corners at the early stage of deep drawing. The experimental result for Al 1.0/Cu 1.0 mm (bonded thickness 1.3 mm) points out that reducing the blank dimensions is helpful for forming with a low ductility limit when the holding force is fixed. In the next section, the fracture prediction of these experimental results is validated, using previous forming limit data in FE simulations.

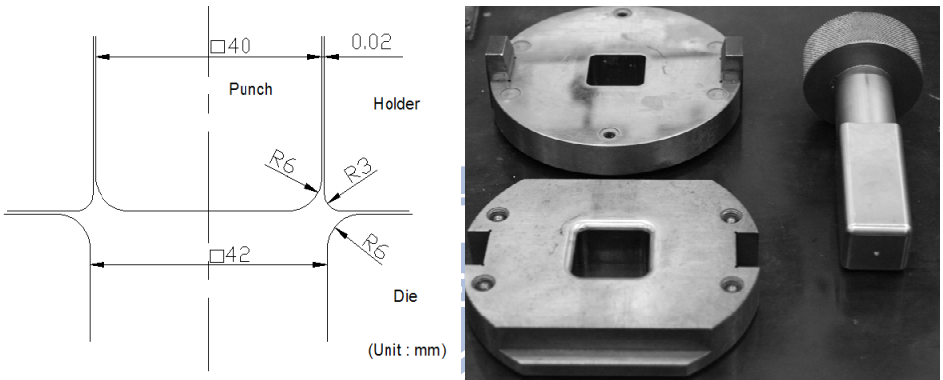


Figure 3.5 Tooling and blank geometry of the deep drawing test

Table 3.2 Type of facture conditions of clad metal sheets with different thickness combinations of holding force and specimen diameter (***OK, FT-Fracture on top, FS-Fracture on side***)

| *Combination material (Bonded Thickness)* | *Specimen diameter* | | |
|---|---|---|---|
| | **70 mm** | **80 mm** | **90 mm** |
| | *Holding force (result)* | | |
| **Al 2.0 mm/Cu 1.0 mm (0.97 mm)** | 5 KN(OK) | 50 KN(FT) | 5 KN(FT) |
| **Al 1.5 mm/Cu 1.0 mm (0.97 mm)** | 50 KN(FT) | 15 KN(FS)<br>20 KN(FT) | 5 KN(FT) |
| **Al 1.0 mm/Cu 1.0 mm (1.3 mm)** | 15 KN(OK) | 15 KN(FT) | 10 KN(FT) |

### 3.3 Numerical simulation of deep drawing test

#### 3.3.1 Finite element model of deep drawing

In this section, the fracture prediction of Al/Cu clad metal sheets using finite element simulations will be analyzed and verified with deep drawing tests. The deep drawing test was modeled using ABAQUS/CAE. For the numerical simulation of the deep drawing test, ABAQUS/Explicit was used to simulate large deformation behavior of the clad metal sheet. In this case, a 1/4 symmetric model was used; the Al/Cu clad metal sheet was considered as an equivalent isotropic single layer material, with material properties previously determined from tensile tests and used to simulate the actual flow rule of the Al/Cu clad metal sheet with the residual stresses effect considered. The blank was meshed with quadrilateral shell elements, while the die, punch and holder plate were considered to be discrete rigid bodies. A finite element model was constructed as shown in Figure 3.6.

For boundary conditions, the punch was specified to move in the z direction, and a holding force was applied on the blank through the holder. Three contact pairs (punch-blank, holder-blank, and blank-die) were defined in this study. The Coulomb coefficient of friction was set to 0.1 for all of contact surfaces.

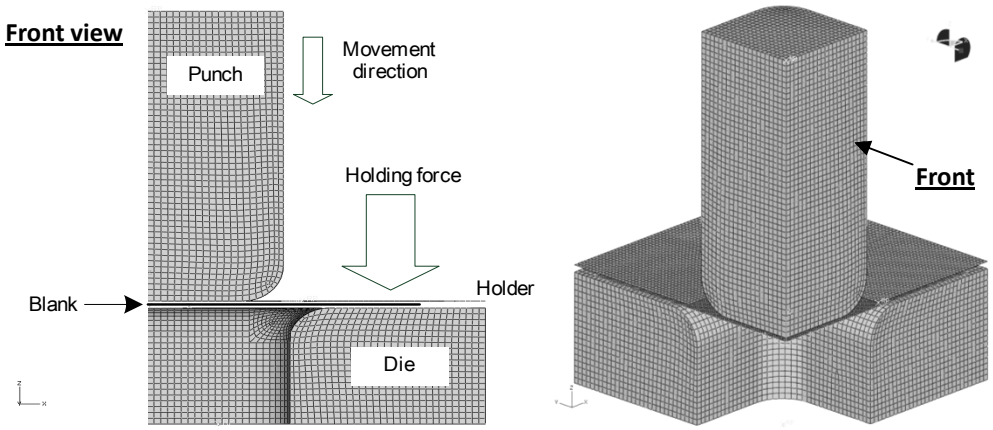


Figure 3.6 The finite element model of the deep drawing (1/4 symmetry)

### 3.3.2 Damage initiation criterion

For fracture prediction, the damage initiation option was used in the deep drawing forming simulation. The damage initiation criterion associated with the FLD is given by the condition $\omega_{FLD} = 1$, where the variable is a function of the current deformation state and is defined as the ratio of the current major principal strain, $\varepsilon_{\text{major}}$ to the major limit strain on the FLD evaluated at the current values of the minor principal strain, $\varepsilon_{\text{minor}}$. For the deformation state given by point A in Figure 3.7, the damage initiation criterion is evaluated as follows:

$$\omega_{FLD} = \frac{\varepsilon_{major}^{A}}{\varepsilon_{major}^{B}} \tag{5}$$

The parameters for the forming limit of the clad metal sheets were determined from the forming limit tests as discussed above.

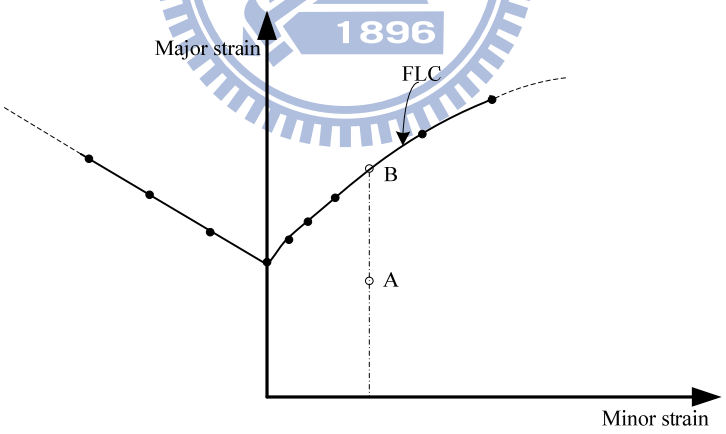


Figure 3.7 Forming limit diagram in ABAQUS [35]

### 3.4 Results and discussion

The deformation conditions and sheet fracture are shown in Figure 3.8(a). For the clad metal sheet with Al 1.5 mm/Cu 1.0 mm (blank dimension=80 mm), Figure 3.8(b) reveals that the maximum drawing depth was 23.5 mm when the holding force

was set to 15kN. It was observed that the fracture occurs on the side wall of the blank. When the holding force was increased, the metal flow of the clad metal sheet was constrained by larger frictional forces, with the result that the blocked metal flow caused fracture at the top corner of the blank for other fracture cases.

In this study, the applicability of FLDs on the fracture of clad metal sheets was verified. Al 1.0 mm/Cu 1.0 mm blanks with a thickness of 1.3 mm and three diameters (70, 80, and 90 mm) were used in the finite element analysis, and the simulation results were compared to those of the experiments. From the results shown in Figures 3.9-11, we can examine the fracture of clad metal sheets. When the blank dimension was 90 mm, the simulation of deep drawing indicated that the possible fracture site is at the corner of the blank where the higher holding area effect causes too much resistance for drawing. This fracture is caused by the near biaxial tensile mode. In FLD, the strain distribution is located on a minor strain of positive value. The experimental results verified this prediction.

When the blank dimension was 80 mm, the experimental fracture was at the corner. This fracture was caused by the biaxial tensile mode. The strain distribution was located on a positive minor strain in the FLD. In the simulation result, the strain distribution at the corner and side wall of the blank approached the high fracture criterion value. Therefore, the predicted fracture site of the blank was similar to the experimental result.

When the blank dimension was 70 mm and the holding force was set to 15 kN, the blank was drawn without fracture. From the simulation result, the forming limit factor is 0.573, and the strain distribution is located on a safe zone.

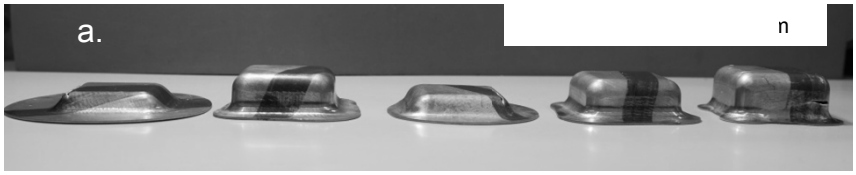

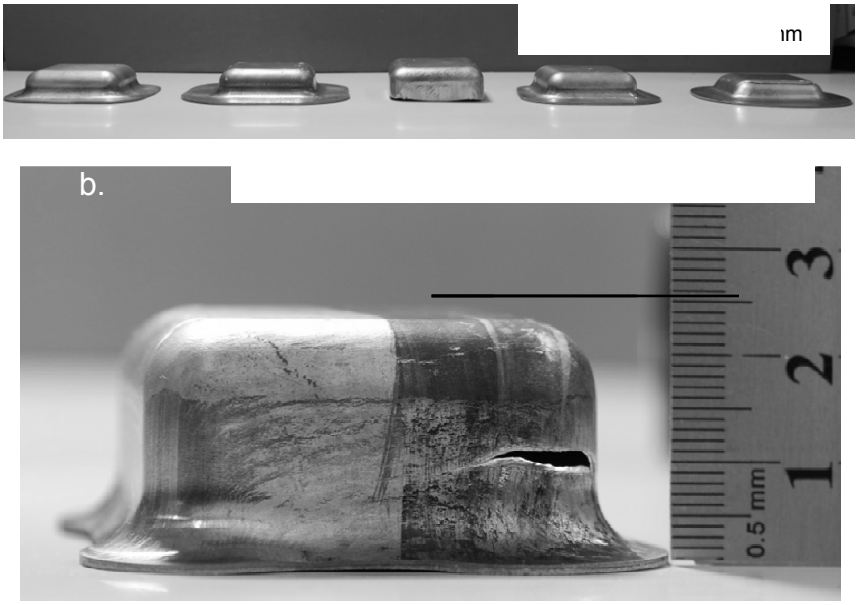


Figure 3.8 (a) The deformation conditions of blank with different initial thickness; (b) The maximum drawing depth of 23.5 mm (Al 1.5 mm/Cu 1.0 mm)

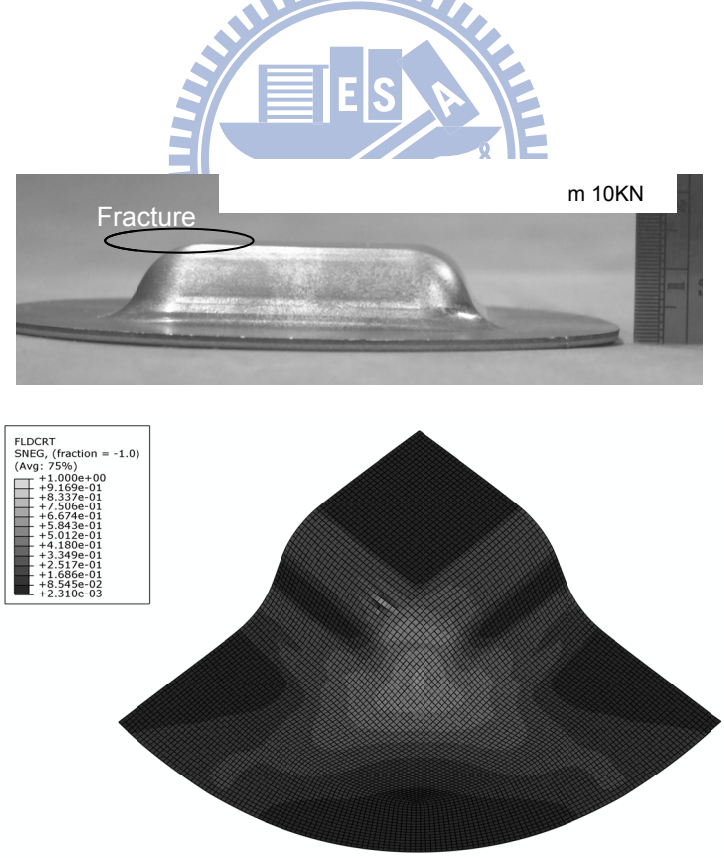


Figure 3.9 Experimental verification of deep drawing (d=90 mm)

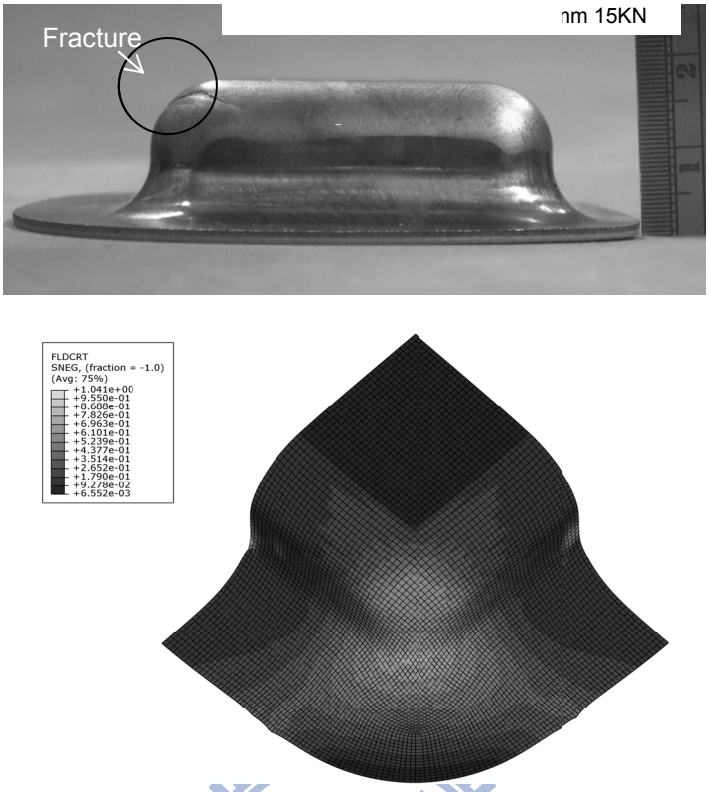


Figure 3.10 Experimental verification of deep drawing test (d=80 mm)

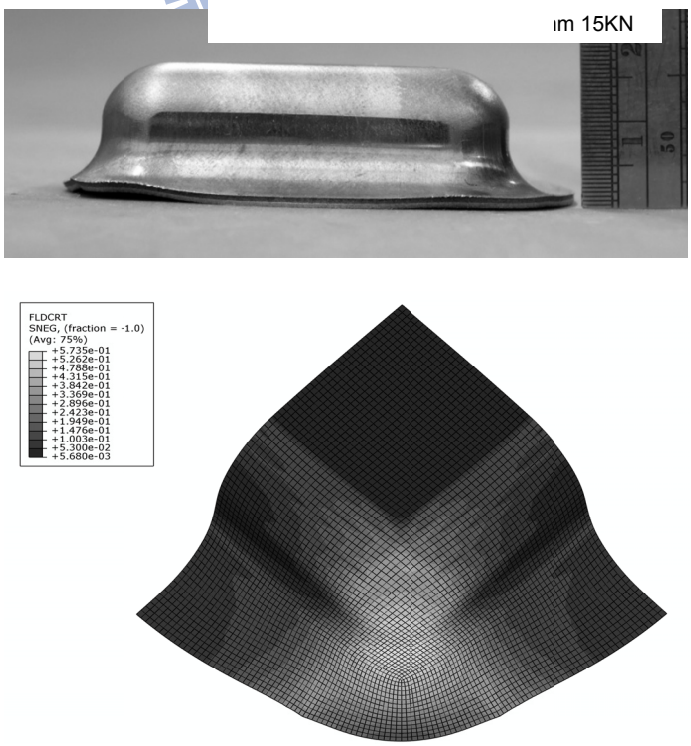


Figure 3.11 Experimental verification of deep drawing test (d=70 mm)

# CHAPTER 4 ANALYSIS OF PROCESS PARAMETER OF SHF

In this chapter, preliminary researches were studied for application of clad metal sheet in SHF. Some critical process parameters were analyzed on formability of clad metal sheet by FEA. The research in this section approach was divided into three tasks as follows:

- Obtained material property of clad metal sheet.
- Created FE model for SHF.
- Compared numerical simulation with experimental validation.

## 4.1 Material properties of Ti/Al clad metal sheet

All specimens of Ti / Al clad metal sheets were prepared in the following manner. The raw materials were cold-rolled aluminum sheets with thicknesses of 0.5 mm and cold-rolled Titanic sheets 0.3 mm thick. The bonded thickness was 0.45 mm thick by 1 stage rolling process. However, because the clad metals are produced at low temperature, the residual stresses generated in the rolling process cannot be released by the conventional annealing process because the melting temperatures of the individual layer sheets are often different from each other. For strain releasing, the specimen was heated to 500℃, and then air cooling during 5 hours. However the clad metal was assumed to anisotropic material.

The plastic strain ratio, $r$, is considered a direct measure of sheet metal's drawability and is useful for evaluating materials intended for forming shapes by deep drawing. The $r$ value is the ratio of the true strain in the width direction to the true strain in the thickness direction when a sheet material is pulled in uniaxial tension beyond its elastic limit. The plastic strain ratio is calculated as shown in Equation 6.

$$r = \frac{\varepsilon_w}{\varepsilon_t} \tag{6}$$

Where

$\varepsilon_w$ ：True width strain、$\varepsilon_t$ ：True thickness strain

In order to measure the mechanical properties of Ti / Al clad metal sheets, tensile tests were carried out on the MTS-810 tensile machine. Figure 4.1 shows the specimens dimension according to ASTM E8 tensile standard. The specimen dimensions were minified for bonded limitation of rolling mill. Figure 4.2 shows the true stress–strain curves obtained from Ti / Al clad metal sheets with three different directions (0∘, 45∘, and 90∘). Each curve stands for the average result of these specimens. These tensile properties will be used in the finite element simulation described below. Table 4.1 shows the plastic strain ratio of Ti / Al clad metal.

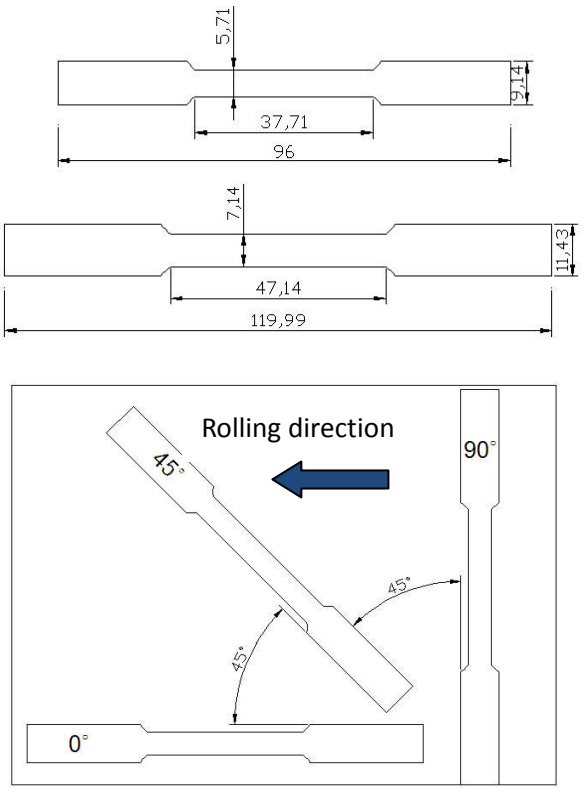


Figure 4.1 The specimen dimension

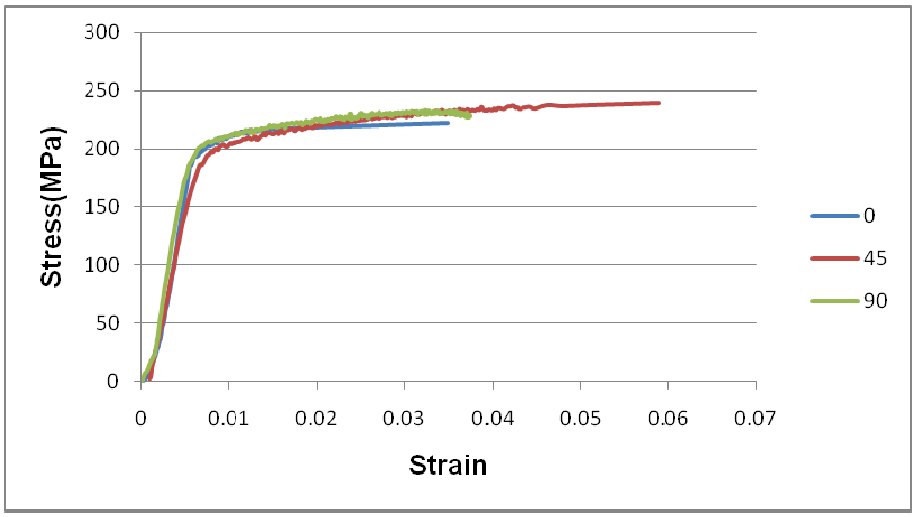


Figure 4.2 The true stress / strain curves of Ti / Al clad metal

Table 4.1 Plastic strain ratios of Ti / Al clad metal

| $r_0$ | $r_{45}$ | $r_{90}$ |
|---|---|---|
| 0.913 | 2.591 | 0.941 |

**4.2 FE simulation**

In this section, the deformation of Ti / Al clad metal using FE simulations will be analyzed and verified. The investigated SHF has been modeled using ABAQUS/CAE. For the numerical simulation of the SHF, ABAQUS/EXPLICIT was used. Two models of 3C housing were adopted. CAD models were show as Figures 4.3～4. In housing A, the 1/4 symmetric model was utilized. In housing B, the 1/2 symmetric model was utilized. The Ti / Al clad metal was regarded as an equivalent single material, with material properties previously determined from tensile tests. The layer of clad metal was assumed as perfect bonding. The blank was meshed with quadrilateral shell elements while the die, punch, and holder plate were considered to be discrete rigid bodies. Figure 4.5 shows the cross-section of SHF machine. The FE models were constructed as shown in Figures 4.6~7, respectively.

In fact, the real SHF has many extrinsic variations that will affect the forming results. In simulation case, some assumptions and effects were applied to simplify and clarify. Furthermore, the following assumptions are made: The clad metal assume to anisotropic, homogenous material.

- Bonding layer is perfect, clad metal assumed an equivalent single material.
- The deformation of punch, holder, and die were neglected.
- Leakage was neglected.
- The interface friction coefficient was assumed to be constant.

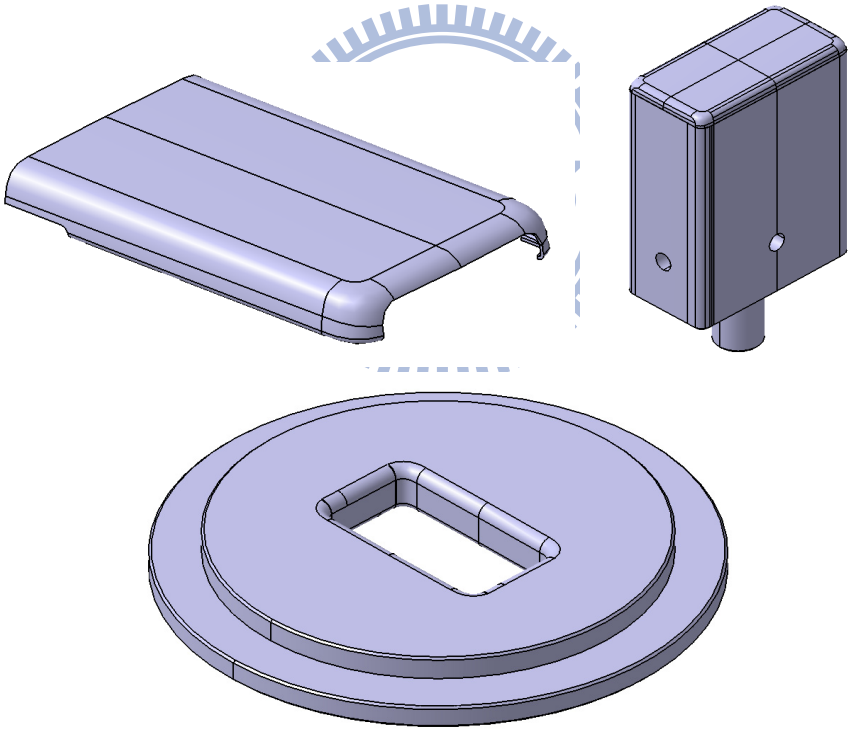

Figure 4.3 The CAD model of housing A, holder, and punch

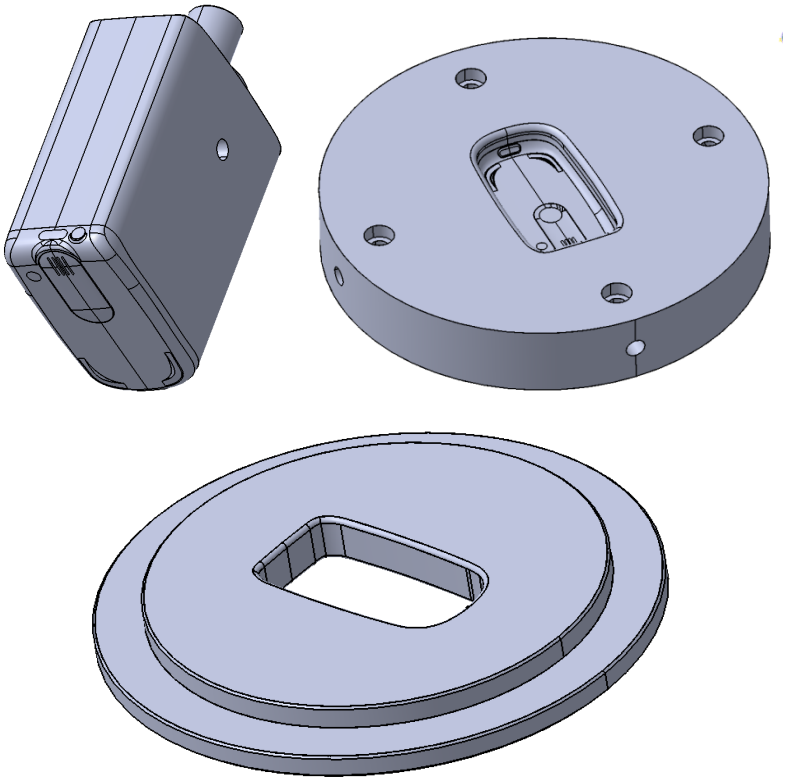

Figure 4.4 The CAD model of housing B, holder, die, and punch

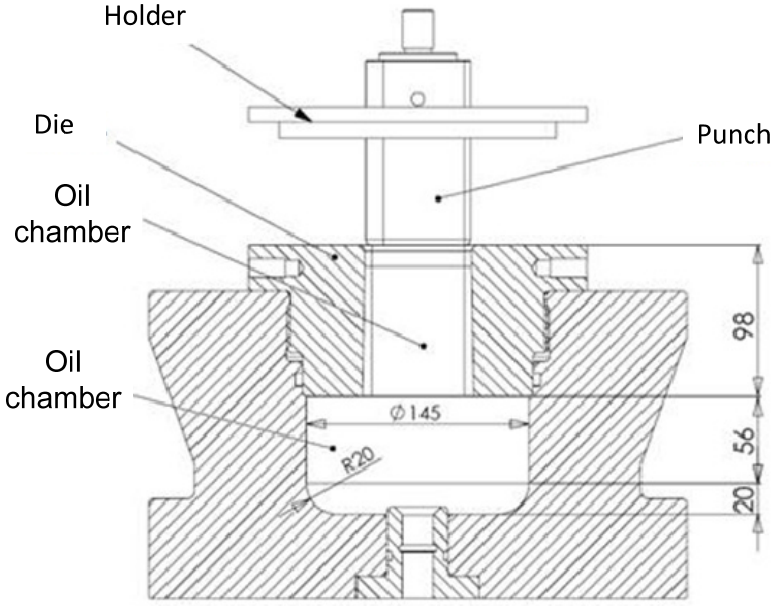


Figure 4.5 The cross-section of SHF machine

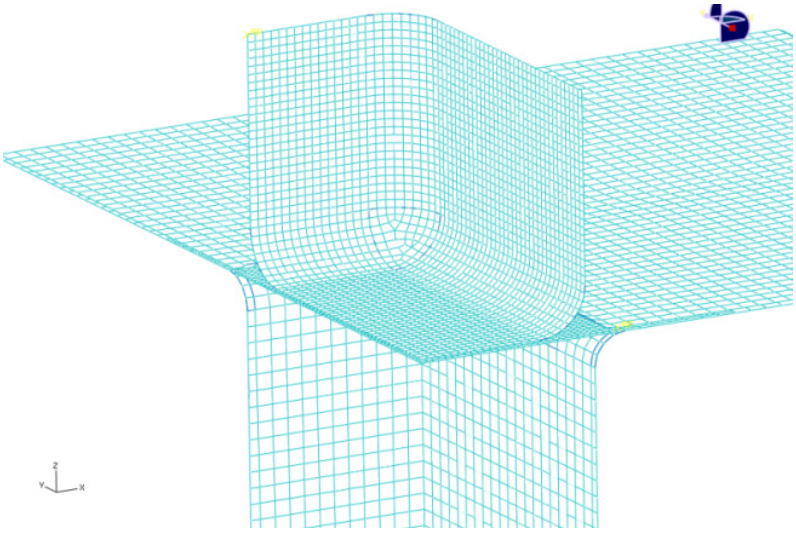

Figure 4.6 FE model of housing A

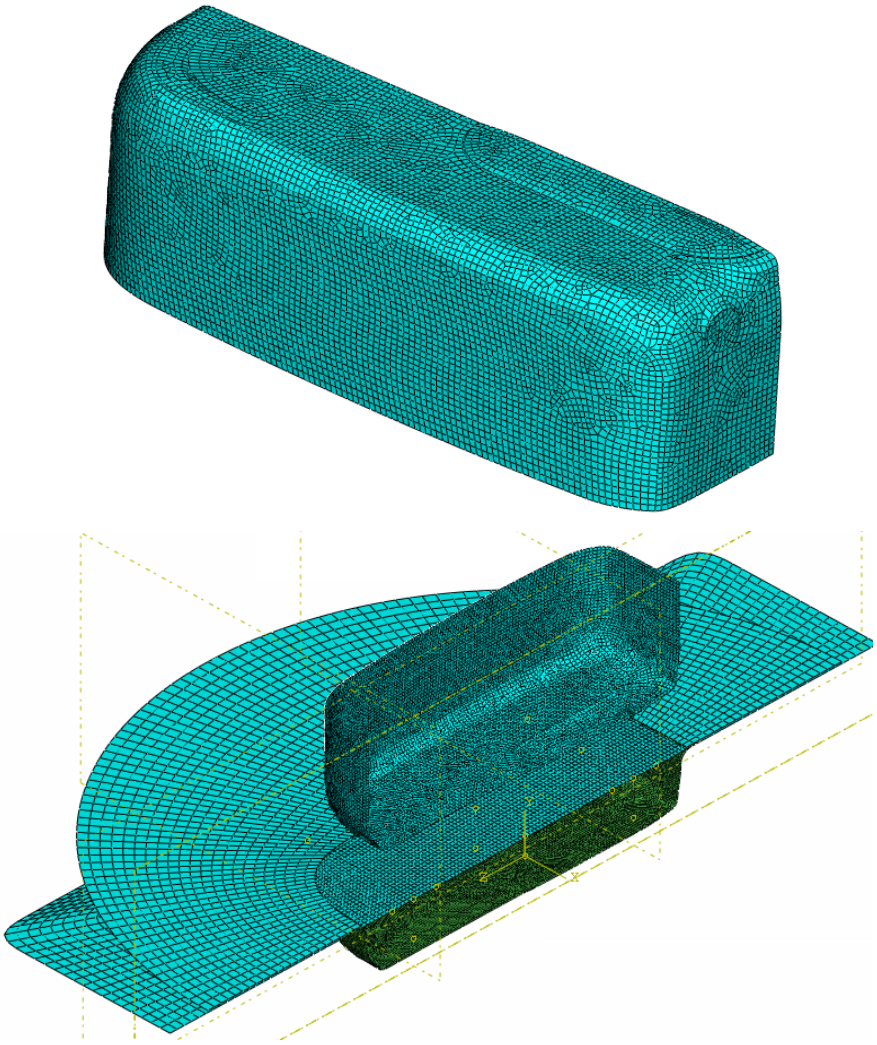

Figure 4.7 FE model of housing B

**FE simulation - Contact**

Three contact pairs (punch-blank, holder-blank, and blank-die) were defined in this study. The Coulomb coefficient of friction was set to 0.05, 0.1 for contact surfaces with and without lubrication [25, 36].

In the SHF process, the leakage was prevented by o-ring element. The deformation of o-ring was simplified to save computing time in FE simulation. So, three conditions were simulated in this section.

a. die with channel, and o-ring

b. die with channel without o-ring

c. die without channel, and o-ring.

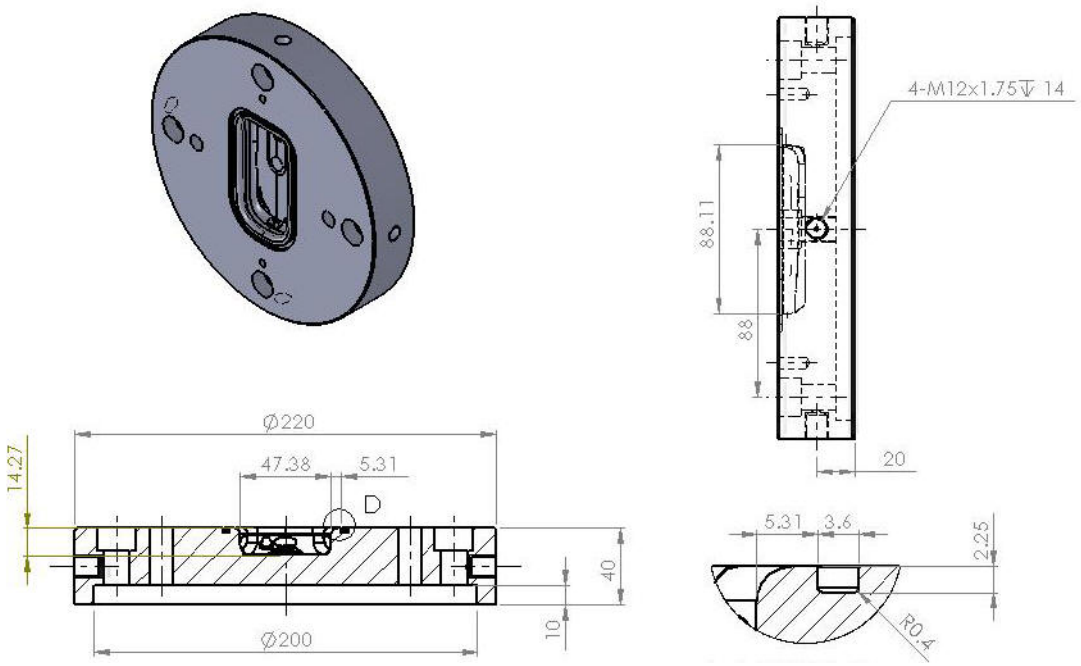


Figure 4.8 The drawing of sealing channel dimension

Here the o-ring was considered to incompressibility material, the elastic coefficient is 1.08GPa, and Poisson's Ratio is 0.475. The effective strain distributions of sheet were compared with different conditions, as Figures 4.9~4.11 shows. Because these simulation results were insignificant, the simplest condition c was adopted for

saving CPU time.

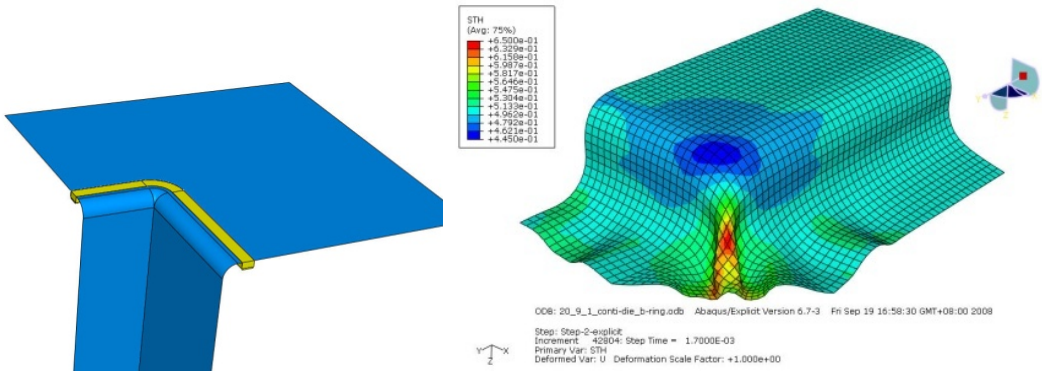


Figure4.9 The effective strain distribution of sheet with condition a

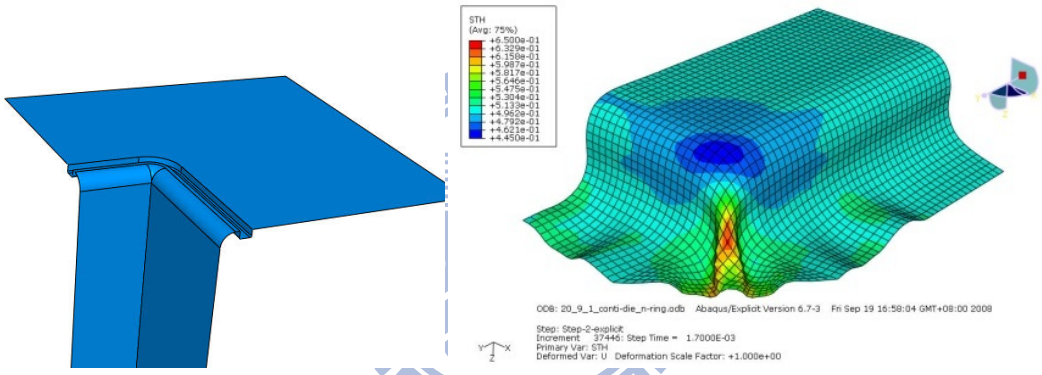


Figure 4.10 The effective strain distribution of sheet with condition b

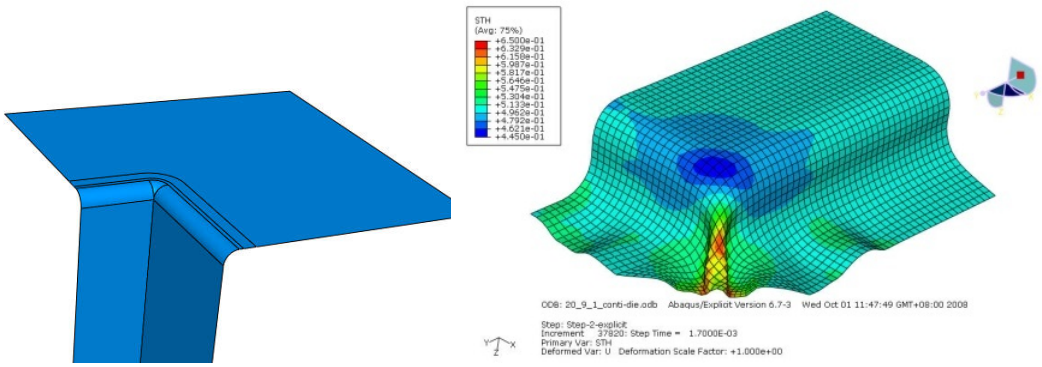


Figure 4.11 The effective strain distribution of sheet with condition c

**FE simulation - Boundary condition**

In simulation, the punch was specified to move in the z direction, and a holding

force was applied on the blank through the holder. The counter pressure was applied to blank, and the working area of blank was varied according to punch moving, as Figure 4.12 shows. A virtual film concept was proposed to realistically simulate the hydraulic loading for clad metal sheet during SHF. The friction coefficient of contact pair blank-virtual film was set to zero. Figure 4.13 shows the operation of virtual film with die and punch.

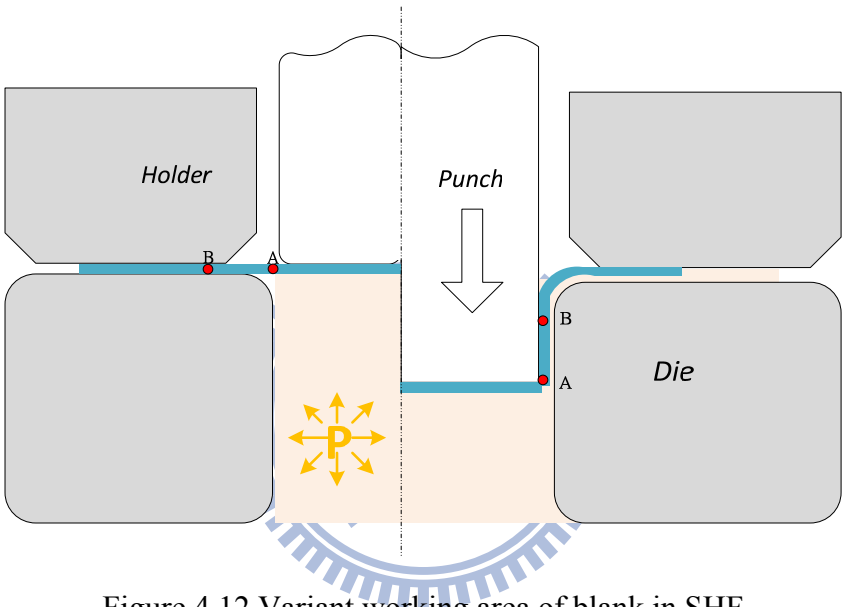


Figure 4.12 Variant working area of blank in SHF

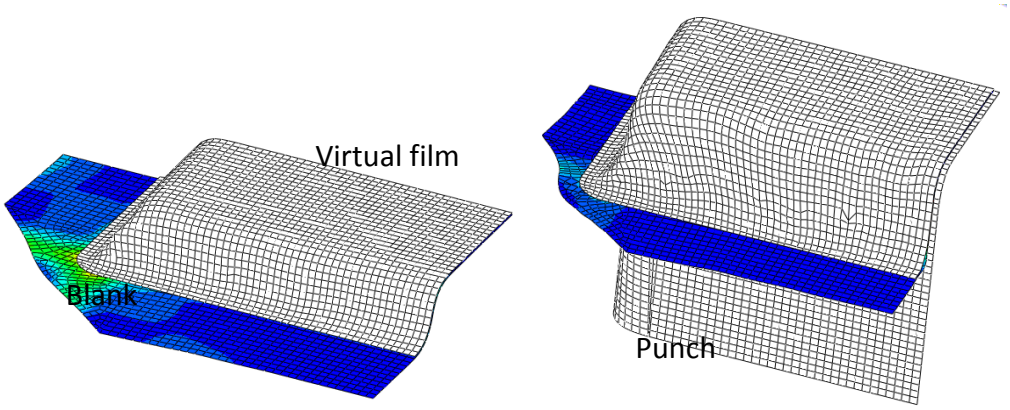


Figure 4.13 The operation of virtual film with punch and blank

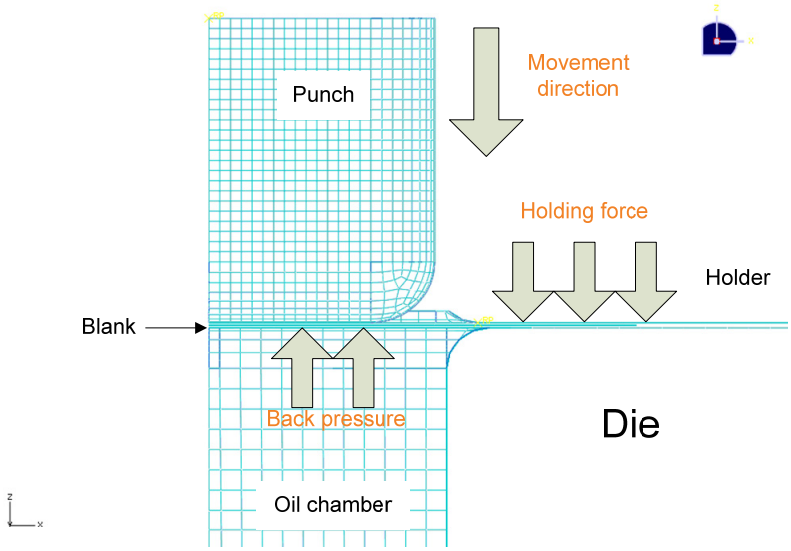


Figure 4.14 Boundary condition in SHF

**FE simulation - FE Model verification**

In this section, FE model was verified with experiment by thinning distribution. The AMINO SHF machine as Figure 4.15 shows. Figure 4.16 shows the blank dimension of housing A (1/4 symmetry). Figure 4.17 shows the locations of measured points on sheet,

Experiment parameters: the punch displacement was 13.5mm, the holding force was 2 ton, and counter pressure history was measured by pressure sense. Figure 4.18 shows the pressure history. Figure 4.19 shows the comparisons of thickness distribution of experiment with simulation. Those results were similar, and the histories of internal and kinetic energy were satisfied for quasi-steady problem, as Figure 4.20 shows.

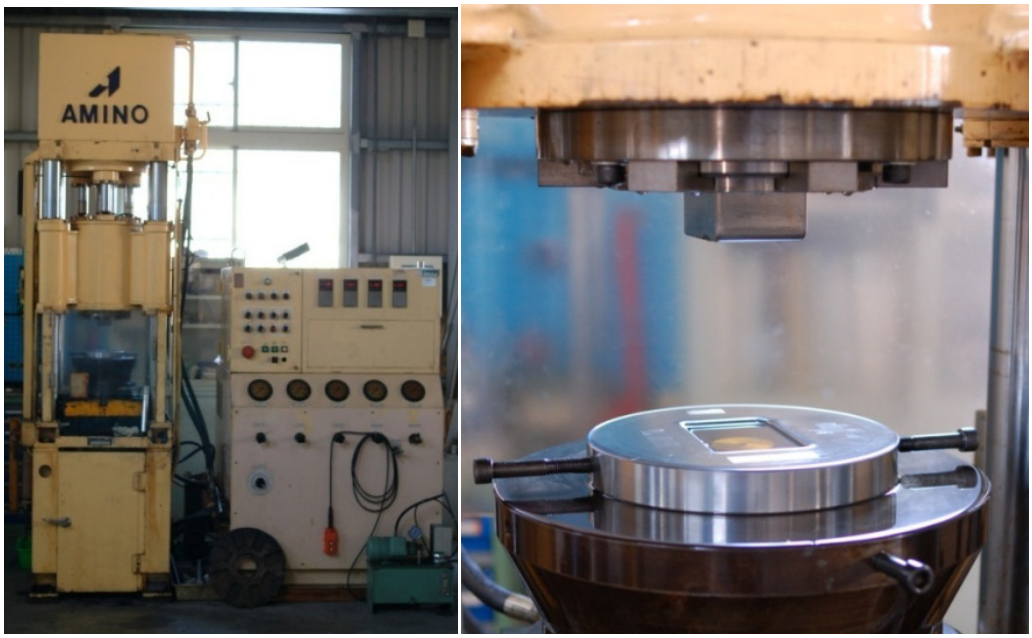


Figure 4.15 SHF machine

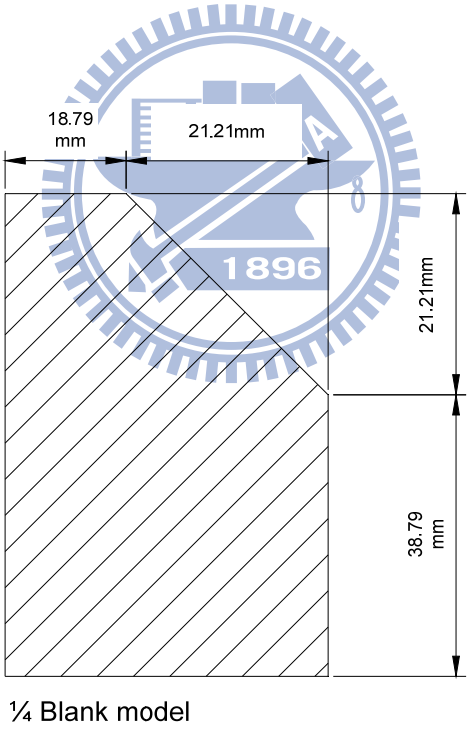


Figure 4.16 Blank dimensions for housing A

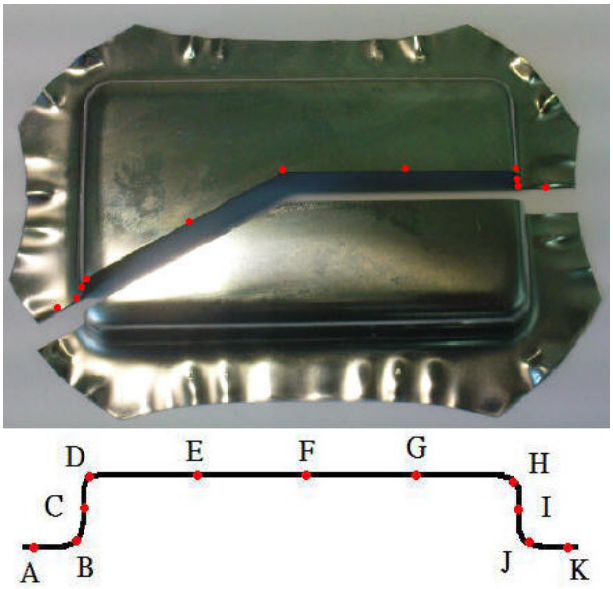


Figure 4.17 The locations of measuring points on housing A

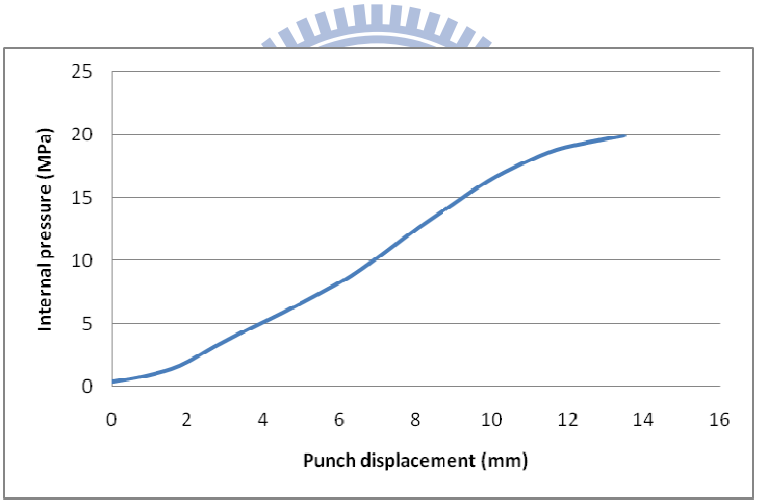


Figure 4.18 Pressure histories during SHF

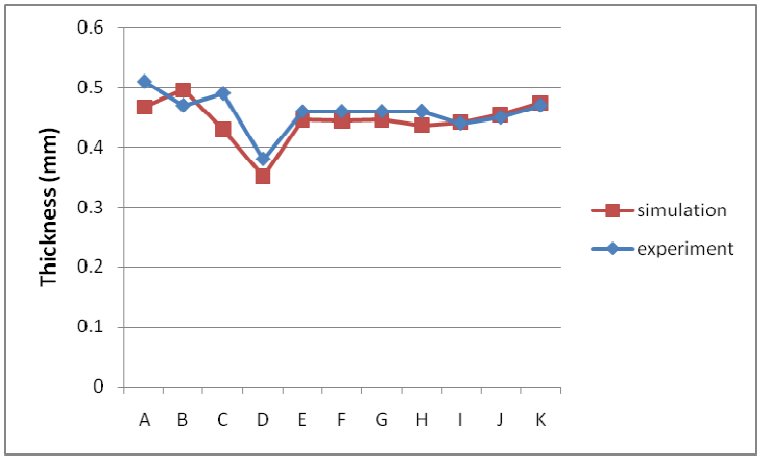


Figure 4.19 Comparison of thickness distribution of experiment with simulation

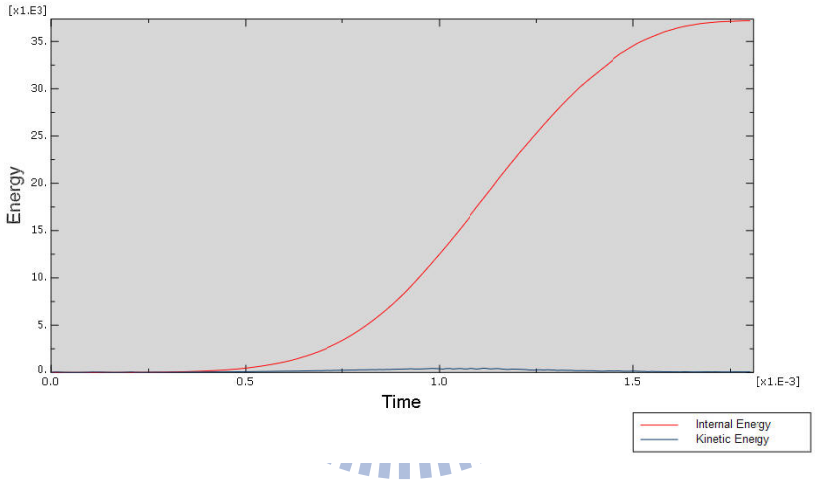


Figure 4.20 The histories of kinetic and internal energy

## 4.3 Process parameter analysis of SHF (housing A)

In this section, some critical process parameters were discussed by FE analysis. The housing A was adopted. The thinning distributions of blank were determined. The thinning ratio as Equation 7 shows. Table 4.2 shows combinations of process parameter.

$$Thinning \quad ratio = \frac{T_1 - T_0}{T_0} \times 100\% \tag{7}$$

$T_1$ ：Final blank thickness, $T_0$ ：Initial blank thickness

Table 4.2 Combinations of process parameter for housing A

| Parameters of Forming Process | Original value | Varied values |
|---|---|---|
| **Holding force (tons)** | 2 | 0.25, 1, 3 |
| **Internal Pressure (MPa)** | 10 | 5, 15, 18<br>11, 12, 13, 14 |

### 4.3.1 Influence of friction coefficient

In this research, the friction condition was different with and without lubricant because the contact materials of clad metal were different for holder and die (outside of seal), respectively.

The variant friction combinations were assigned in simulation. The friction coefficient was set to 0.05 in oil chamber. Figure 4.21, the setting for different friction pairs. Table 4.3 shows combinations of friction coefficient for different contact pair.

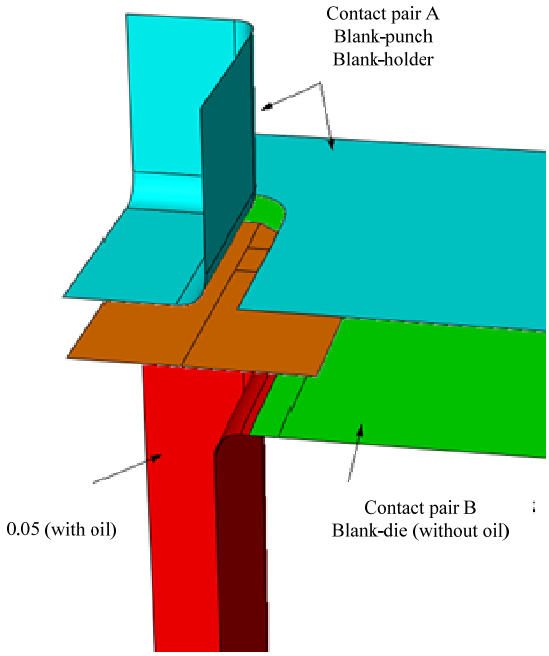


Figure 4.21 Schematic representation of setting of different contact pairs in SHF

Table 4.3 Combinations of coefficient of friction $\mu$

| | Contact pair A | Contact pair B |
|---|---|---|
| **Condition 1** | 0.1 | 0.05、0.1、0.2 |
| **Condition 2** | 0.05、0.1、0.2 | 0.1 |

The Figure 4.22~23 shows the thickness and the thinning distribution with condition 1. The thinning of blank occurs when the friction coefficient of blank-die outside was rising.

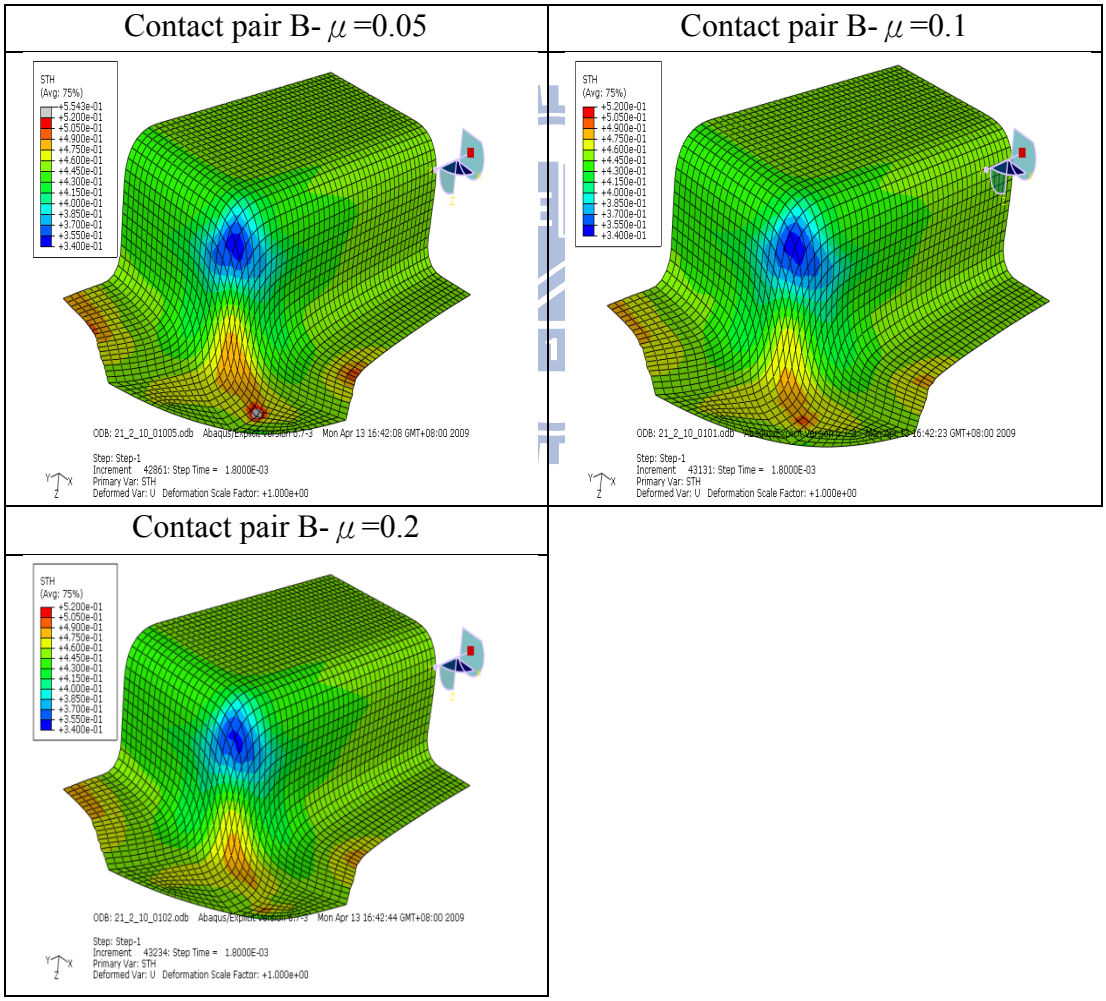


Figure 4.22 Thickness distributions with condition 1 (contact pair A- $\mu$ =0.1)

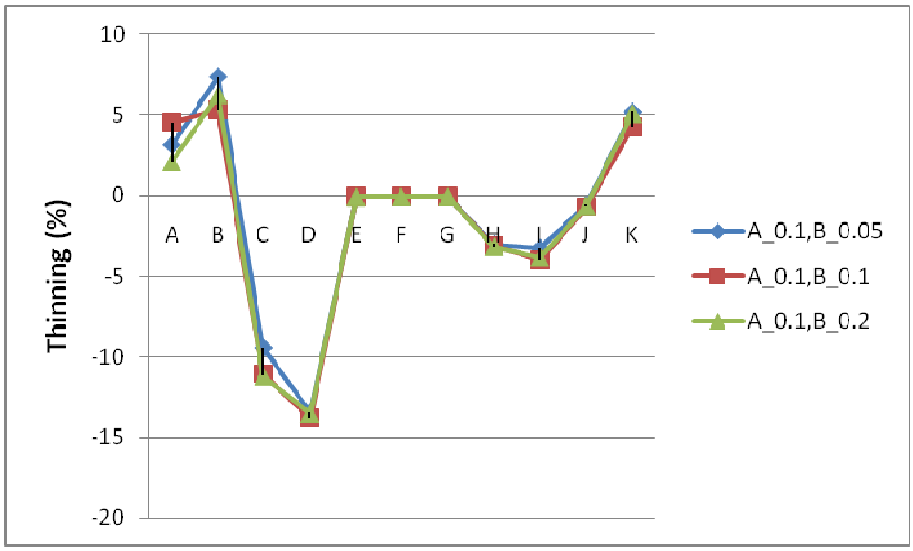


Figure 4.23 Thinning distribution with condition 1 (contact pair A- $\mu$ =0.1)

The Figures 4.24~25 shows the thickness and the thinning distribution with condition 2. From simulation results, the point C and D have opposite trend on thinning when friction coefficients of blank-punch, and blank-holder were rising. Large friction force causes the limited sliding between blank and punch, as Figure 4.26 shows. Thus thinning of blank was easing at point D (corner). Furthermore sufficient friction force has been helpful to draw-in. The restraining force of metal flow was rising at point C (sidewall) when large friction force oppositely. As Figure 4.27 shows.

| Contact pair A- $\mu$ = 0.05 | Contact pair A- $\mu$ =0.1 |
|---|---|
| 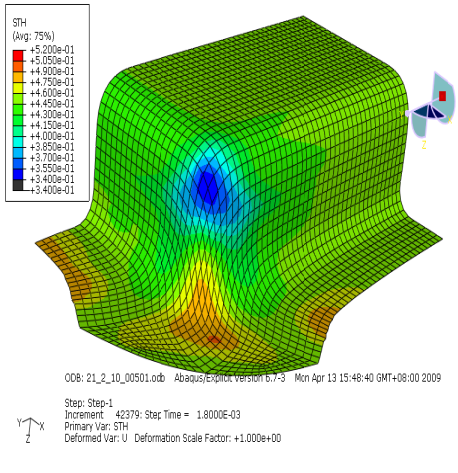 | 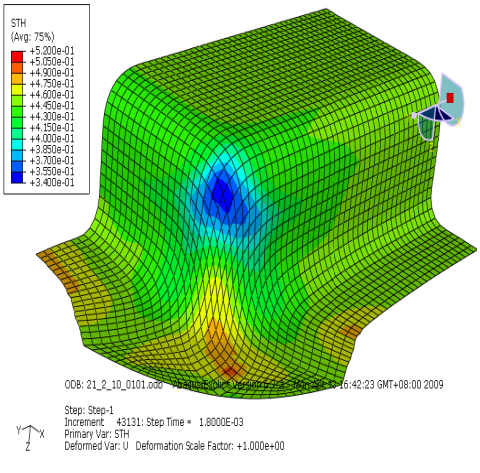 |

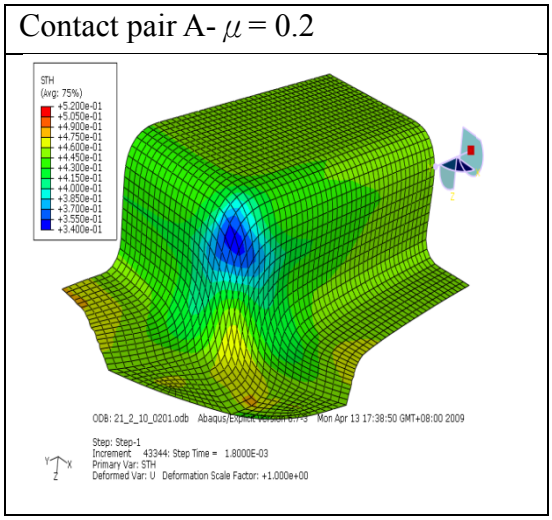


Figure 4.24 Thickness distributions with condition 2 (contact pair B- $\mu$ =0.1)

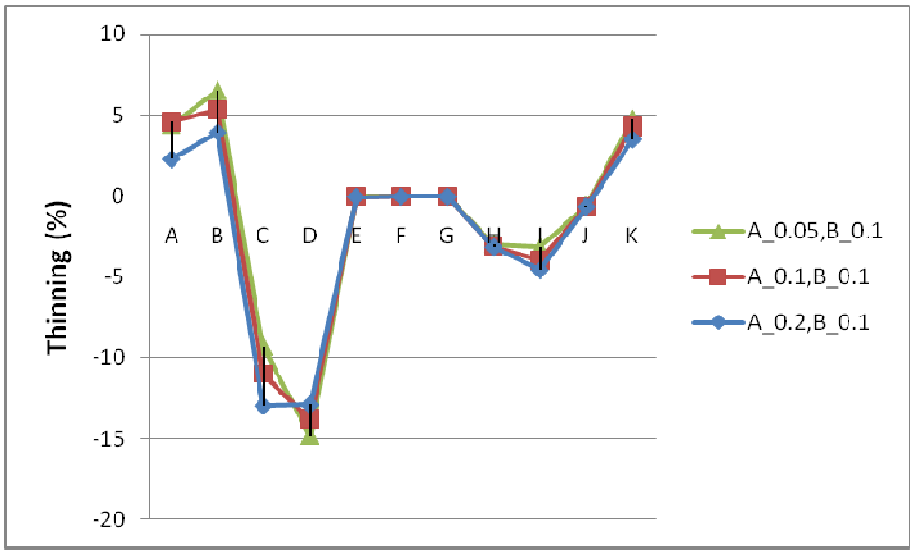


Figure 4.25 Thinning distribution with condition 2 (contact pair B- $\mu$ =0.1)

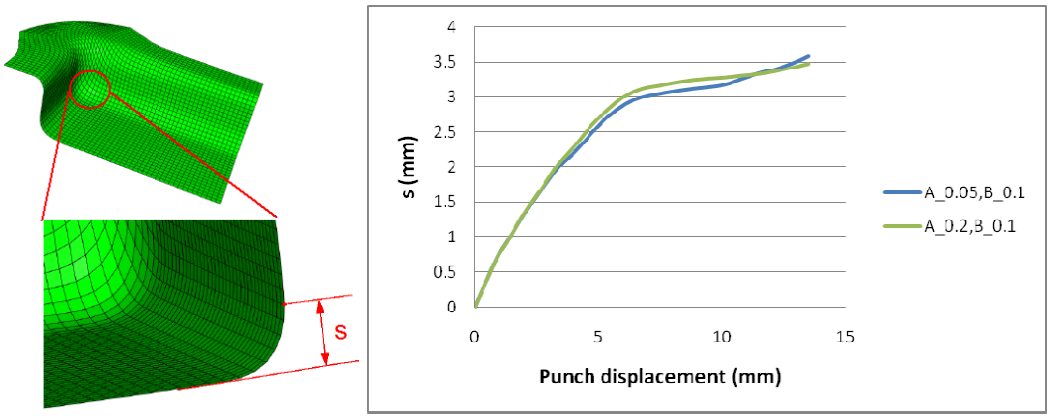


Figure 4.26 The displacement of blank at point D

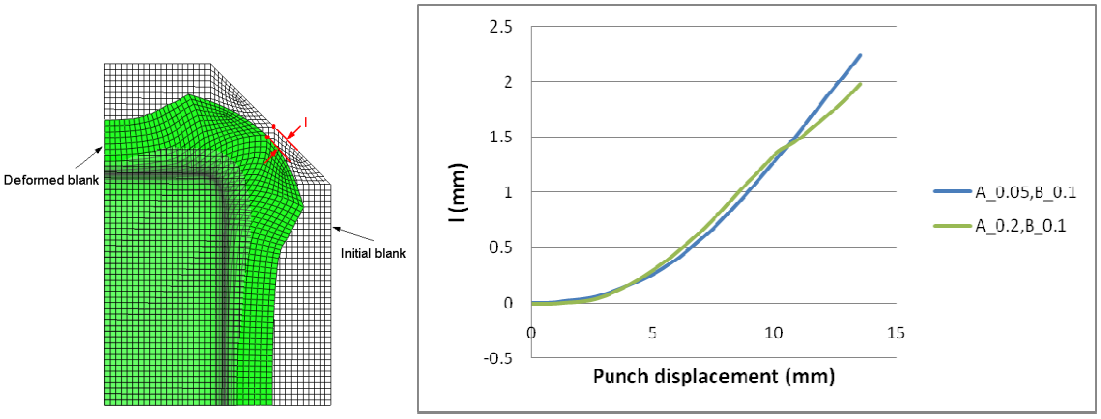


Figure 4.27 The displacement of blank at point C

### 4.3.2 Influence of holding force

In metal forming process, holding force is very important parameter for formability. Undue holding force made too much restraining force during forming. For SHF, insufficient holding force causes wrinkling, that may be made leaking problem (pressure lose). In this section, the effects of different holding forces were simulated. The combinations of process parameter shows, Table 4.2. Figures 4.28~29 show the thickness and thinning distributions with different holding forces.

| HF=0.25 tons | HF=1 tons |
|---|---|
| 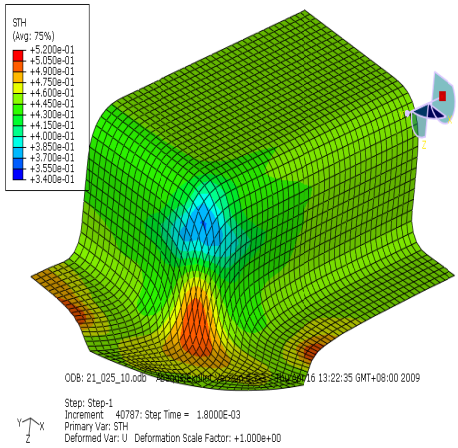 | 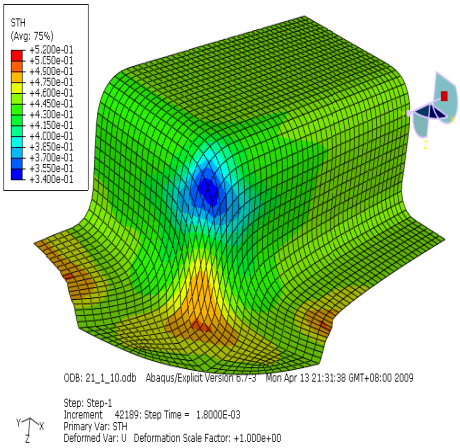 |
| HF=2 tons | HF=3 tons |

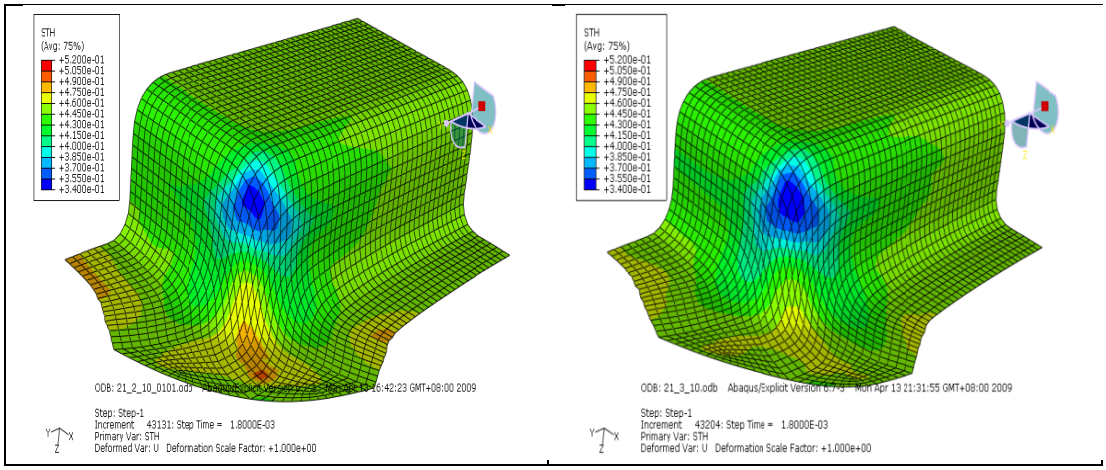


Figure 4.28 The thickness distributions of blank with different holding forces

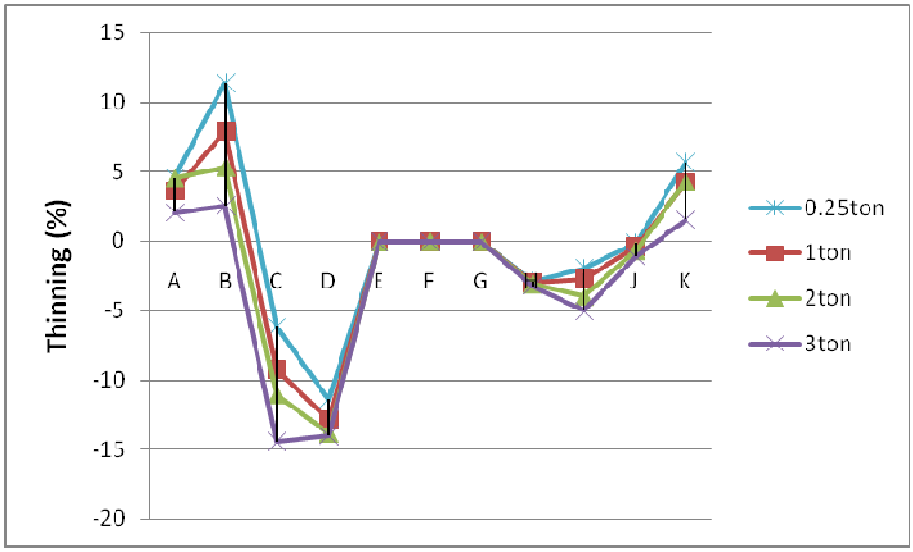


Figure 4.29 The thinning distribution of blank with different holding forces

From simulation results, the thinning of blank was be effected by holding force. The wrinkling of blank couldn't result; small holding force was adopted in this application.

### 4.3.3 Influence of pressure history

Compared SHF with conventional stamping process, SHF provides counter pressure to blank, which press the blank to punch. Counter pressure was helpful to

reduce the friction effect between die-blank.

For existing hydraulic system design, the maximum pressure always depends on drawing depth of product. Maybe too large pressure causes the failure of blank during forming. In this section, different final pressure histories were simulated for improving the formability of the clad metal. Table 4.2 shows the combinations of process parameter. Figure 4.30, different final pressure histories. Figures 4.31～32 shows the simulation results.

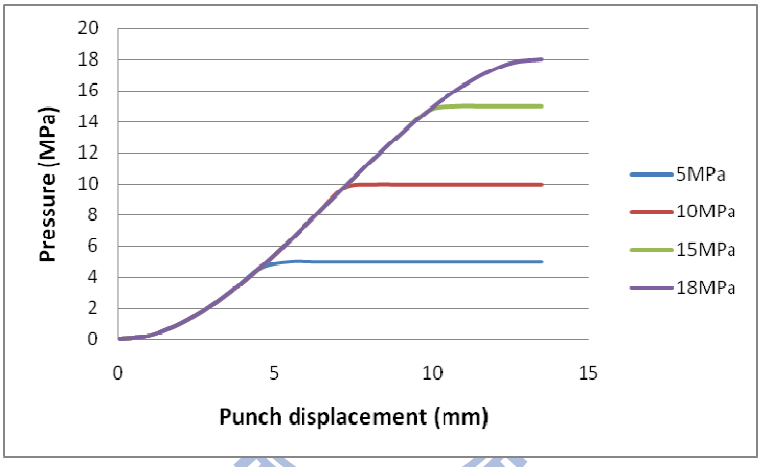


Figure 4.30 Different pressure histories (final pressure 5, 10, 15, 18MPa)

| Final pressure=5MPa | Final pressure=10MPa |
|---|---|
| 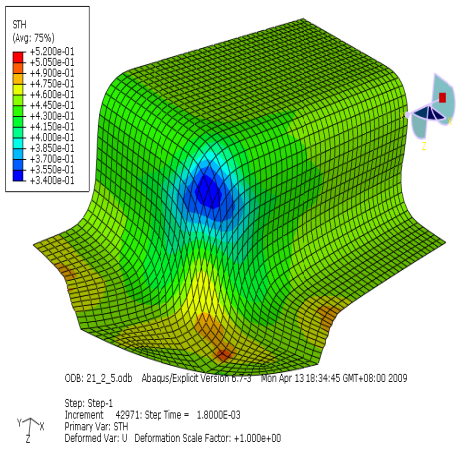 | 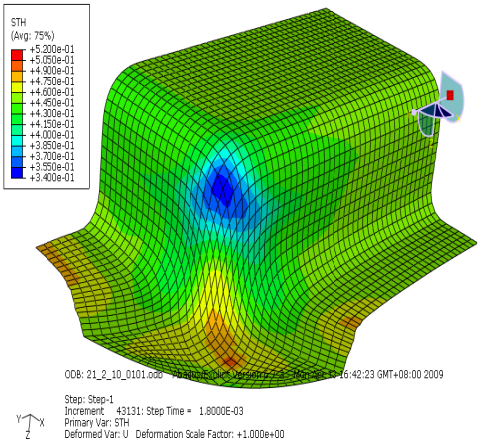 |
| Final pressure=15MPa | Final pressure=18MPa |

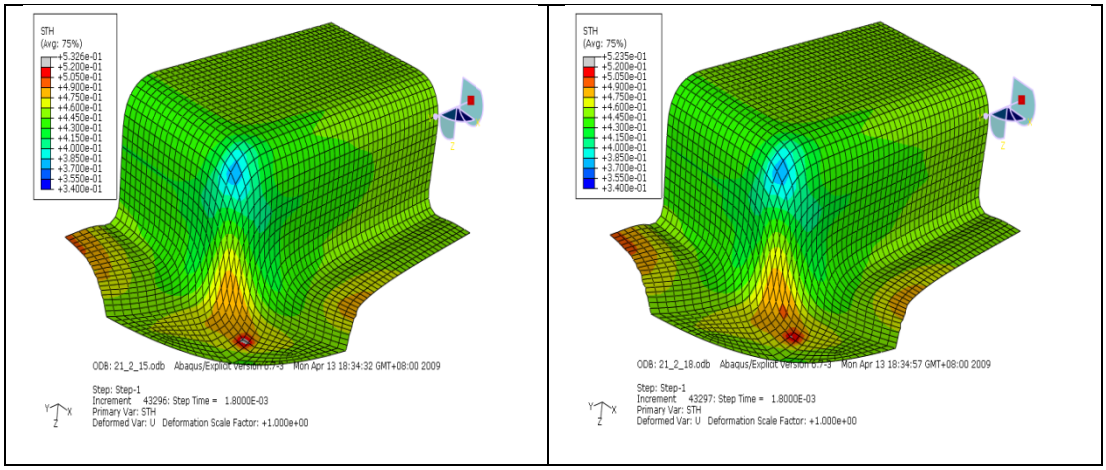


Figure 4.31 The thickness distribution with different final pressure histories

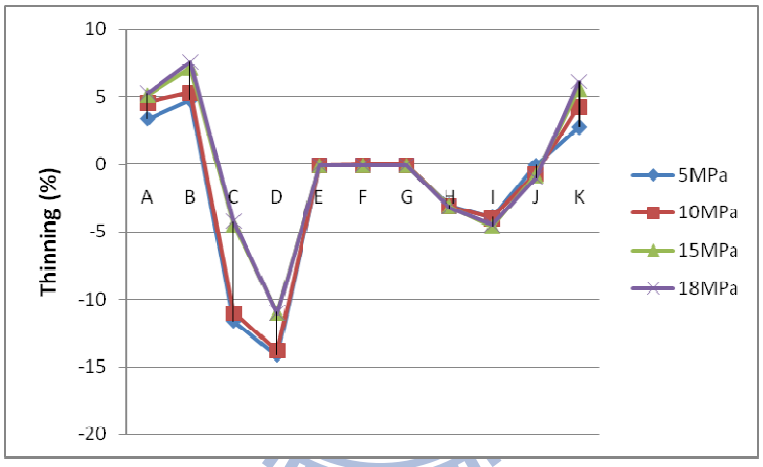


Figure 4.32 The thinning distribution with different pressure histories (final pressure 5, 10, 15, 18MPa)

From above results, the thinning of blank was retarded by counter pressure rising. Compared results of 5 with 10 MPa, and 15, with 18 MPa, the thinning distribution were similar. In order to correct the effect of counter pressure for formability of blank. Four different final pressure histories (11, 12, 13, and 14MPa) were simulated again. Figure 4.33 shows the pressure histories. Figure 4.34 shows the thinning distribution of blank with different pressure histories. Large final pressure helpful improves the formability of blank.

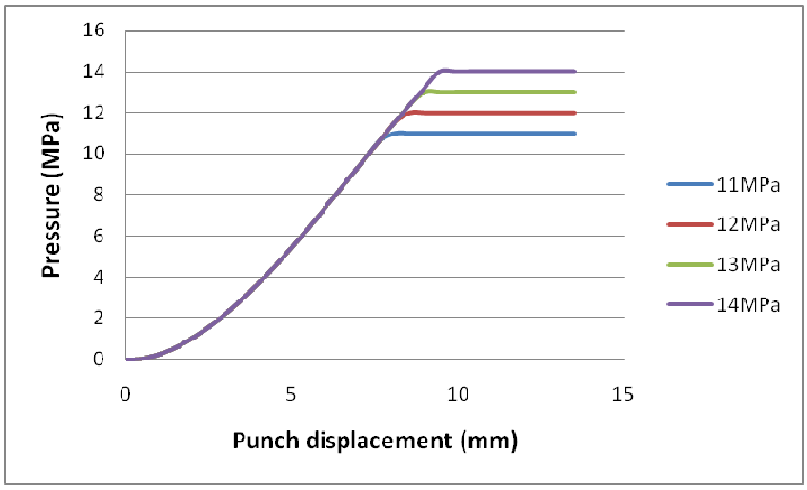


Figure 4.33 Different pressure histories (final pressure 11, 12, 13, 14MPa)

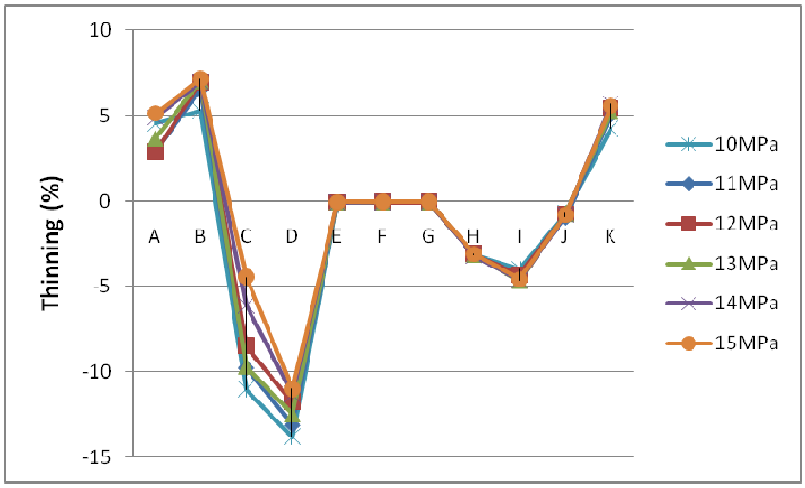


Figure 4.34 The thinning distribution with different pressure histories (final pressure 11, 12, 13, 14MPa)

## 4.4 Analysis of SHF-application-housing B

### 4.4.1 Comparison of FE results with experiments

In this section, the housing B was adopted; significant process parameters such as blank dimension and holding force continue to analyze by experiment and FE. In some case, the stainless steel (SUS 304) was adopted. The material property of SUS 304 was referred from the reference [37]. Table 4.4 shows the combinations of process parameter for housing B. Figure 4.35 shows the locations of measured points on housing B.

Table 4.4 Combinations of process parameter for housing B

| **Material** | **SUS 304** | | | **Ti/Al** | |
|---|---|---|---|---|---|
| **Holding force (ton)** | 0.7 | 1 | 2 | 0.7 | 1 |
| **Chamfer width (blank dimension)** | 20 (114×74) | 21.21 (120×80) | 20(114×74)<br>21.21(120×80)<br>23(120×80) | 20 (114×74) | |

*Length Unit: mm*

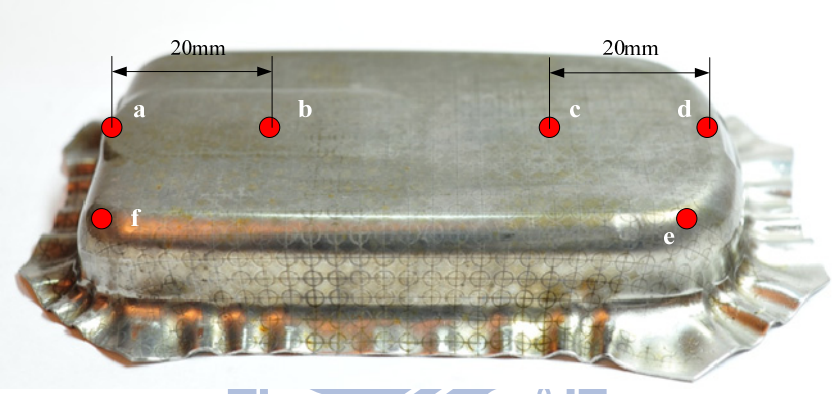


Figure 4.35 The locations of measuring points on housing B

**Comparison of thinning distribution (blank dimension, SUS 304)**

In this section, three different blank dimensions were simulated for housing B. The holding force was 2 tons, and counter pressure history was measured by pressure sense. Figures 4.36~38 show the thickness distributions with different chamfer width. Figure 4.39 shows the thinning distribution of blanks.

| Min. thickness = 0.3618 (Chamfer width = 21.21mm) | |
|---|---|
| 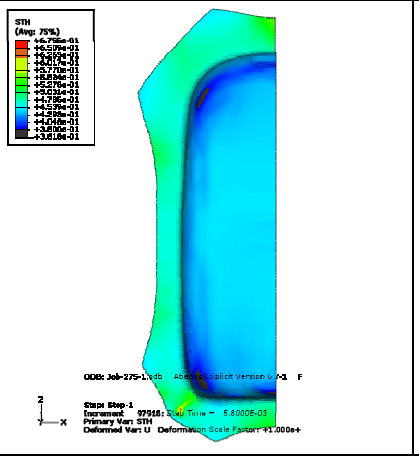 | 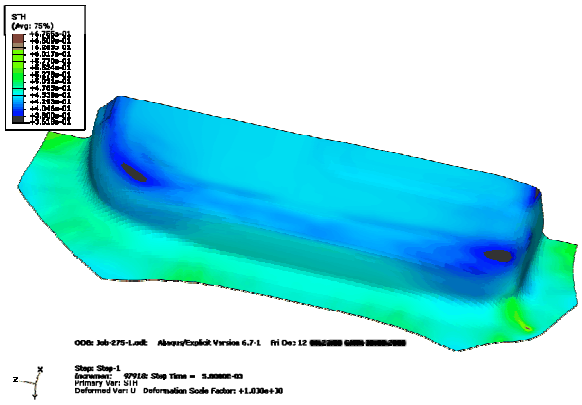 |
| Boundary condition: Material SUS 304, Holding force=2 ton, Final pressure=18.2MPa | |

Figure 4.36 The thickness distribution (chamfer width=21.21mm)

| Min. thickness = 0.3643 (Chamfer width = 23mm) | |
|---|---|
| 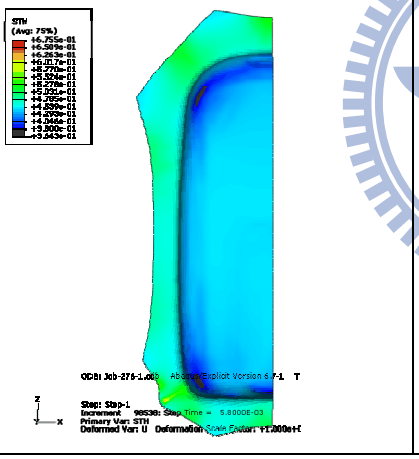 | 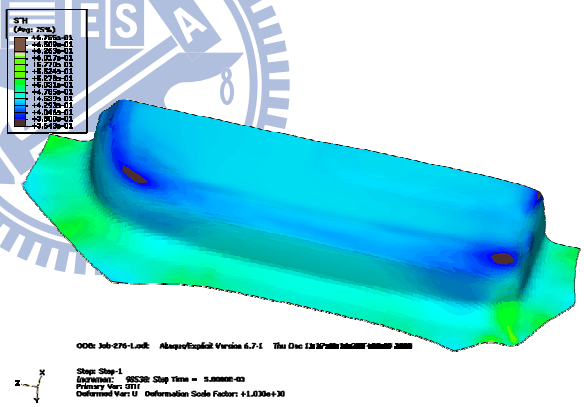 |
| Boundary condition: Material SUS 304, Holding force=2 ton, Final pressure=16.1MPa | |

Figure 4.37 The thickness distribution (chamfer width=23mm)

| Min. thickness = 0.3773 (Chamfer width = 20mm) |
| --- |
| 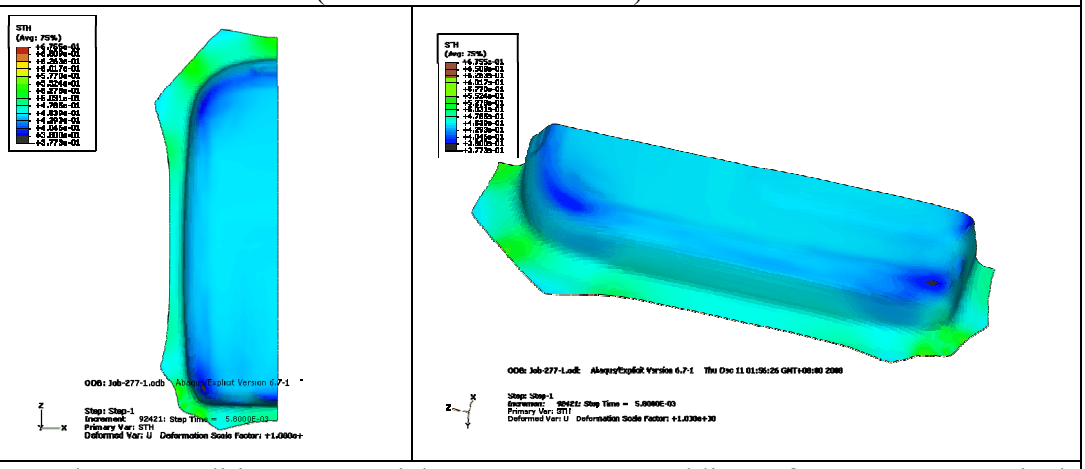 |
| Boundary condition: Material SUS 304, Holding force= 2ton, Final pressure=16.6MPa, |

Figure 4.38 The thickness distribution (chamfer width=20mm)

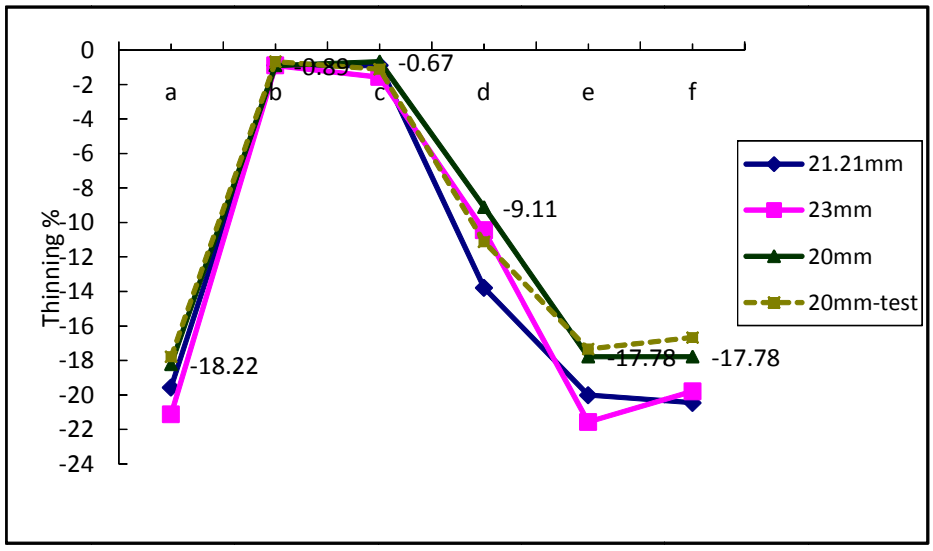


Figure 4.39 The thinning distributions with different chamfer widths (material: SUS 304)

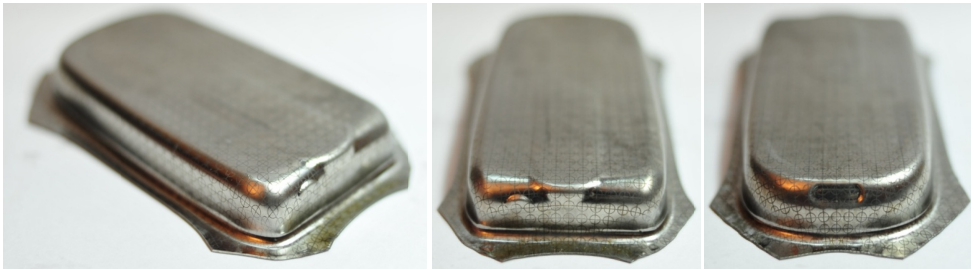

Figure 4.40 The deformation of SUS 304 with mesh (holding force: 2 ton, chamfer width: 20mm)

From simulation results as Figures 4.36~37, the thinning results of cases (21.21, 23 mm) were obvious for case of 20mm. An insignificant wrinkling occurs at side of blank. From Figure 4.39 shows, the thinning distribution of case 20mm was stable; that was similar to experiment data. Deformation of blank was shown as Figure 4.40.

**Comparison of thinning distribution (SUS 304, Ti/Al clad metal)**

In this section, Ti / Al clad metal and SUS 304 were simulated with different holding; that formability of materials was compared. Figures 4.41~44 show the thickness distribution with different holding force and material. Figure 4.45 shows the thinning distribution of blank with different parameter combinations. Figure 4.46 shows the failure occurs at a point (holding force: 1 ton, chamfer width: 20mm). Figure 4.47 shows the deformation of Ti / Al clad metal sheet without failure (holding force: 0.7 ton, chamfer width: 20mm).

| Min. thickness = 0.365 mm (HF = 1 tons) |
| --- |
| 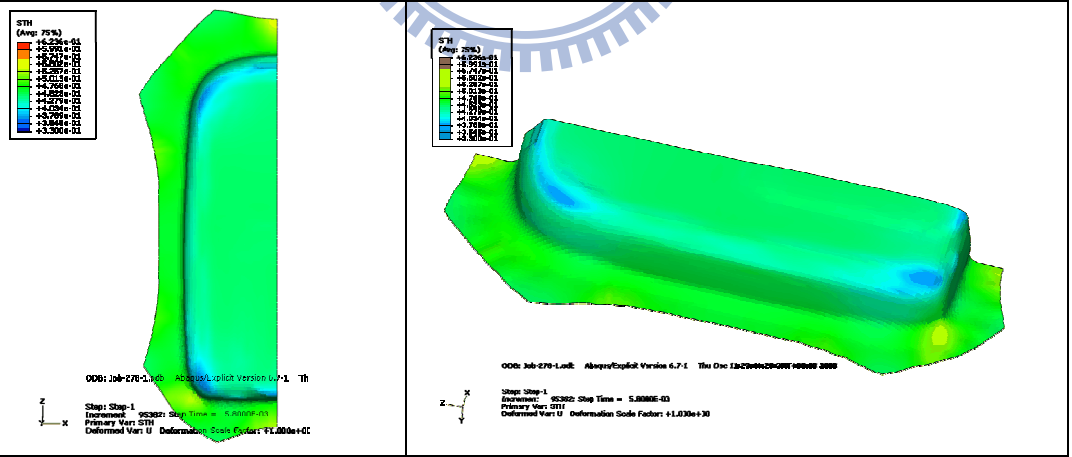 |
| Boundary condition: Material SUS 304, Chamfer width = 21.21mm, Final pressure=12MPa, |

Figure 4.41 The thickness distribution of blank (HF = 1ton, SUS 304)

| Min. thickness = 0.3897 mm (HF = 0.7 tons) | |
|---|---|
| 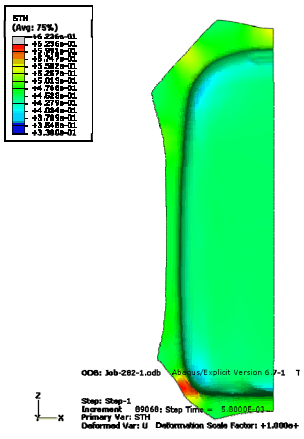 | 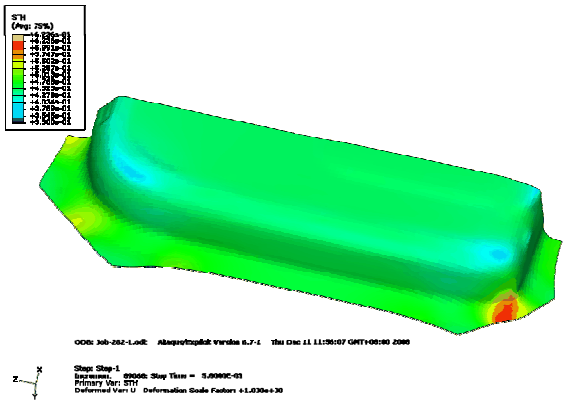 |
| Boundary condition: Material SUS 304, Chamfer width = 20mm, Final pressure=10.4MPa, | |

Figure 4.42 The thickness distribution of blank (HF= 0.7tons, SUS 304)

| Min. thickness = 0.33 mm (HF = 1 tons) | |
|---|---|
| 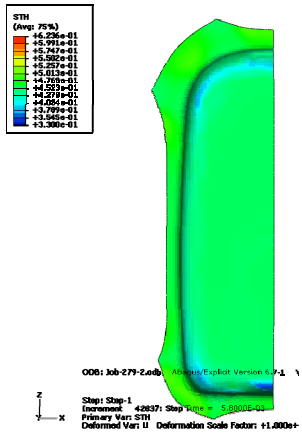 | 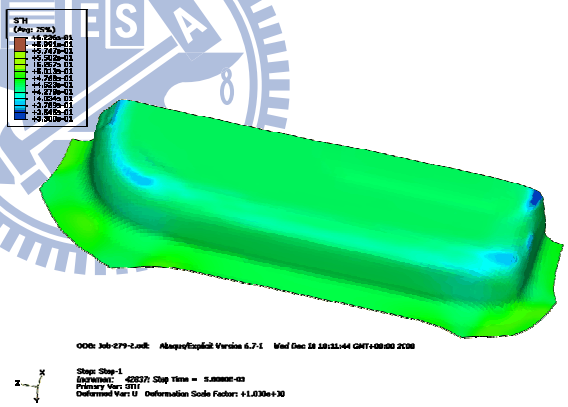 |
| Boundary condition: Material Ti/Al clad metal, Chamfer width = 20mm, Final pressure=10.4MPa, | |

Figure 4.43 The thickness distribution of blank (HF= 1tons, Ti/Al clad metal)

| Min. thickness = 0.343 mm (HF = 0.7 tons) | |
|---|---|
| 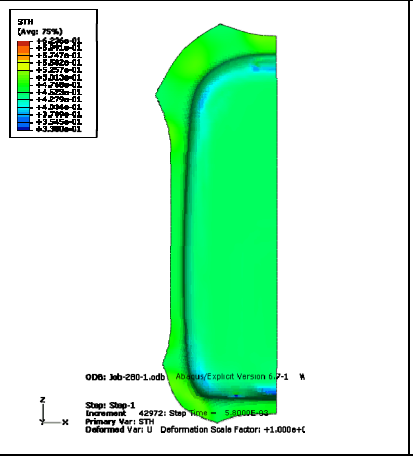 | 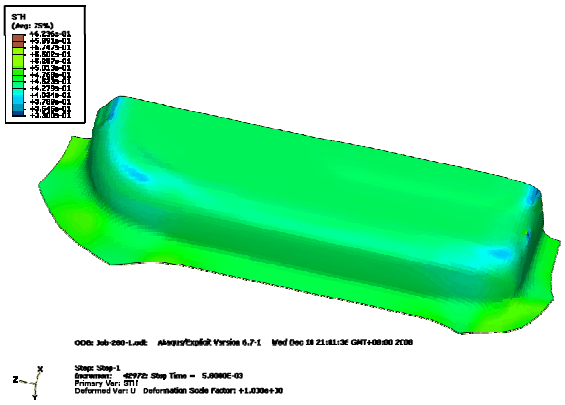 |
| Boundary condition: Material Ti/Al clad metal, Chamfer width = 20mm, Final pressure=11.5MPa, | |

Figure 4.44 The thickness distribution of blank (HF= 0.7tons, Ti/Al clad metal)

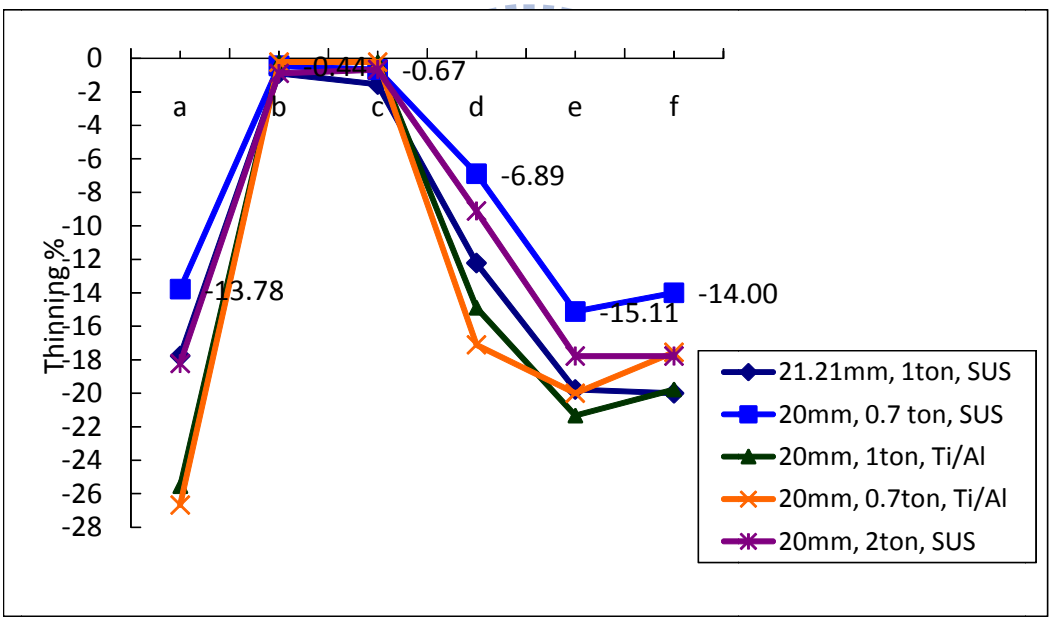


Figure 4.45 The comparisons of thinning distribution with different holding force, chamfer width, and material

Figure 4.46 The failure of Ti Al clad metal sheet occurs at a point (HF= 1 ton, chamfer width: 20mm)

Figure 4.47 The Ti / Al clad metal sheet without failure (HF= 0.7 ton, chamfer width: 20mm)

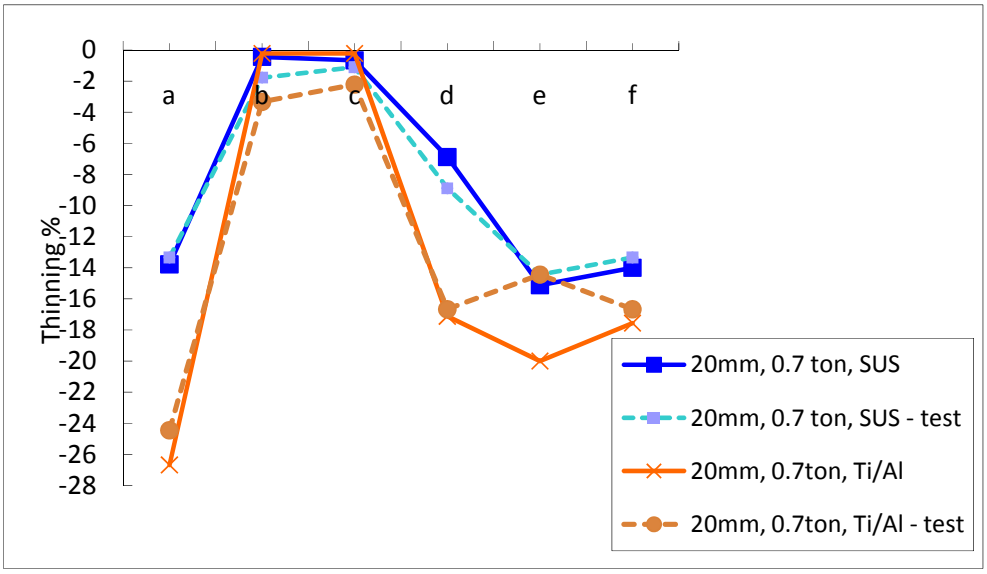


Figure 4.48 The comparison of thinning distribution by experiment and FE (different holding force)

From above simulation results, the formability of blank was better, which blank dimensions were 114mm lengths, and 74mm width with 20mm chamfer width.

Compared the thinning ratio of Ti / Al clad metal with SUS 304 in particular case (holding force were 0.7, 1 tons, and chamfer width was 20mm), thinning ratio was high (-26%) than other SUS 304 cases. Compared that with experiment result, the failure of blank occurs at point a similarly as Figure 4.46 shows.

Overall, the tendency of thickness distributions of Ti / Al clad metal and SUS 304 were similar in simulation. Figure 4.47 shows the Ti / Al clad metal sheet without failure (holding force: 0.7 ton, chamfer width: 20mm), which proves that Ti / Al clad metal with low formability were manufactured for current 3C product application by choosing suitable process parameter.

Figure 4.48 shows the comparisons of thinning distribution by experiment and FE simulation. The tendency of thinning was similar; the difference of result was only at point e. Because the thickness was be measured according to a single element. If an

average of thickness was measured from around elements, which result was close to experimental data.

From above simulation results, the holding force was significant parameter for metal flow. In housing A, the holding force can choose 2~3 tons to better formability. In housing B, the holding force can choose 0.7 tons. For pressure history, high final pressure can helpful for draw-in. That supplies the blank with more normal force. For blank dimension, suitable blank dimension can helpful for thinning. For above applications, the chamfer width 20mm was used for initial blank shape. However compared with SUS 304, the Ti / Al clad metal with low formability can achieve same product quality by choosing suitable parameters.

# CHAPTER 5 APPLICATION OF THE CLAD METAL

In this chapter, the Ti/Al clad metal housing with complex shape was formed by SHF. First, the FE model was verified by comparing the deformation of the blank obtained from experiments. Through finite element simulations, several significant process parameters such as holding force, tooling geometry, blank dimensions, single-stage (with pre-bulging effect) and multi-stages SHF were analyzed for improving formability of the Ti / Al clad metal housing during SHF.

## 5.1 Research method

### 5.1.1 Material property tests

For the material tests, all thin clad metal sheets were made by cold roll-bonding from MIRDC. The layer materials were aluminum sheets 1.0 mm thick and titanium sheets 0.5 mm thick. The roll-bonded thickness of Ti/Al clad metal sheet was 0.9 mm with one stage rolling process. For strain release, the Ti/Al clad metal sheet specimens were heated evenly to 500℃ and then air cooled for 1 h. To measure the mechanical properties of the Ti/Al clad metal sheets, tensile tests were carried out on a MTS-810 tensile machine. Figure 5.1 shows the true stress–strain curves obtained from the Ti/Al clad metal sheets. This curve represents the average result of three specimens. For verification FE model, A1050 with a 0.8 mm thickness was also tensile tested. These metal sheets were regarded as isotropic in numerical simulation.

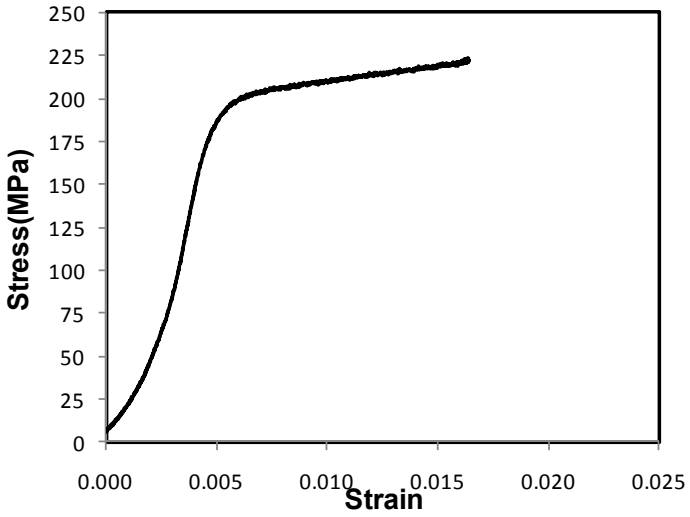


Figure 5.1 The true stress / strain curves of the Ti / Al clad metal sheet

### 5.1.2 FE simulation

This study investigated SHF with Ti/Al clad metal sheets by using ABAQUS/Explicit. The formability of camera housing with complex shape was analyzed by explicit FE code. The CAD model was shown in Figure 5.2. During FE simulation, the interface bonding condition of clad metal sheet was assumed to be perfect bonding, and the Ti/Al clad metal sheet was regarded as an equivalent single material, with its material properties determined from previous tensile tests. The blank was meshed with quadrilateral shell elements, while the die, punch, and holder were simplified as discrete rigid bodies in simulation. The FE model is shown in Figure 5.3.

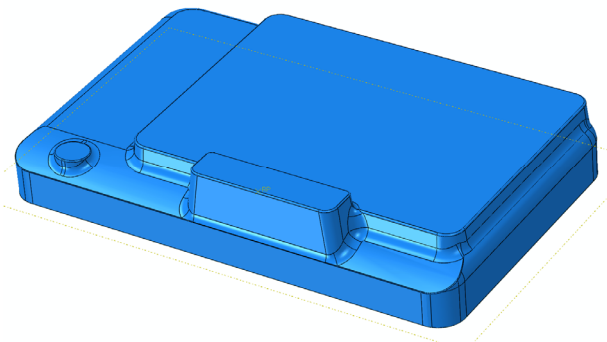

Figure 5.2 The CAD model of the housing

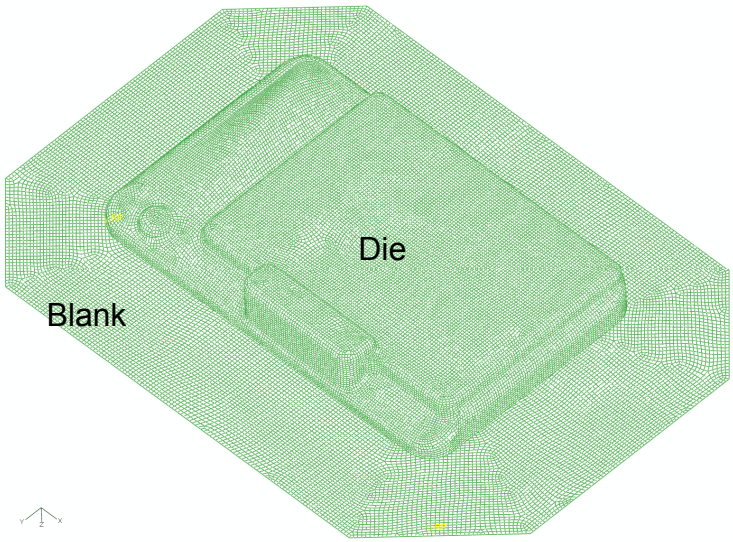


Figure 5.3 The FE model of the housing

For boundary conditions, three contact pairs (punch-blank, holder-blank, and blank-die) were defined in the FE model. The Coulomb coefficient of friction was set to 0.05 and 0.1 for contact surfaces with and without lubrication.

The punch was specified to move in the z direction, and a holding force was applied to the blank through the holder. In SHF, the pressurized area of the blank was varied according to movements of the punch, as shown in Figure 4.12. Therefore, a virtual film was also applied to simulate the hydraulic loading on blank. The coefficient of friction for the contact pair of blank-virtual film was set to zero. Figure 5.4 shows the boundary conditions of FE model for SHF.

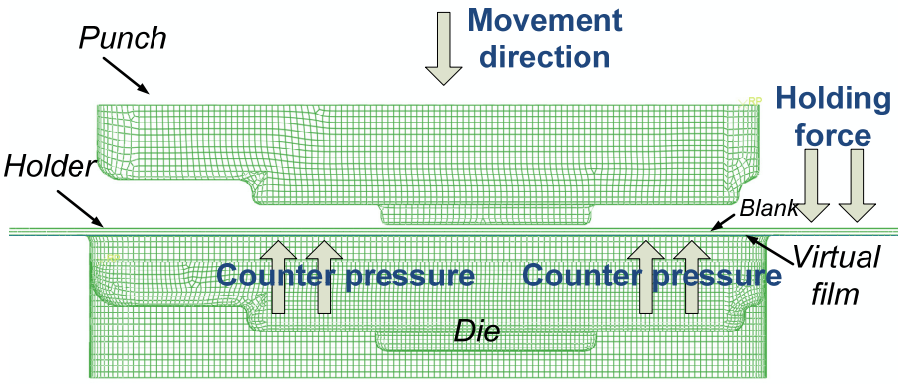


Figure 5.4 Boundary conditions of the FE model

### 5.1.3 Verification

Before further analysis, the FE model of SHF was verified by comparing the deformation of a product from experiment. In verification, the A1050 and the Ti/Al clad metal were individually used to compare the deformation during multi-stages SHF. Figure 5.5 shows the preliminary blank dimension (length of blank, 128 mm, width of blank, 95 mm, and 25 mm chamfer width). Preliminary process parameters were: the holding force was 9800 N; the counter pressure history was measured by pressure gauge, and the final pressure was 18MPa, as shown in Figure 5.6. In this research, the shape of part is complex and unsymmetrical. Before measurement, the deformed part needs to cut carefully on corner by wire cut electrical discharge machining (WEDM). When the cutting path of WEDM has a lapse, the measured and simulation value of blank diverge greatly. In the verification section, the authors used shape comparison to verify rationality of the FE model is reasonable.

The comparison between simulation and experiment shows an agreement in deformation shape, as depicted in Figure 5.7. In next sections, the authors analyzed the formability of Ti/Al clad metal with different combinations of process parameter of SHF by this verified FE model.

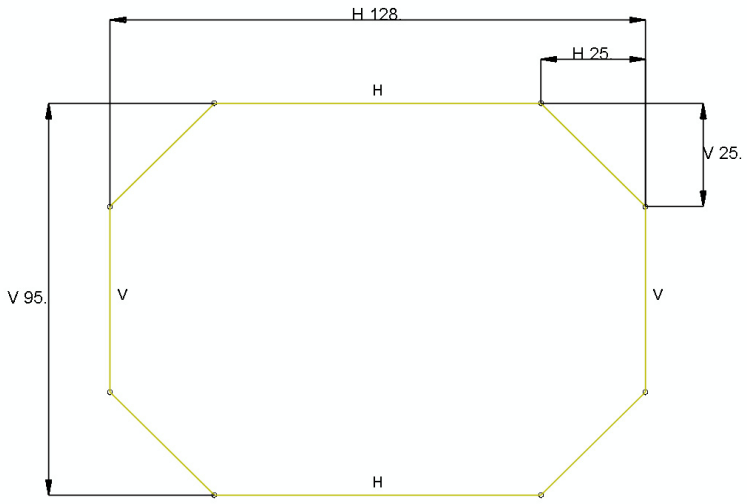


Figure 5.5 Preliminary blank dimensions (unit: mm)

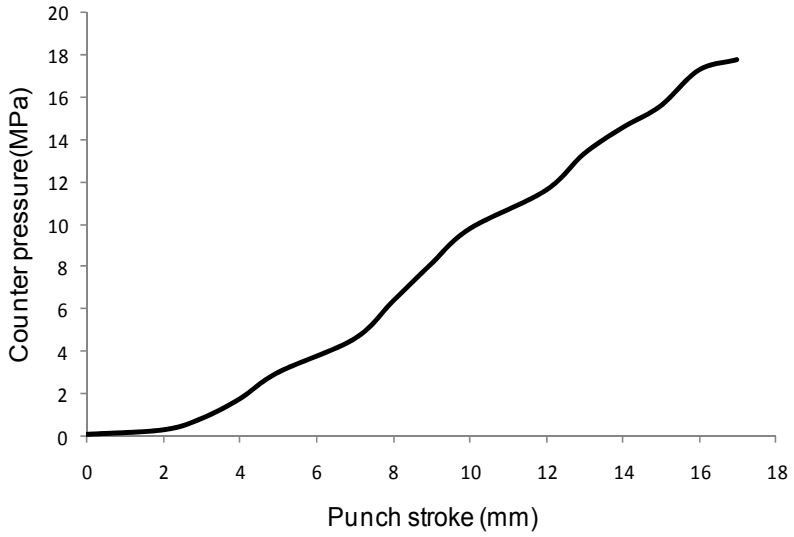


Figure 5.6 The measured counter pressure history from experiment

Figure 5.7 The deformation comparison of Ti/Al clad metal between simulation and experiment

**5.2 Analysis of SHF-application-housing C**

First, the oil-less condition (without pressure effect on blank) was simulated during drawing process as a comparison base. The holding force was 9800 N, the blank dimensions was shown in Figure 5.5. Figure 5.8 shows the thickness distribution of blank under oil-less condition. The minimum thickness of blank is 0.492 mm. It can be compared to following simulation results. In next sections, the effect of counter pressure was considered and simulated during SHF.

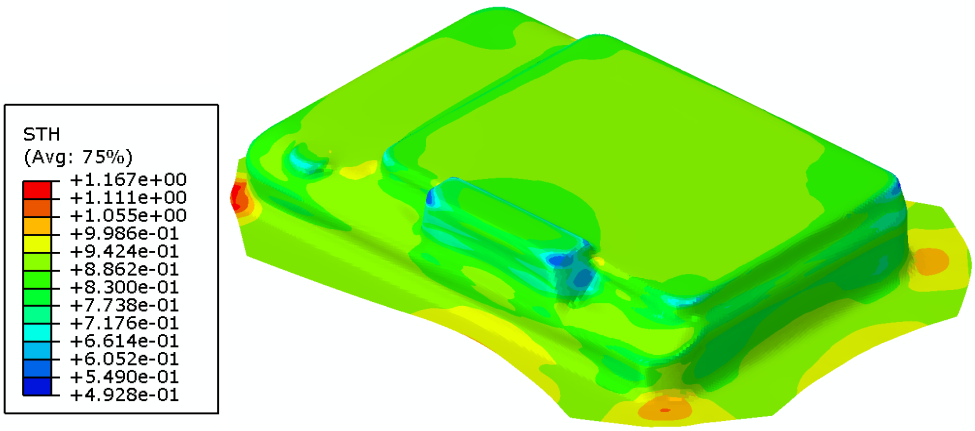


Figure 5.8 The thickness distribution of the blank under oil-less condition (unit: mm)

### 5.2.1 Influence of holding force (two stages SHF)

In this section, the effects of different holding forces were analyzed. Other process parameters are: the maximum counter pressures were 2 MPa and 18 MPa at first and second stage; the counter pressure curve was assumed to be linear in simulation. Figures. 5.9 to 5.11 show the thickness distributions of the blank.

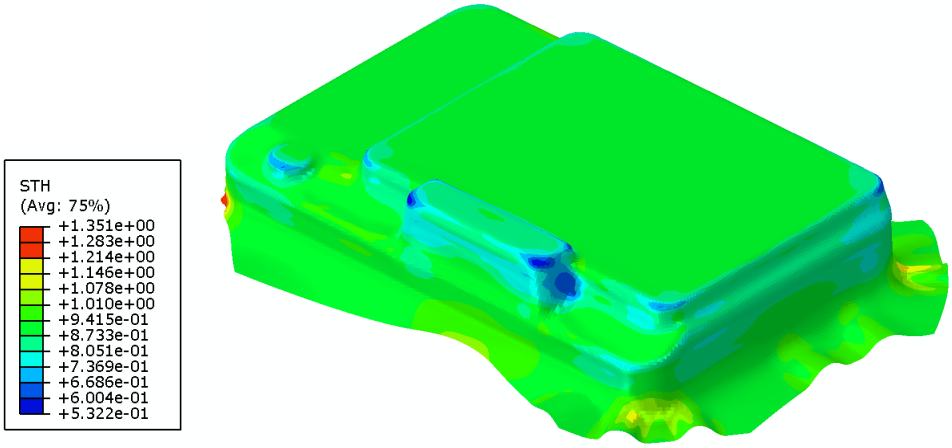


Figure 5.9 The thickness distribution of the blank with holding force 4900 N (unit: mm)

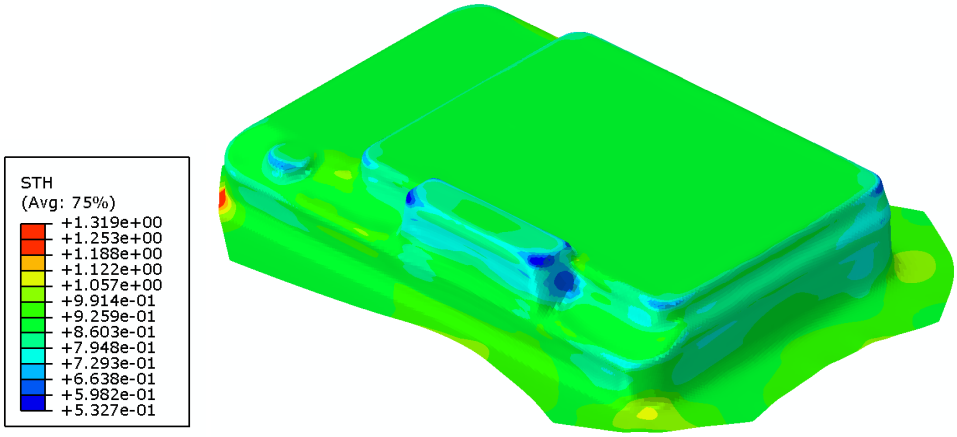


Figure 5.10 The thickness distribution of the blank with holding force 9800 N (unit: mm)

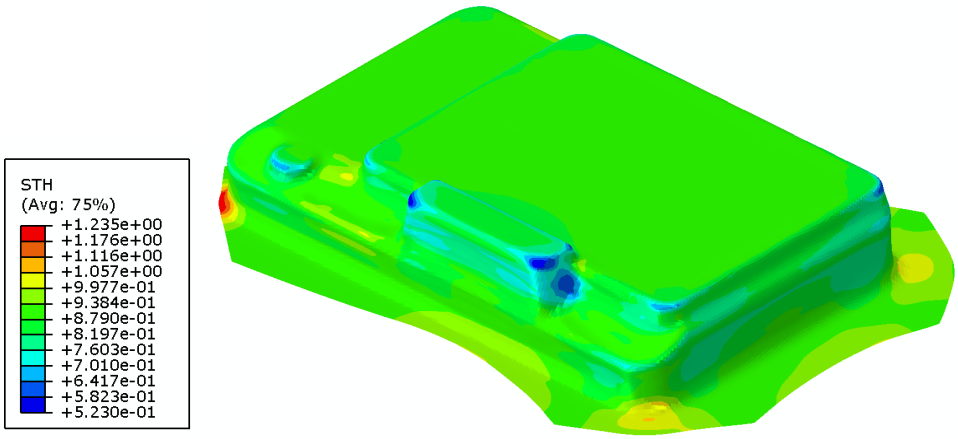


Figure 5.11 The thickness distribution of the blank with holding force 14700 N (unit: mm)

Overall, the tendencies of the thickness distributions of the blank were similar. Comparison of these simulation results reveals that the minimum thickness is lower (0.523 mm) at final stage when holding force is 14700 N. Note that the wrinkle of the blank can be observed in Figure. 5.9 (when holding force is 4900 N). These simulation results show that the formability of the blank was best when the holding force is 9800 N (min. thickness = 0.532 mm).

In addition, comparing these cases with oil-less condition shows that it applies a

counter pressure on blank, which can provide frictional support at the corner of product during forming. From above, suitable final counter pressure is also helpful in reducing thinning of blank during SHF.

### 5.2.2 Influence of pre-bulging (single stage SHF)

Many process parameters can influence the formability of blank in SHF; one of important is the pre-bulging. As show in the literature, pre-bulging technique can be used to reduce the number of operation stages. Pre-bulging means that at the initial stage of SHF, one pre-bulging unit is applied to increase the pressure in the die cavity, meanwhile, the punch is fixed at a position. When the pre-bulging pressure has reached the setting value, the punch will go down. Two critical factors for pre-bulging are bulging height and pressure. A sufficient bulging process can improve material flow and decrease holder constraint.

In this section, single stage SHFs with different pre-bulging heights (the definition of pre-bulging height as Figure 5.12 shown) were simulated to analyze the formability of Ti/Al clad metal sheet. Figure 5.13 shows the counter pressure history for single stage SHF (with and without pre-bulging). Other process parameters were: two pre-bulging heights are 2.8 and 12.8 mm, pre-bulging pressure is 2 MPa, final pressure is 18 MPa, and the holding force is 9800 N.

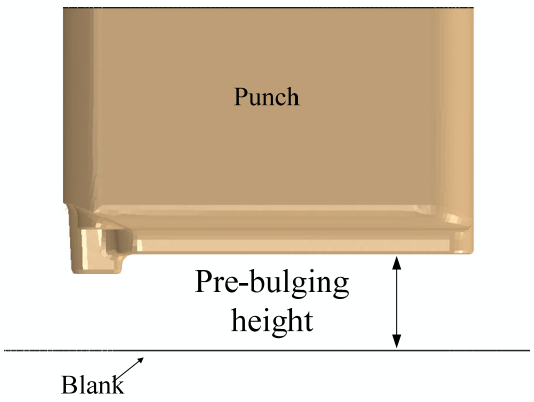


Figure 5.12 The definition of the pre-bulging height

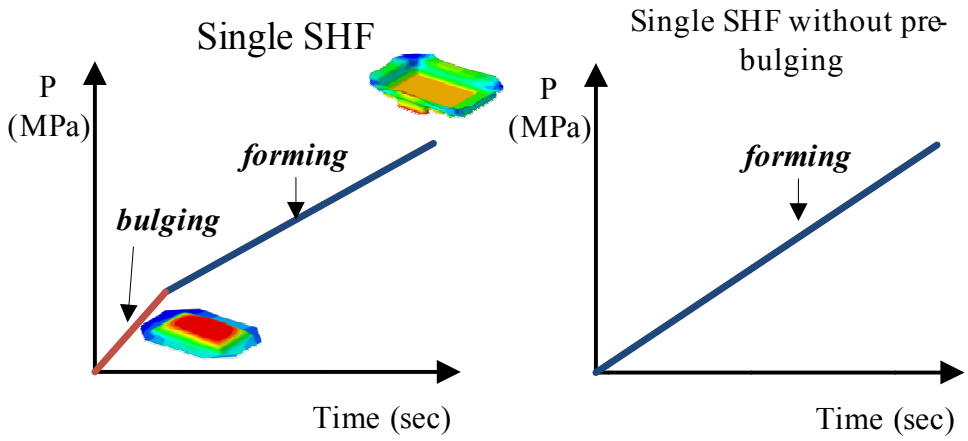


Figure 5.13 Different counter pressure histories (pre-bulging pressure = 2 MPa, final pressure =18 MPa)

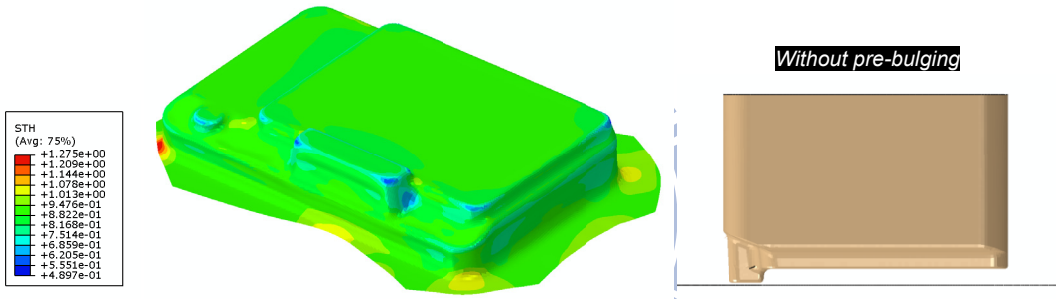


Figure 5.14 The thickness distribution of the blank without pre-bulging (unit: mm)

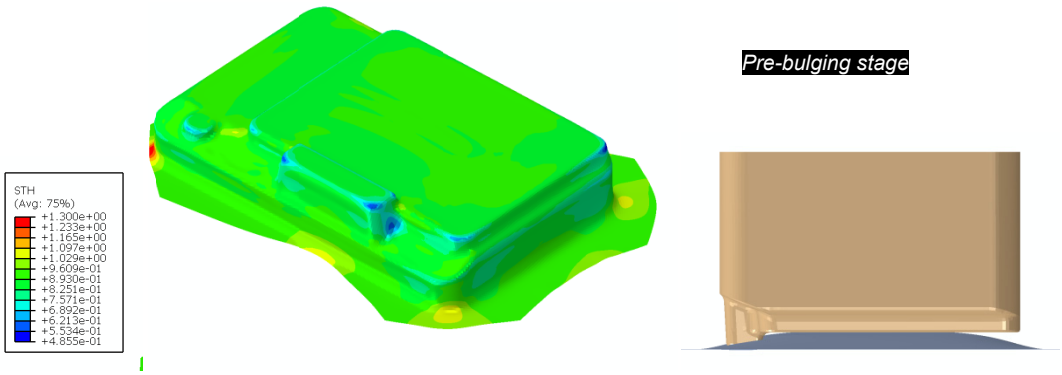


Figure 5.15 The thickness distribution of the blank with pre-bulging height of 2.8 mm (unit: mm)

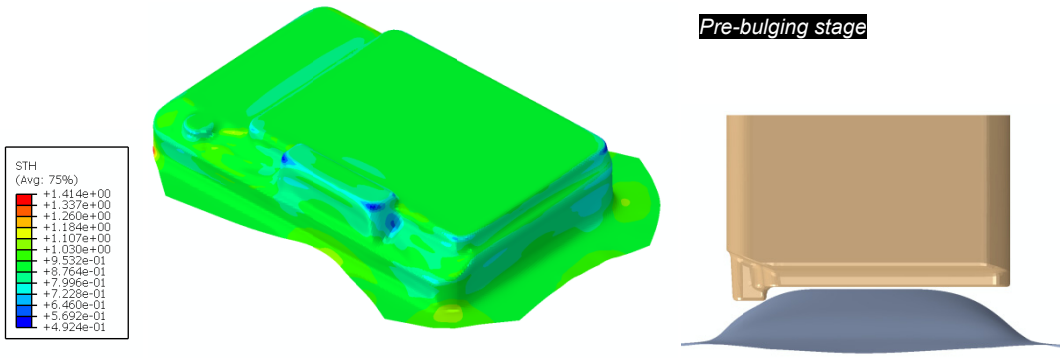


Figure 5.16 The thickness distribution of the blank with pre-bulging height of 12.8 mm (unit: mm)

Figure 5.14 shows the simulation result without pre-bulging. Figures 5.15 and 5.16 show the simulation results with two different pre-bulging heights. Compared these simulation, the thinning distributions of these cases are similar. The higher minimum thickness of 0.4924 mm was obtained when the pre-bulging height is 12.8 mm. The improvement of pre-bulging is non-significant; the material flow was still constrained because of the complex shape of the product. Nevertheless, compared to the result of multi-stage SHF under oil-less condition (Figure 5.8, with minimum thickness 0.4928 mm), the results of minimum thickness are close; that proves the pre-bulging process is helpful for reducing the number of operation stages.

### 5.2.3 Influence of dimensions

In this section, the geometry of first stage punch was modified for decreasing thickness strain during stage 1. Figure 5.17 shows the original and modified punch shapes. Because the geometry of camera product is unsymmetrical, unsuitable blank dimensions make too much constraint that can cause thinning problem on corner of blank. The symmetry blank dimensions (Figure 5.5) were modified for improving

metal flow. Figure 5.18 shows the modified blank dimensions.

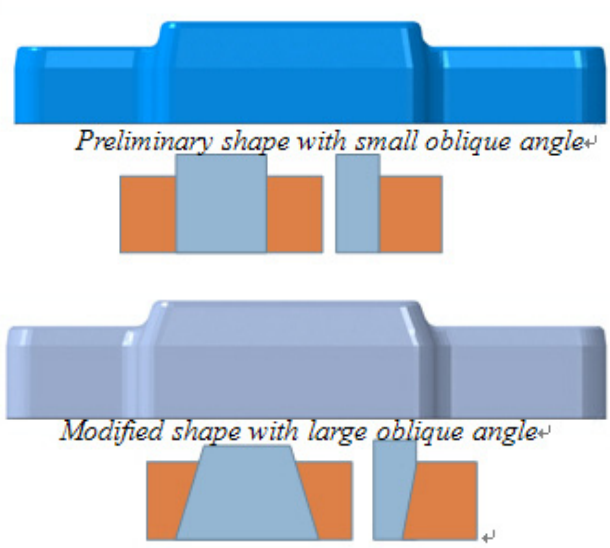


Figure 5.17 The preliminary and modified punch shapes for SHF stage 1

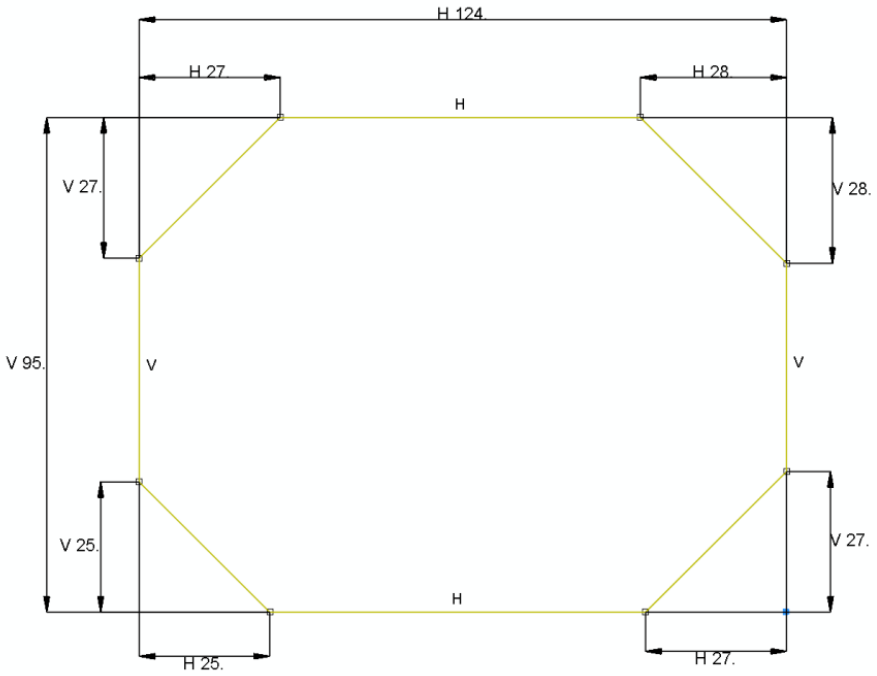


Figure 5.18 The modified blank dimensions (unit: mm)

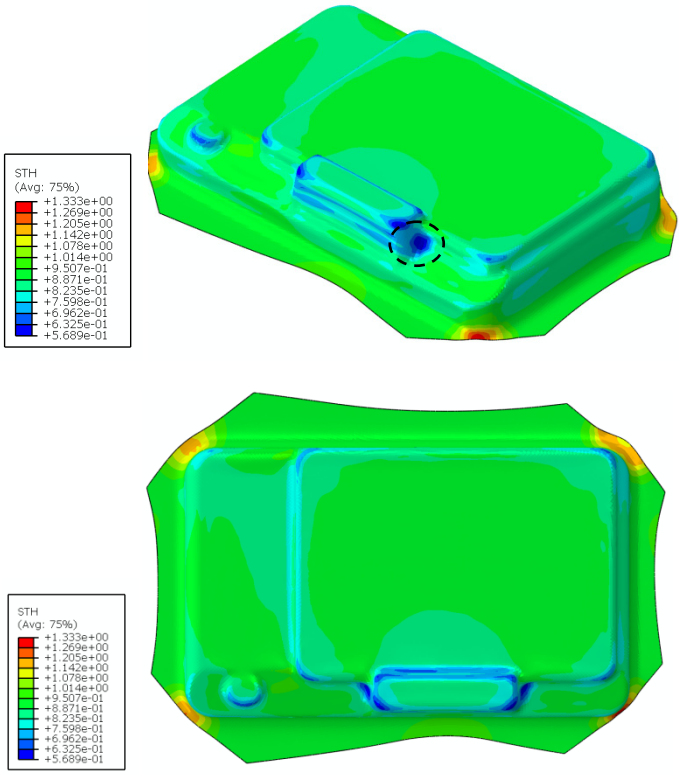


Figure 5.19 The thickness distribution of the blank with modified condition (unit: mm)

Figure 5.19 shows that the minimum thickness of blank is 0.568 mm. Compared with other cases in this research, material flow of the blank is uniform, the minimum thickness of the corner at the dotted line region is over 0.6 mm. That means the modified blank dimension and punch shape can be helpful for decreasing thickness strain of the blank during multi-stages SHF.

# CHAPTER 6 CONCLUSIONS AND FUTURE WORKS

## 6.1 Conclusions

### Cold roll bonding

In this research, first, the bonding performance of clad metal with different initial thickness and reduction rate were discussed. The plastic heat of material and frictional heat were considered in FE simulation. The temperature and pressure distributions of clad metal sheet at maximum reduction region were obtained during roll bonding process. The simulation results pointed out that the asymmetry, high rotation speed and reduction of material can improve the bonding performance for clad metal.

The results show that high reduction rate (gap=1.2mm) were effective for increasing material temperature and maximum pressure, which in turns increase the bonding performance.

In cases of symmetric rotational speed (cases 1~4, 7~10), the magnitudes of temperatures were increased by rising rotational speed.

From experimental validation, the Al/Cu clad metal sheet was bonded successfully with case 1, unsuccessfully with case 7; thus by comparing magnitudes of the temperature, pressure distribution, and diffusion coefficient, cases 3~6 are possible for good bonding with increasing rotational speed. For case 10, and 12, the results of diffusion coefficient were closed to case 1, which proves that those parameter combinations are possible for bonded.

In asymmetric rotation speed (case 5, 6, and 11, 12), the magnitudes of temperature, pressure distribution, and diffusion coefficient are higher than those of symmetric cases (case 3, and 9). It might result from the relative displacement which causes more friction heat between bonding layers. Furthermore, sufficient pressure and relative displacement can extrude more new material, and improve the bonding

energy, which were significant for bonding performance.

**FLDs of clad metal sheet**

In this section, the secondary formability and fracture prediction of Al/Cu clad metal sheets with different initial thickness ratios were analyzed. From the results of punch-stretching tests, the formability of single materials was shown to be better than that of clad metal sheets. It is expected that the formability of clad metal sheets is affected by the residual stresses during the cold rolling process. Given the different ductility of two base materials, higher plastic deformation occurred in the aluminum during the roll-bonding process. Therefore, in this research, reduction rate of the material was a significant factor for the formability of the clad metal sheets when the bonded thickness was the same. As for the fracture predictions in Al/Cu clad metal sheets, the use of forming limit diagrams with FEM has been verified by this research. The thickness distribution, the fracture prediction and the deformation behavior of Al/Cu clad metal sheets were accurately predicted using the FLD criterion option in ABAQUS.

Finally, the formability of clad metal sheets can be manipulated by changing the process parameters such as the holding force and the blank diameter in deep drawing tests. In these tests, the maximum drawing depth of 23.5 mm for clad metal sheets (Al 1.5 mm/Cu 1.0 mm) was obtained when the blank diameter was 80 mm and the holding force was 15 kN.

**Process parameters analysis and application of SHF**

In this research, some significant process parameters were discussed for formability of clad metal sheet during SHF. Some tasks were finished as follows:

- Obtained material property of Ti / Al clad metal sheet (0.45mm, and 0.9 mm thick).
- Single and multi-stages SHF FE models were created
- Validated FE model.
- Compared simulation result with experiment for application of clad metal sheet.

In simulation, a virtual film technique was proposed to realistically simulate the hydraulic loading for clad metal sheet during SHF.

From above simulation results, the holding force was significant parameter for metal flow. For pressure history, high final pressure can helpful for draw-in. For blank dimension, suitable blank dimension can helpful for decreasing thinning. However compared with SUS 304, the Ti / Al clad metal with low formability can achieve same product quality by choosing suitable parameters.

For decreasing numbers of operation stage, a high pre-bulging height and pressure can be helpful for draw-in the blank, by supplying the blank with larger normal force. By considering metal flow, suitable blank dimension can be helpful for decreasing thinning effect. For applications closed to the cases in the research, multi-stages SHF, suitable modified punch geometry at stage 1, and suitable blank dimension (124×95mm) are recommended for improving the formability of the Ti/Al clad metal sheet.

### 6.2 Future works

In future, advanced works about thin clad metal sheet and sheet hydroforming must be continued to study.

1. In this study, the most significant index to estimate whether the metals can bonded together was not clearly identified. In future, more experiments (cold roll-bonding and microscopy) should be carried out to validate numerical result.

2. In this study, tensile test are carried out to obtain true stress/strain curve of thin clad metal sheet. Experimental FLDs were applied to predicate fracture of the sheets. For complex deformation behavior, a biaxial bulging text will carry out to obtain precise material properties of thin clad metal sheets. According to theoretical facture criterion and the material properties, the facture of thin clad metal sheet will be predicted more efficiently.
3. FEA has become an established tool for predicting the formability of sheet metals. It has enabled significant reduction in the cost and time for design, and facilitation in improving the quality of products. In SHF, there exist several factors which cause the formability of metal sheet, for instance, the holding force, and the blank shape etc. In future works, current SHF simulation will be integrated with optimization procedure to efficiently obtain the most suitable process parameters.

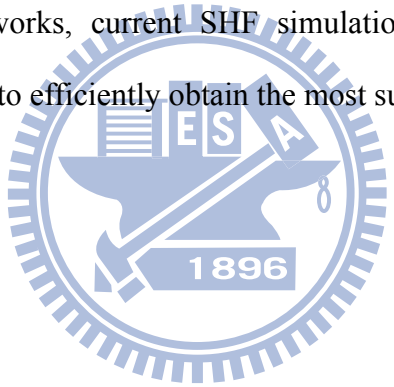

# REFERENCES


1. Bay, N., “Cold Welding : Influence of surface preparation on bond strength”, Metal Construction, 8, pp.486-490, 1986.
2. Li, L., Nagai, K., and Yin, F., “Progress in cold roll bonding of metals”, Sci. Technol. Adv. Mater., 9, 023001, 2008.
3. Kim, K.J., Kim, D., Choi, S.H., Chung, K., Shin, K.S., Barlat, F., Oh, K.H., and Youn, J.R., “Formability of AA5182/polypropylene/AA5182 Sandwich Sheets”, Journal of Material Processing Technology, 139, pp. 1-7, 2003.
4. Takuda, H., Mori, K., Fujimoto, H., and Hatta, N., “Prediction of Forming Limit in Deep Drawing of Fe/Al Laminated Composite Sheets using ductile Fracture Criterion”, Journal of Material Processing Technology, 60, pp. 291-296, 1996.
5. Dyja, H., Lesik, L., Milenin, A., and Mroz, S., “Theoretical and Experimental Analysis of Stress and Temperature Distributions during the Process of Rolling Bimetallic Rods”, Journal of Material Processing Technology, 125-126, pp. 731-735, 2002.
6. Dyja, H., Mroz, S., and Milenin, A., “Theoretical and Experimental Analysis of the Rolling Process of Bimetallic Rods Cu-steel and Cu-Al”, Journal Material Processing Technology, 153-154, pp. 100-107, 2004.
7. Mahendran, C., Balasubramanian, V., and Senthilvelan, T., “Developing Diffusion Bonding Windows for Joining AZ31B Magnesium and Copper Alloys”, International Journal of Advanced Manufacture Technology, 42, pp.689-695, 2009.
8. Nowicke, Jr.F, Zavaliangos, A., and Rogers, H.C., “The Effect of Roll and Clad Sheet Geometry on the Necking Instability during Rolling of Clad Sheet Metals”,

International Journal of Mechanical Sciences, 48, pp. 868-877, 2006.

9. Özdemir, N., and Bilgin, B., "Interfacial Properties of Diffusion Bonded Ti-6Al-4V to AISI 304 Stainless Steel by Inserting a Cu Interlayer", The International Journal of Advanced Manufacturing Technology, 35, pp. 814-820, 2009.
10. Masahashi, N., Komatsu, K., Kimura, G., Watanabe, S., and Hanada, S., "Fabrication of Iron Aluminum Alloy/Steel Laminate by clad rolling", Metallurgical and Materials Transactions A, 37A, pp. 1665-1673, 2006.
11. Kim, J.K., Huh, M.Y., and Lee, J.C., "Evolution of Strain States and Textures during Roll-cladding in STS/Al/STS Sheets", International Journal Material Sciences, 39, pp. 5371-5374, 2004.
12. Kang, H.G., Kim, J.K., Huh, M.Y., and Engler, O., "A Combined Texture and FEM Study of Strain States during Roll-cladding of Five-ply Stainless Steel / Aluminum Composites", Materials science and engineering A, 452-453, pp. 347-358, 2007.
13. Cave, J. A., and Williams, J. D., "The mechanism of cold pressure welding by rolling", J. Inst. Met., 101, pp. 203-207, 1973.
14. Bay, N., "Mechanism Producing Metallic Bonds in Cold Welding", Weld. Res. Suppl., 5, pp. 137-142, 1983.
15. Bay, N., "Cold Welding I : Characteristics, Bonding Mechanisms, Bond Strength", Metal Construction, 18, pp.369-372, 1986.
16. Vaidyanath, L. R., Nicholas, M. G., and Milner, D. R., "Pressure Welding by Rolling", Brit. Welding Journal, 6-3, pp. 13-28, 1959.
17. Park, D.H., and Yarlagadda, Prasad K.D.V., "Effects of Punch Load for Elliptical Deep Drawing Product of Automotive Parts", The International Journal of Advanced Manufacturing Technology, 35, pp. 814-820, 2008.

18. Keeler, S.P., “Determination of Forming Limits in Automotive Stamping”, Sheet Metal Ind, 42, pp.683-691, 1965.
19. Goodwin, G.M., “Application of Strain Analysis on Sheet Metal Forming Problems in the Press Shop”, SAE Paper No.680093, 1968.
20. Cockcroft, M.G., and Latham, D.J., “Ductility and Workability of Metals”, Journal Institute of Metals, 96, pp. 33-39, 1966.
21. Kim, J., Kang, Y.H., Choi, H.H., Hwang, S.M., and Kang B.S., “Comparison of Implicit and Explicit Finite Element Methods for the Hydroforming Process of an Automobile Lower Arm”, The International Journal of Advanced Manufacturing Technology, 20, pp. 407-413, 2002.
22. Shim, H., “Determination of Optimal Shapes for the Stampings of Arbitrary Shapes”, Journal of Material Processing Technology, 121, pp. 116-122, 2002.
23. Pegada, V., Chun, Y., and Santhanam, S., “An Algorithm for Determining the Optimal Blank Shape for the Deep Drawing of Aluminum Cups”, Journal of Material Processing Technology, 125, pp. 743-750, 2002.
24. Lang, L., Li, T., An, D., Chi, C., Nielsen, K.B., and Danckert, J., “Investigation into Hydromechanical Deep Drawing of Aluminum alloy-Complicated Components in Aircraft Manufacturing”, Materials Science and Engineering A, 499, pp. 320-324, 2009.
25. Kim, T.J., Yang, D.Y., and Han, S.S., “Numerical Modeling of the Multi-stage Sheet Pair Hydroforming Process”, Journal of Materials Processing Technology, 151, pp. 48-53, 2004.
26. Chen, W., Liu, Z.J., Hou, B., and Du, R.X., “Study on Multi-stage Sheet Metal Forming for Automobile Structure-Pieces”, Journal of Materials Processing Technology, 187-188, pp. 113-117, 2007.
27. Palumbo, G., Zhang, S.H., Tricarico, L., Xu, C., and Zhou, L.X.,

"Numerical/Experimental Investigations for Enhancing the Sheet Hydroforming Process", International Journal of Machine Tools & Manufacture, 46, pp. 1212-1221, 2006.

28. Zhang, S.H., Zhou, L.X., Wang, Z.T., and Xu, Y., "Technology of Sheet Hydroforming with a Moveable Female Die", International Journal of Machine Tools & Manufacture, 43, pp. 781-785, 2003.
29. Thiruvarudchelvan, S., and Tan M.J., "Fluid-Pressure-Assisted Deep Drawing", Journal of Materials Processing Technology, 192-193, pp. 8-12, 2007.
30. Kleiner, M., Krux, R., and Homberg, W., "Analysis of Residual Stresses in High-Pressure Sheet Metal Forming", CIRP Annals - Manufacturing Technology, 53-1, pp. 211-214, 2004.
31. Danckert, J., and Nielsen, K. B., "Hydromechanical Deep Drawing with Uniform Pressure on the Flange", CIRP Annals - Manufacturing Technology, 49-1, pp. 217-220, 2000.
32. William D. and Callister, JR., Materials Science and Engineering an Introduction 6/e, John Wiley & Sons, Inc.
33. Kobayashi S., Oh S. I. and Altan T., Metal Forming and the Finite Element Method, Oxford University Press, Oxford.
34. 張志毅，金屬工業研究中心，「輕構件及板材成形接合技術開發與應用」，合作計畫研究成果報告，民國 95 年。
35. ABAQUS Theory manual, Version 6.8, Hibbitt, Karlsson & Sorensen, Inc.
36. Groche P., and Metz C., "Hydroforming of Unwelded Metal Sheets Using Active-Elastic Tools", Journal of Materials Processing Technology, 168, pp. 195-201, 2005.
37. 洪景華，金屬工業研究中心，「高階數位產品構件複合成形技術開發」，合作

計畫研究成果報告，民國97年。

# RESUME

Name : Tseng, Huang-Chi

Birthplace : Taiwan, Nantou

Birthday : 1979/09/20

Specialties : Gear theory and design, Finite element analysis, and Sheet metal forming

## Academic background

2005~2010 Ph.D. National Chiao Tung Univ., ME.

2002~2004 Master National Formosa Univ., PME.

1999~2001 Bachelor National Chin-Yi Univ. of Technology, ME

1997~1999 College National United Univ., ME.

1994~1997 National Nantou Senior High School

## Work experience

2004~2005 Flotrend corporation company, Structure engineer.

## Publication list

A. Journal papers

1. **Tseng H.C.**, Hung J.C., Hung C., Lee M.F., 2010 “Experimental and numerical analysis of titanium/aluminum clad metal sheets in the sheet hydroforming. ” The international journal of advanced manufacturing technology (accepted) DOI: 10.1007/s00170-010-2911-0.
2. **Tseng H.C.**, Hung C., Huang C.C., 2009 ” An analysis on formability of aluminum/copper clad metal with different thickness by finite element method and experiment,” The international journal of advanced manufacturing

technology, Vol. 49, Numbers 9~12, pp. 1029-1036.

3. **Tseng H.C.**, and Hung C., 2009 “The Finite Element analysis on Diffusion Bonding of Al / Cu Clad Metal in Cold Rolling Process,” Journal of the Chinese society mechanical engineers. (accepted)
4. Hsieh, J. K., **Tseng, H.C.**, and Chang, S. L., 2008, “A Novel Hob Cutter Design for the Manufacture of Spur-typed Cutter,” Journal of Materials Processing Technology, DOI:10.1016/j.jmatprotec.2008.02.071.
5. Chang, S. L., **Tseng, H.C.**, Hsieh, J. K., Liu, J. H. and Hung, C. H., 2008, "Optimum design of a cutting tool for manufacturing rotary knives," 2nd revision for Proceedings of the Institution of Mechanical Engineers, Part C: Journal of Mechanical Engineering Science.
6. Chang, S. L. and **Tseng, H.C.**, 2005, “Design of a Novel Cutter for Manufacturing Helical Cutting Tools,” Journal of Mechanical Engineering Science, Part C, Vol. 219, pp. 395-408. (NSC91-2212-E-150-022, NSC92-2212-E-150-033) (SCI, EI)

B. Conference papers

1. **Tseng H.C.,** Wu Z.C., Hung C., Lee M.F., 2010 “Investigation on sheet hydroforming process of Titanium/Aluminum clad metal housing, ” Proceedings of the 2010 ASME International Manufacturing Science and Engineering Conference, MSEC2010, October 12-15, 2010, Erie, Pennsylvania, USA.
2. 韓忠諭、**曾煌棊**、洪景華、李明富，2009 ”鈦/鋁複合金屬板件板液壓成形之有限元素分析,” 中國機械工程學會，第 26 界全國學術研討會，11 月 20~21 號，台南，台灣。
3. **Tseng H.C.**, Wu Z.C., Hung C., Lee M.H., Chin-Chuan Huang 2009 ” Investigation of Optimum Process Parameters on the Sheet Hydroforming of

Titanium / Aluminum Clad Metal for Battery Housing," 4th International Conference on Tube Hydroforming September 6-9, 2009 – Kaohsiung, Taiwan.

4. **Tseng H.C.**, Hung C., Huang C.C., 2008, "An Analysis on Forming Limits of Aluminum/Copper Clad Metal with Different Thickness Ratio by Finite Element Method and Deep Drawing Process," The 9th International Conference on Technology of Plasticity, Gyeongju, Korea, September 7-11, pp.702-707.
5. Chang, S. L. and **Tseng, Huang-Chi**, 2004, "Mathematical Model Development and FEM Analysis of a Plastic Rotary Knife Manufactured by a Novel Designed Cutter," The 4th IASTED International Conference on Modelling, Simulation, and Optimization, Hawaii, August 17-19, pp.365-370.

C. Patent

1. **曾煌棋**，洪景華，"具背壓式密封調節之一體式模具"，中華民國發明專利，公開/實體審查中。